Design and fabrication of a device to characterize the electromechanical behavior of Superconducting Nb_3Sn 3-strand cables under transverse load.

Submitted by
Konstantin Derman

IN PARTIAL FULFILLMENT OF THE REQUIREMENTS FOR THE DEGREE OF

MASTER OF SCIENCE IN MECHANICAL ENGINEERING

School of Engineering
Tufts University
Medford, Massachusetts

May 2012

Author: Konstantin Derman
Department of Mechanical Engineering
Tufts University

Certified By: Dr. Luisa Chiesa
Assistant Professor
Department of Mechanical Engineering
Tufts University
Research Advisor

Certified By: Dr. Makoto Takayasu
Research Scientist
Plasma Science and Fusion Center
MIT

Certified By: Douglas M. Matson
Associate Professor
Department of Mechanical Engineering
Tufts University

Abstract

Nb_3Sn superconducting wire is currently in use in the Toroidal Field (TF) and Central Solenoid (CS) coils of the ITER fusion machine because of its ability to remain in the superconducting state at the high magnetic fields required to confine a plasma. However, this conductor is sensitive to strain, which degrades its electromagnetic performance. In the past 15 years, a lot of research has been focusing on the understanding of the mechanisms behind the degradations due to bending, transverse, and axial strains. This thesis work focused on the design, fabrication and preliminary functionally tests of a mechanical system to apply transverse load on a 3-strand Nb_3Sn cable. The design of a completely new loading mechanism has been developed to apply transverse load to the 3-strand cable and the device has been fabricated. The mechanism is designed so that a load cell and an extensometer are used to record vertical load and displacement respectively. This information is used to evaluate the transverse load applied to the sample. The mechanism allows an overall transverse deformation of the cable from a 1.78 mm to a 1.16 mm diameter. The mechanism is designed to sustain and react transverse forces up to 60 kN on a cable length of ~215 mm. Finite Element Analysis (FEA) was performed using Solidworks Simulation to confirm the structural integrity of the mechanism and preliminary tests were performed to verify the operational functionality of the device.

Acknowledgements

Firstly, I would like to thank Dr. Luisa Chiesa, for providing support and invaluable guidance on this journey. I would like to thank Dr. Makoto Takayasu, who has been a source of great design insight and limitless attention to detail. I would also like to thank Dr. Douglas Matson being on my masters degree committee.

This work was supported in part by the U.S. Department of Energy under GRANT DE-SC0004062.

I would also like to thank my family, who been my biggest fans. Mom and dad, you have been the best parents one could ever ask for. You have showed unconditional love and encouraged me to reach for the stars. Ira, you're the best sister one could ever ask for. Now it is your turn to get another degree. I would also like to thank my grandparents, Polina, Tanya, Abram and Lev, who have cheered for me every step of the way.

Thank you to my girlfriend Zoya. You are amazing! I love you with all my heart.

Thank you to Joe for being a great friend. You are a great friend and I look forward to having you in my life for years to come.

A very warm and special thank you to my grandpa Lev. Sadly you could not make it to see me finish this degree. You are the shining star I always have and always will look up too. Your warm smile and blue piercing eyes are forever on my mind. All of us are lucky to have had the pleasure to be with you. You will never be forgotten.

Table of Contents

Table of Figures

Design and fabrication of a device to characterize the electromechanical behavior of Superconducting Nb_3Sn 3-strand cables under transverse load.

Chapter 1 Introduction and Background

1.1 Background of Superconductivity

Scientists have been studying and characterizing the properties of superconducting materials since it was discovered by Onnes Kamerlingh in 1911. A discovery that was made possible by the ability to liquefy helium, also achieved by Onnes, only a few years prior. [1]. The discovery of a new superconducting material, Nb_3Sn, in 1954 was a breakthrough in the superconducting field. Nb_3Sn maintains superconductivity state for larger currents and fields compared to the more conventional superconductor used for magnets NbTi, making it a good candidate conductor for high magnetic fields applications [2]. One weakness of Nb_3Sn is that it's sensitive to stress and strain, which degrade its electromagnetic performance. In order to better predict the performance of a magnet, stresses experienced by the Nb_3Sn strands inside a cable must be understood.

Other applications are made possible by superconductivity. One of the great properties of superconductors is their ability to magnetically levitate objects by expelling a magnetic field applied to them. Using this ability, one can levitate trains on strong superconducting magnets, eliminating most of the friction between the train and the train tracks. Doctors, can utilize strong superconducting magnetic fields to non-invasively see the insides of a human body. In a scientific community, the use of superconducting magnets is used in high-energy particle research, accelerating sub-atomic particles to near speed of light. CERN, a European Laboratory for Particle

Physics, on the border of France and Switzerland has been successfully working and demonstrating the importance of superconductivity.

Three types of strains act on a superconducting strands in a cable during cool down and operations; axial strain caused by thermal contraction, bending strain caused by thermal contraction and the Lorentz load and the transverse strain caused by the Lorentz Load [3]. This thesis will focus on designing a mechanism to measure the transverse strain and how it affects the performance of the Nb_3Sn strands used in large cables for fusion machines. A new experimental device to electromechanically characterize a 3-strand cable will be presented. While large cables for fusion machines are composed of more than 1000 strands, studying a small sub-cable using this device will highlight the fundamental behavior of Nb_3Sn conductor under transverse strain.

1.2 Properties of Superconductors.

A superconductive material is said to exhibit distinctive characteristics, its ability to conduct the electric current without any resistance in a DC current and expelling the magnetic field from within the interior of the material. The second characteristics is called the Meissner effect and it describes the absence of magnetic induction (B), within the bulk of a superconductor, i.e. B=0. The complete diamagnetism of a superconductor is more fundamental than the complete absence of electrical resistivity (ρ), i.e., $\rho = 0$. A material's perfect diamagnetism automatically requires it to be a perfect electrical conductor [3]. Meaning, in order for normal material to go into a superconducting state, it has to actively exclude magnetic fields from its interior. This behavior is the Meissner effect and it produces absence of

electrical resistance, thus a perfect conductor. More details on this effect will be discussed in section 1.3.

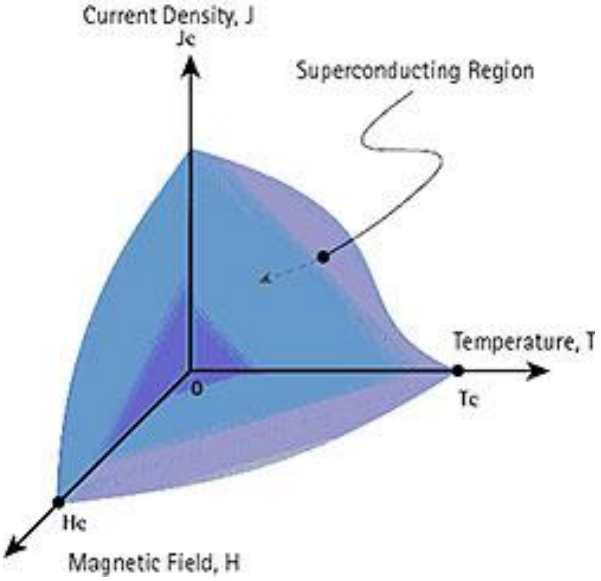

Fig. 1.1 Conditions for Superconductivity

When cooled below a critical temperature, a superconducting material loses all its resistance to the flow of direct electrical current, and therefore is 100% efficient. To maintain its superconductive behavior, three conditions must be met, as shown in Fig. 1.1. Material must be cooled below a certain temperature, known as its superconducting transition, or critical temperature (T_C). The current passing through a given cross-section of the material must be below a characteristics level known as the critical current density (J_C). Lastly, the magnetic field to which the material is exposed to, must be below a characteristic value known as the critical magnetic field (H_C), Fig. 1.1, [4]. Some materials, such as Nb_3Sn, also exhibit sensitivity to strain, ε. Only when the critical temperature, critical current density (as the amount of current flowing through a given cross sectional area), critical strength level of the magnetic fields are below their critical values can you have a material in a

superconductive state [5]. The strain effect will effectively shift the critical surface described by those three parameters, mostly making it smaller.

Superconductors can be of two types, Type I and Type II, depending on their magnetic characteristics. First described by London's Theory in 1935, Type I superconductors exhibit perfect diamagnetism behavior. They also show no resistance in both AC and DC conditions below the critical field. When an external magnetic field is applied, a field equal and opposite is induced inside the superconductor [6]. They generally are not used in magnets because their critical field is very small. Type II superconductors exhibit a partial penetration of the magnetic fields while maintaining the superconducting state and can carry much higher current up to a very high critical magnetic field.

1.3 Type I and Type II Superconductors

Type I superconductors exhibit a unique magnetic characteristic called Meissner effect, Fig. 1.2, where the magnetic flux resides on the exterior surface of the material in the superconductive state, independent of the existence of the magnetic field in the material before it was cooled below its critical temperature. Unlike Type I, Type II superconductors show partial penetration when external field is applied without destroying the overall superconductive state Fig. 1.2. It is important to understand the behavior of a single superconductive strand in an external applied field environment, as this behavior is similar inside of a magnet where the field is generated by adjacent strands.

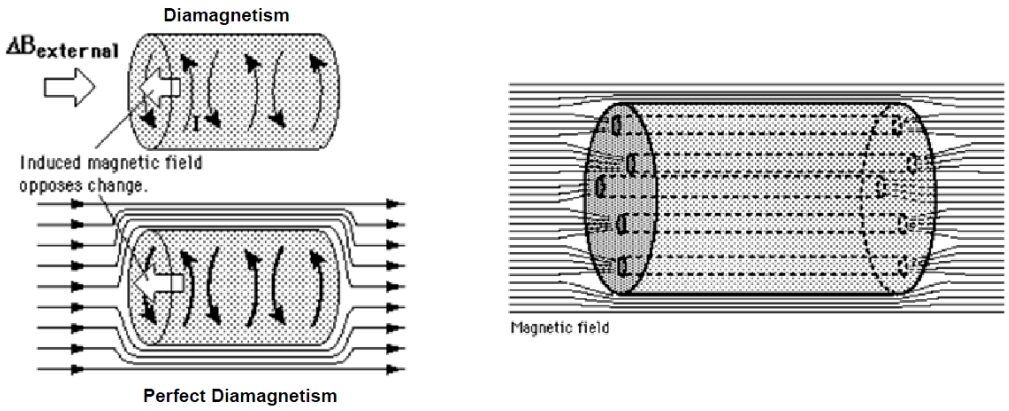

Fig. 1.2 Behavior exhibited by superconductors during application of external magnetic field.

Fig. 1.3 compares the electromagnetic behavior of a perfect conductor and a superconductor to illustrate the Meissner effect. It shows that perfect conductor has zero electrical resistance, but does not exhibit Meissner effect. A perfect conductor opposes any change to the existing magnetic state. As it can be seen in Fig. 1.3 from (a) to (d) when the conductor is cooled and magnetic field is applied and removed the conductor goes back to its original state and opposes the change of field by expelling the filed in (c). When the magnetic flux is applied prior to the cooling as shown from (e) to (g), and then removed, in a cooled state, the conductor will resist the magnetic field change and trap the magnetic field in the conductor indefinitely. Superconductor exhibits diamagnetic behavior and the magnetic flux is always expelled via Meissner effect. This behavior is represented in (h) to (k) and from (l) to (n), when the magnetic flux is applied, it is always expelled by the surface of the superconductor. This phenomenon was first explained by Fritz and Heinz London in 1935 [7].

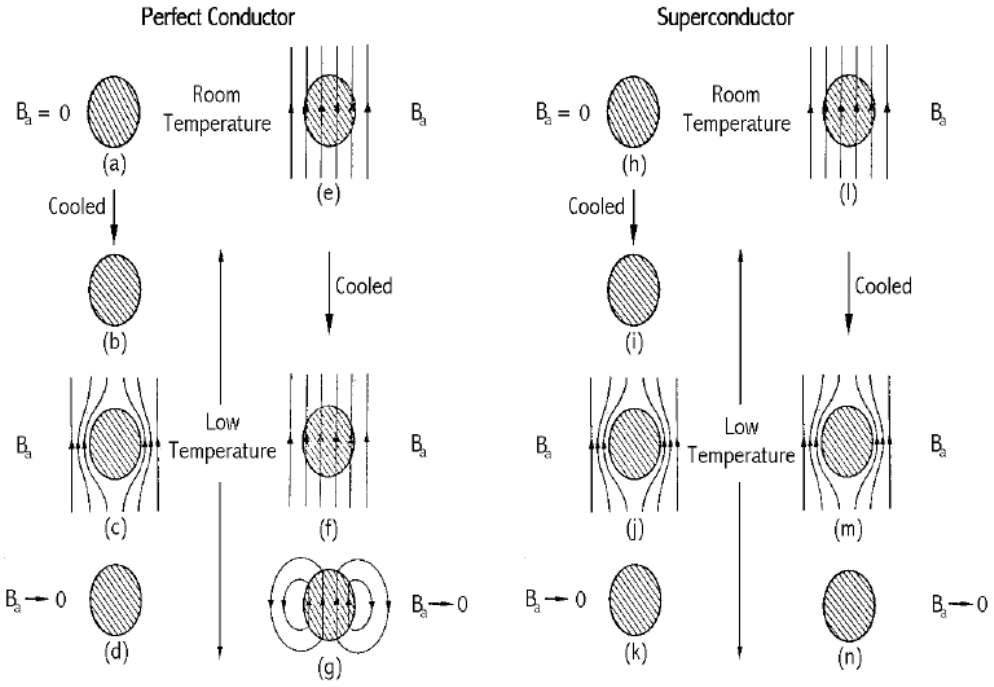

Fig. 1.3 Comparison of the magnetic behavior of a perfect conductor and a superconductor. For both the perfect conductor (a, b, c and d) and the superconductor (h, i, j and k) magnetic flux exclusion occurs when the materials are first cooled and then exposed to a magnetic field. When the materials are exposed to a magnetic field and then cooled, the perfect conductor traps the magnetic flux (e, f and g), while the superconductor excludes the magnetic flux (l, m and n)[8]

The difference between a "perfect" conductor and a superconductor is the ability to attain zero resistance in combination with the Meissner effect. However, in Type I superconductors when the external magnetic field is strong enough, screening currents cannot provide enough opposing magnetic field and the Meissner effect is broken down. The loss of the Meissner effect brings the superconductor back to a normal conductive state.

1.4 Type II Superconductors

Type II superconductors exhibit a mixture region in which while maintaining superconductivity, they allow partial penetration of the magnetic field. The local

islands of resistive regions allow magnetic flux lines to penetrate through the mixture without destroying the overall superconductive state [9]. If a current is applied to an ideal Type II superconductor in the presence of magnetic field, it will result in Lorentz force which causes magnetic flux lines to move and redistribute across the material as shown in Fig. 1.4.

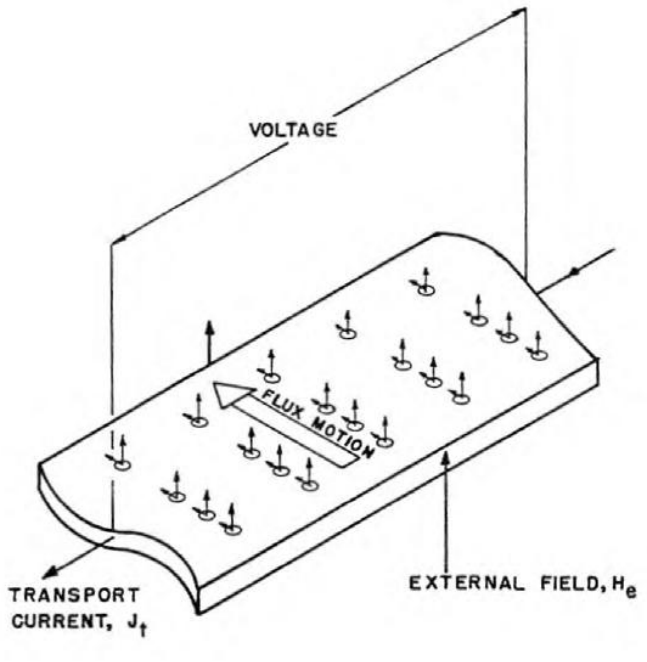

Fig. 1.4 Dissipative flux motion in a Type II superconductor [9].

The flux lines can be prevented from moving, be "pinned", by lattice imperfections such as impurities, defects or grain boundaries [10]. When a current is applied to the superconductor in this mixed state, the current will flow without resistance in a path around the normal cores, which are now pinned. The pinning force establishes how the vortices of magnetic flux penetrate through the normal regions and are surrounded by shielding currents. This force keeps the flux from moving and has the effect of raising the upper critical field level of material. To

minimize the energy state, the vortices contain one flux quantum and arrange in a triangular lattice pattern. This is illustrated in Fig. 1.5(a) and the picture of the flux lattice in Fig. 1.5(b).

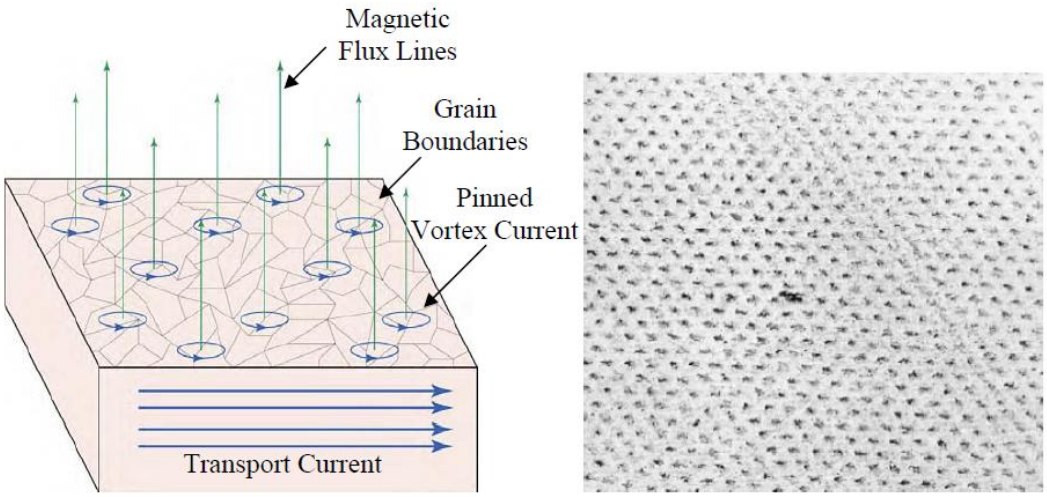

Fig. 1.5 (a) Flux penetration in Type II superconductor, (b) picture of actual lattice [9]

As the external field increases the number of normal cores increase until it occupies the entire material at $B_{c2,}$ Fig. 1.6, and the material becomes normally conducting [6]. When a Type II, superconductor is in a magnetic field lower than B_{c1}, the currents will flow on the surface opposing any external field to penetrate the material (perfect diamagnetism). When the external field exceeds B_{c1}, surface currents will still flow but normal cores will also form in the material. These normal cores tend to form at the surface and diffuse into the material. The local islands of resistive regions allow magnetic flux lines to penetrate through the mixture without destroying the overall superconductive state.[9]

When the magnetic field is increased, Type I superconductors, Fig. 1.6, have a single critical field B_{c1} above which the material stops being superconductive and becomes resistive. Below this critical field condition, the material shows perfect diamagnetism and no resistance in both AC and DC. Below B_{c1}, Type II superconductors, Fig. 1.6, sustain a perfect diamagnetism, namely the Meissner state. Bounded by both lower and the upper fields, B_{c1} and B_{c2} the material bulk exhibits partial magnetic flux penetration but the overall material remains superconducting. While it's in between the two limits the material is said to be in mixed state, allowing partial flux penetration. Type II superconductors have higher tolerance to external magnetic field and maintain superconductivity.

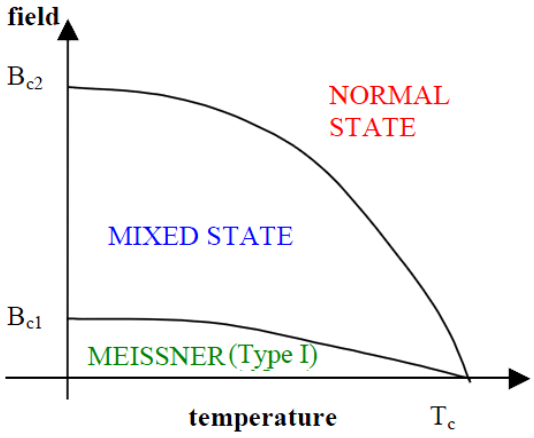

Fig. 1.6 Critical field as a function of temperature for Type I and II superconductors [9]. Type I is superconducting below B_{c1} and Type II is superconducting below B_{c2} in a mixed form.

Material constituents and fabrication process dictate the concentration and type of pinning sites throughout the bulk of superconductor. Cold working and heat treatments can be used to control the quality and quantity of pinning sites, thus improving the critical field and current density limits of the bulk superconductor.

Lots of research in material science is conducted to optimize and improve the properties of a superconductor.

1.5 Production of Nb_3Sn Strand

The design and manufacturing of the Nb_3Sn strand is a difficult process due to the dilemma of producing many twisted small filaments distributed through a stabilizing matrix within a single strand, typically having a diameter of about 1 mm. The filaments need to be finely distributed for electrical and thermal stability reasons. Fine distribution prevents a phenomenon called flux jumping [6]. When the Lorentz force, which acts on the flux-line lattice, becomes larger than the bulk pinning force, a critical current density can be defined. This pinning force, and thus the critical current density, depends on the applied field and temperature [10]. Due to the brittleness of the Nb_3Sn, it cannot be created via normal wire making methods.

A method referred to as the Internal Tin process [11], has been developed where a copper billet is first drilled and filled with niobium and tin rods Fig. 1.7(a). These billets are combined and drawn together to form a single strand. These billets also go through annealing steps as they are drawn. This assembly is wrapped with a tanatalum diffusion barrier, which is usually extruded with the copper stabilizer. These filament sublets are then restacked inside the barrier tube and drawn to final wire size Fig. 1.7(b).

The picture in Fig. 1.7(b) shows that the tin core occupies a significant portion of the area. The tin must diffuse through the copper surrounding the niobium filaments and combine to form the Nb_3Sn compound during the heat treatment. A

bronze matrix is created because tin has a greater affinity for copper than niobium. The tantalum barrier and the copper shell keep the tin from diffusing to the surface and are clearly visible.

Fig. 1.7 (a) Internal Tin billet (b) Picture of uncreated tin strand [9]

The final step of the process (the formation of the superconducting filaments) is achieved during the heat treatment of the wire in the final experimental structure. Handling of the strand after it's been formed and heat treated must be done with extreme care as the material is brittle and can fracture easily.

Several other processes are available for the production of Nb_3Sn wires but for the scope of this thesis only the internal tin process is the one of interest.

1.6 Fusion energy, ITER and the Cable-in-Conduit Conductor (CICC)

The focus of this thesis is on superconducting cables used for highly desired but so far not achieved, fusion energy reactors. Fusion works on the principle of capturing heat from secondary products, typically neutrons, of a nuclear reaction. It generates electricity by collecting heat from a heat exchanger, which produces steam

to drive a turbine and thus generates electricity. The challenge is to create a machine which is capable of creating and confining plasma at a very high density for long enough time in order to produce nuclear power. In order to confine the plasma, a large magnetic field is required, which will trap the charged particles in predetermined orbits [6]. Magnetic confinement is the leading scheme for tokamak reactor and is used because the plasma is at such high temperatures that no material is available to contain it.

High magnetic fields can be generated by magnets. In order to have the highest magnetic field achievable large magnets are required. Cryogenically cooled superconducting magnets are currently the best choice available. Such high magnetic fields (12-15 T) cannot be met by resistive magnets, without using an enormous amount of energy to sustain the currents and compensate for the resistive losses. The smaller size and ability to sustain high magnetic fields, makes cryogenic magnets ideal for this task.

International Thermonuclear Experimental Reactor (ITER) Fig. 1.8 is the current plasma reactor that uses such magnetic confinement with superconducting magnets in hopes of achieving fusion reaction. The computer model shows the scale of the reactor, notice the size of the man in a blue lab coat in the bottom of the reactor.

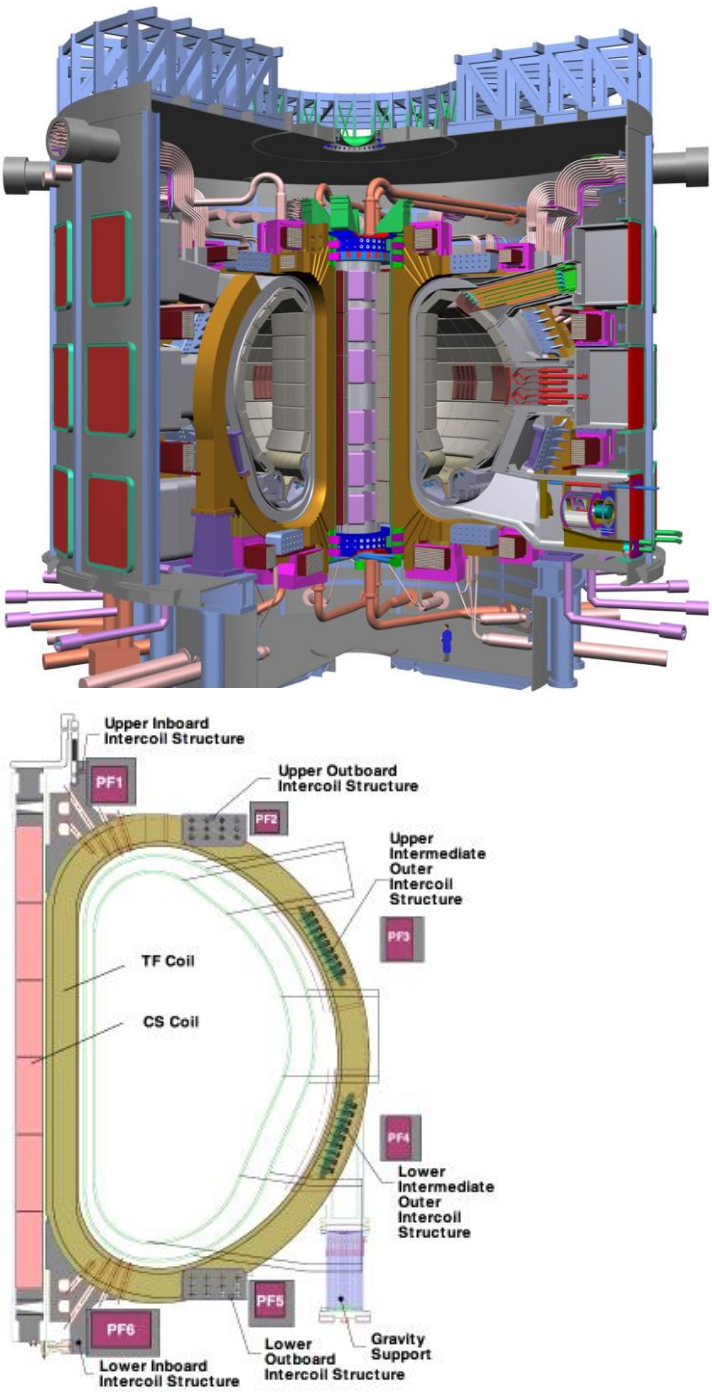

Fig. 1.8 ITER Tokamak Reactor [12]

ITER magnets are wound using Cable-in-Conduit conductors. The first step in creating the cable is to wind the superconducting strands into the conductor configuration. Depending on the magnet design (toroidal field coils or central

solenoid), different design configurations exist. The main goal is to maintain the superconducting magnet below its critical temperature. If the magnet goes above this critical temperature, it becomes resistive with extremely serious consequences to the reactor. The cable-in-conduit conductor used at ITER utilizes forced flow of liquid helium, temperature of 4.2 – 4.5 K. This fluid provides cooling through a non-ferromagnetic stainless steel jacket. An image of such a cable with all the different cabling stages is shown below in Fig. 1.9.

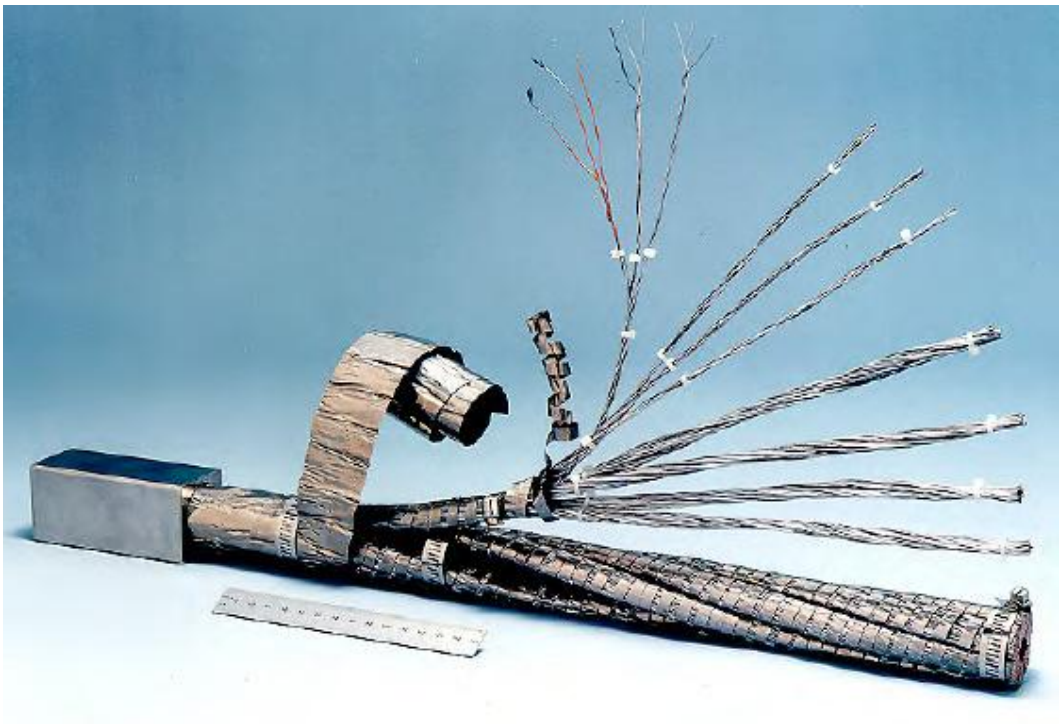

Fig. 1.9 ITER Central Solenoid Model Coil CICC [13]

The ITER magnets were designed to make sure the reactor and its high temperature content does not cause damage to its surroundings and the cryogenically cooled magnets. The CICC was designed with internal tin Nb_3Sn superconductor strands, copper wire for quench protection and a steel spring central cooling channel for the transport of liquid helium. Fig. 1.9. The sub-cable is wound in several stages

to form the final cable. In each stage the strands are twisted together in larger and larger bundles. When the cabling is complete, a jacket of stainless steel 316 is compacted around the cable to provide structure. Stage one cable consists of two Nb_3Sn and one copper strands. Stage two is twisted using three stage one cables. This is done five times during which the sub-cables are twisted together. The pattern for the ITER CICC cable is 3x3x4x5x6. 1080 Nb_3Sn strands are twisted together to create a cable in Fig. 1.10.

Fig. 1.10 provides the scale of the CICC cable, from the individual filament to the final six-petals cable inside its jacket. This experiment was designed for the Central Solenoid US Inner Module for the ITER project. First, 3 Nb_3Sn strands are twisted into a cable. Each strand is roughly diameter of 0.8 mm and is comprised of thousands of superconducting filaments, each with rough diameter of about 3 μm.

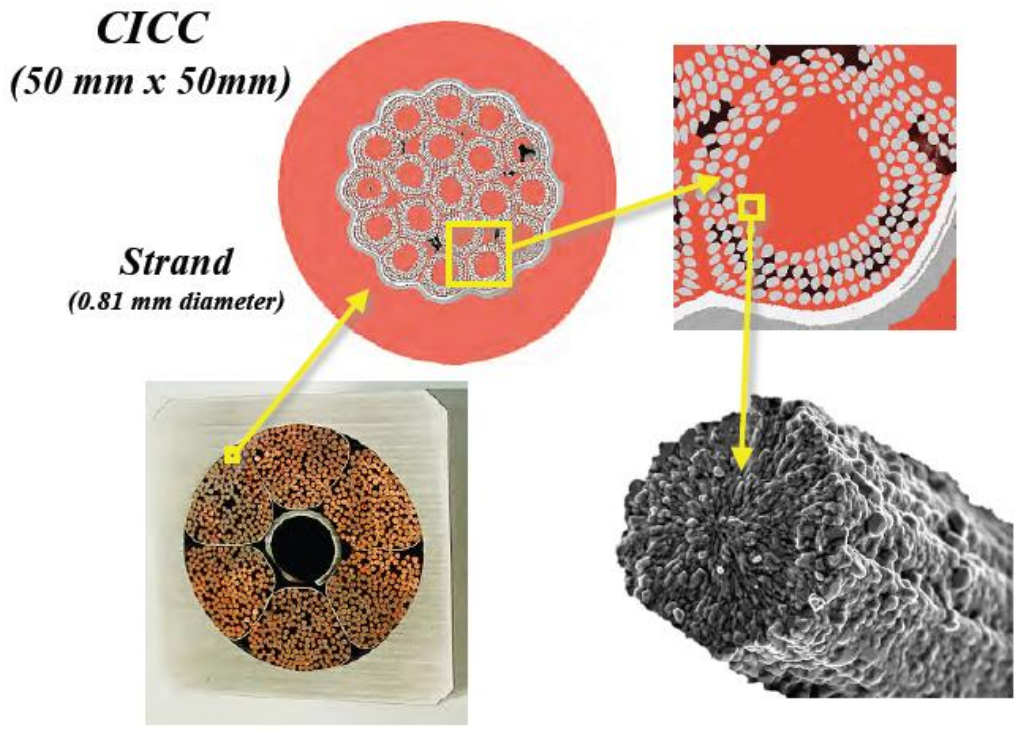

Fig. 1.10 CICC cross-section view at increasing magnification steps [13]

1.7 Strain behavior of Nb_3Sn

Today, Nb_3Sn and NbTi superconducting materials are typically used to build superconducting magnets. As the desire to create more powerful magnets increased, more exotic materials had to be used to create these magnets. It was previously stated that superconductivity depends on three main parameters, Current Density, Temperature and Magnetic Field. These conditions stand true for the Nb_3Sn, which was identified as a superconductor in 1954. Approximately a decade later after Nb_3Sn discovery, Buehler and Levinstein discovered that superconductors are also sensitive to another constraint, mechanical strains. It was almost 20 years later that Ekin presented his strain scaling law that could be used for design of superconductors. His early work was primarily concentrated on characterizing the uniaxial tensile and compressive effects on the current capacity of Nb_3Sn with some thought given to bending strain effects [9].

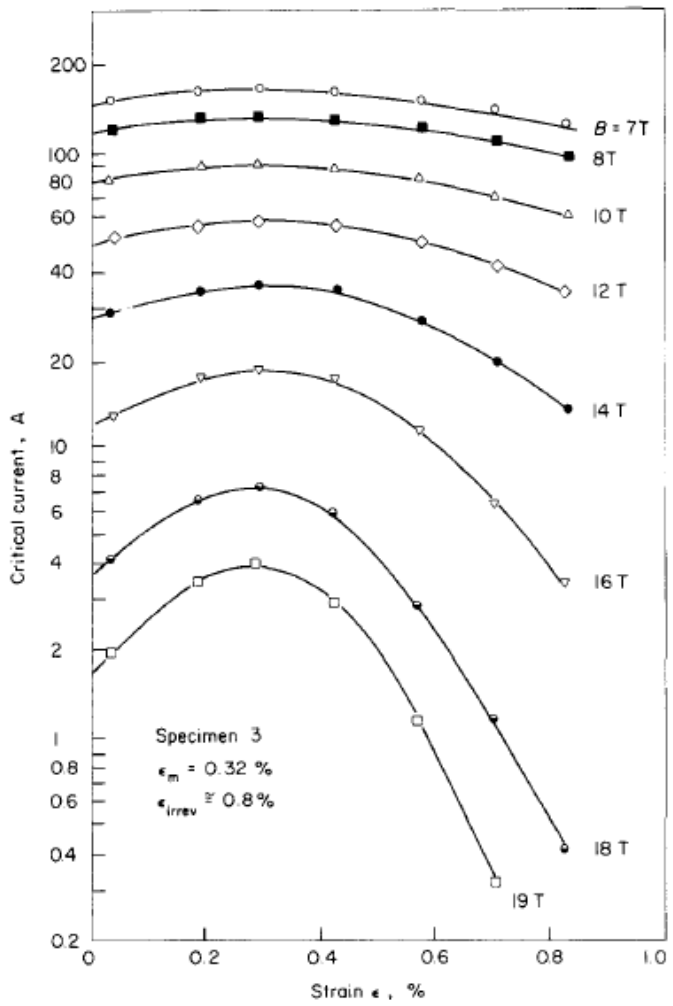

Fig. 1.11 Critical current vs. strain over the range of magnetic fields for Nb_3Sn [13]

Ekin discovered, as shown in Fig. 1.11, that by applying tensile load to a sample first increased its critical current capacity before decreasing it with continued application of tension. He proposed that the source of this was compressive pre-strain: the bronze matrix around the Nb_3Sn contracted more than the superconducting filaments from the drop in temperature. Thus, as the wire was put under tensile strain, the critical current increases as the pre-compression is relieved, then the critical current drops as the superconducting filaments themselves undergo tensile strain. [13]

Mechanical strain in a superconducting cable comes from several sources. Axial strain comes from the thermal mismatch between the superconducting wires and the conduit materials due to the temperature changes from the heat treatment temperature to the liquid helium operational temperatures. The transverse strain is caused by the natural electromagnetic force accumulation across the cable. The bending strain is caused by the cable design and how the strands are twisted together in a configuration with a void fraction higher than 30%.

Ideally one would characterize a single strand and expand upon empirically with a scaling law. Unfortunately, the expansion from a single strand to a cable is not straight forward, and up to now only dependence of a single strand critical current as a function of uniaxial strain can be used to describe with empirical scaling laws.

A brief history of the research that has been undertaken until now will be outlined. Each study investigates different aspects of the strain behavior, and each one is a step closer to developing a unifying strain scaling law.

1.7.1 Uniaxial Strain

Uniaxial strain is felt by a Nb_3Sn during the cooling down process when different components of the strand contracts at different rates, for example the copper matrix contracts more than the superconducting filaments. The wire undergoes a temporary reduction of critical current density, critical field and temperature. When the wire undergoes longitudinal tension, up to a point, these parameters increase. They then further decrease, again, reversibly with increased tension. If the wire is

further put in longitudinal tension, it will eventually fracture to its brittle mechanical properties after heat treatment.

Many devices have been used to measure the uniaxial strain. The U-spring, Pacman strain device, the water spring and others [9], [6].

The U-spring, designed at the University of Twente [9], applies strain to a single strand as well as the tape conductor samples. Through series of worm gears, the device applies tensile stress with minimal bending to the wire. Strain gauges are mounted on the U-spring to measure and to interpolate the strain that's being applied to the sample. Fig. 1.12 shows the workings of the U-spring device.

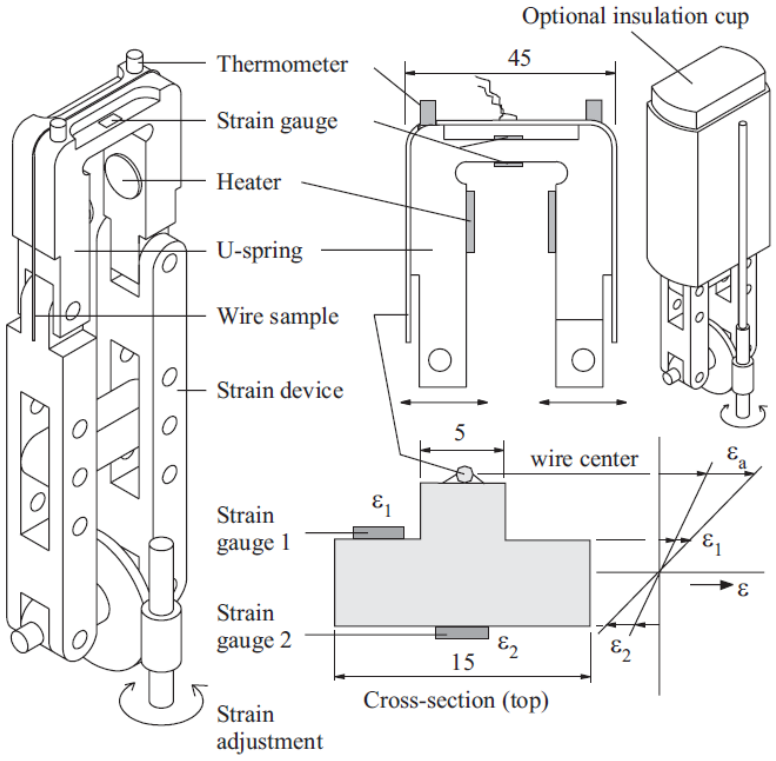

Fig. 1.12 U-Spring device developed by University of Twente [9].

The sample that the U-shape could accommodate was rather small, about 18 mm in length and could cause poor current distribution. To solve this issue, a device

called “Pacman Device” was created. Although the principle behind this device was similar, a bending spring, the sample was mounted on a curved beam. Thus increasing the length of the sample to the circumference of the magnet bore instead of the diameter.

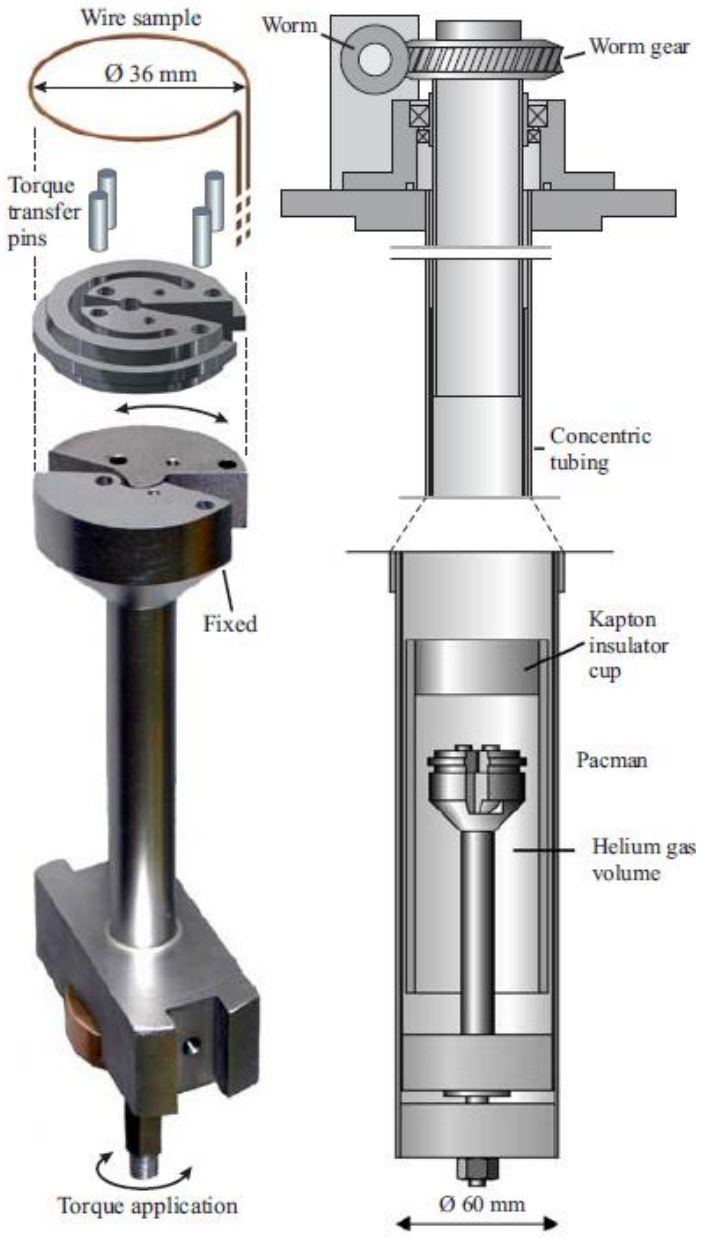

Fig. 1.13 Pacman Device and its drive mechanism [13].

The Pacman device works by rotating the worm gear and concentric tubing. It allows torque to be transferred to the body of the Pacman, which is circular beam section shown in Fig. 1.13. This method of measuring the uniaxial strain show in close up in Fig. 1.14 shows the strain distribution of the sample holder is constant along the sample length.

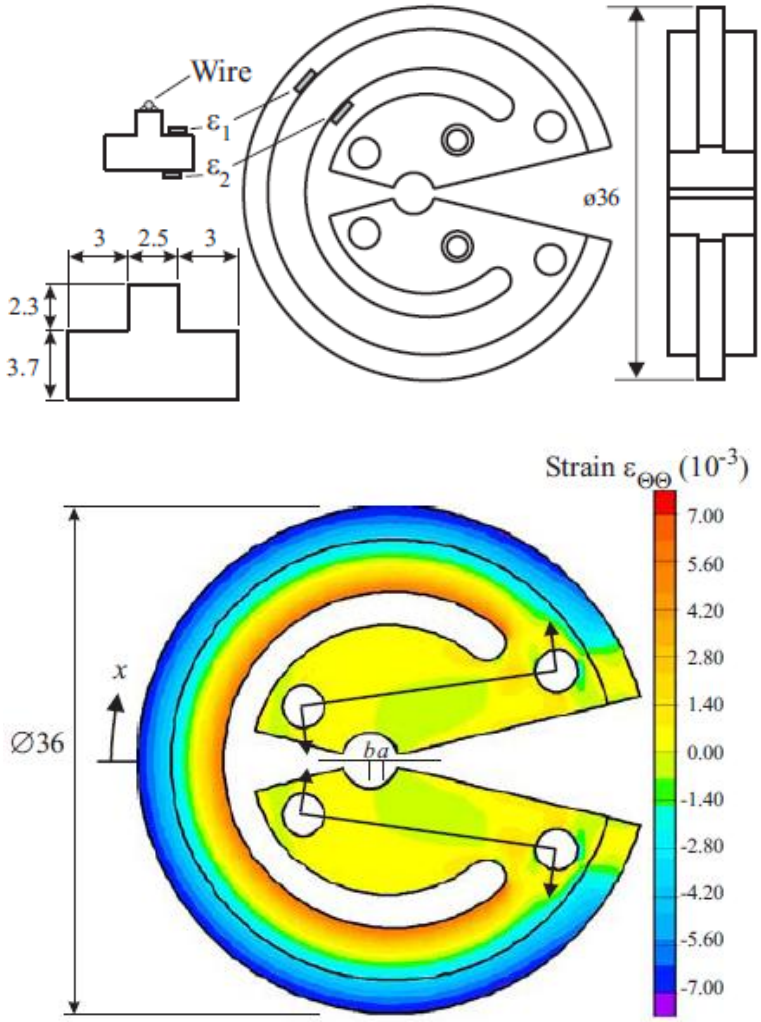

Fig. 1.14 Diagram and Strain distribution of the Pacman device sample holder [13] Units of length are mm.

Since the strain of the samples cannot be measured directly, it has to be inferred by mounting strain gauges on the Pacman device. The advantage of this

device is the increased length from 18 mm in U-spring to 78 mm for the Pacman device.

Walters spring, known as WASP [5] exhibited the longest sample of these experiments. The sample length demonstrated was up to 1 m shown in Fig. 1.15(a). Device made out of Ti-6Al-4V in the shape of a coil spring which allows 1.4% strain to be applied by applying torque on one end of the Walters spring while the other end is fixed. The schematic of the working assembly is shown in Fig. 1.15(b). This setup applied the strain gauges directly to the spring and inferred the strain on the spring is the same as the strain applied to the sample.

(a)

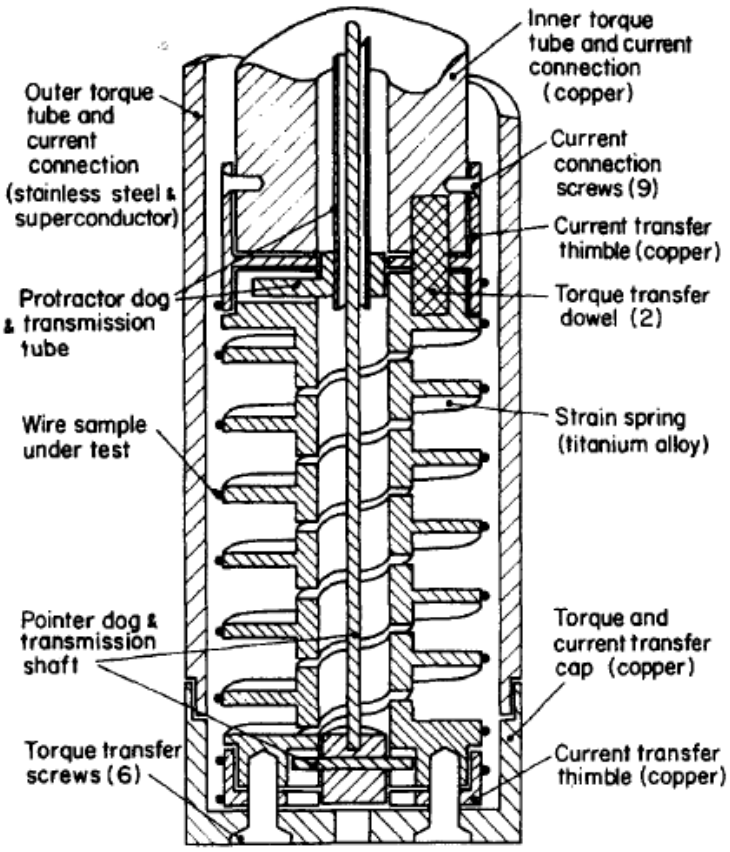

Fig. 1.15 Walters spring (WASP) device (a) photo and (b) functional diagram. [6],[13].

1.7.2 Bending Strain

In the past, there were many attempts to characterize Nb_3Sn under pure bending conditions by Takayasu, Senkowicz and Lee. [14] They statically applied bending to single samples clamped in a fixture of a constant radius, shown in Fig. 1.16. The device was used to measure the progress of bending from 0% bending to 1.4% bending.

Fig. 1.16 Fixed pure bending strain sample holders [9].

This device recorded the critical current data as a function of bending strain. Unfortunately, this device required different fixture for every bending radius of interest. Additionally, the handling of the sample after heat treatment created a potential of wire damage.

In recent years, M. Takayasu, D. Harris, L. Chiesa and P. Mallon have been working on an experiment, which demonstrated the ability of putting a wire in a pure bending state [9], [6], [13]. They were able to secure the wire during the heat treatment, Fig. 1.17, thus eliminating the need to touch or manipulate the wire prior to the experiment. Additionally, the design chosen was able to adjust the angle of the bending allowing for a maximum bending strain of 1.4%. Shown in Fig. 1.17, the bending device has been bent to 1.4%.

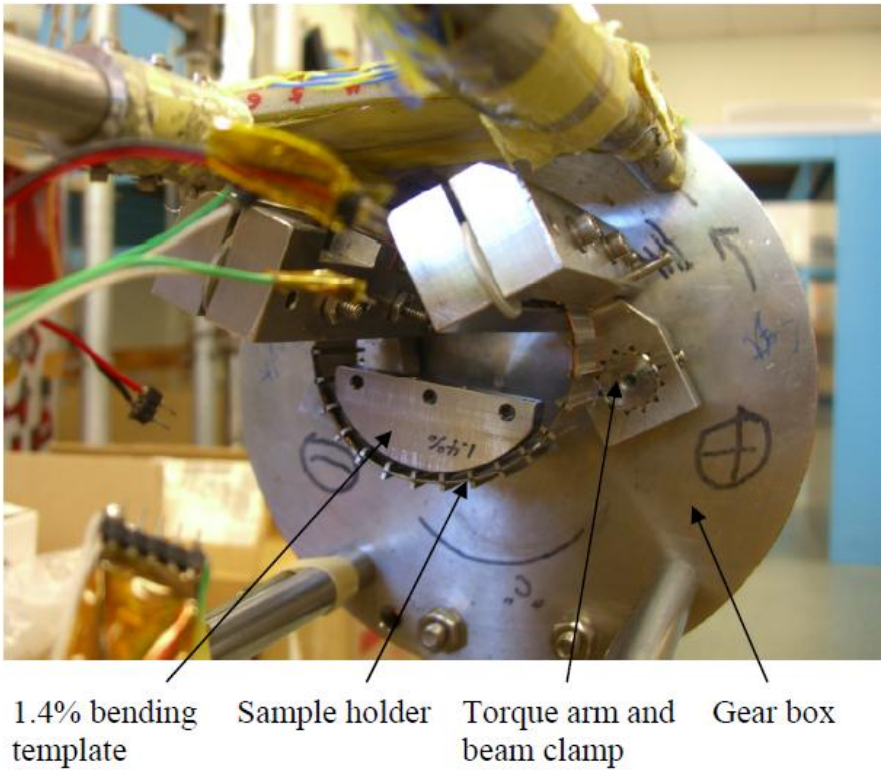

Fig. 1.17 Bending is applied to the support beam during in bending application [13].

Another advantage of this design is the ability to change the wire holders. This allowed the ability to study the wire under different supporting conditions. With the latest improvements by Mallon, the sample holder was applying 1.4% bending as shown. This was done by changing the thickness of the sample holder to avoid plasticity of the holder and putting ribs down the side of the holder to counteract the Lorentz force.

1.7.3 Transverse Strain

Until recently, not a lot of effort was being spent on characterizing degradation of critical current due to the transverse strain effect. The early experiments mostly measured single strand with one experiment performed on a CICC cable. It was thought that the degradation was due to the transverse strain

effect from the accumulation of Lorentz load during charging. Few experiments were performed since then on a sub-sized CICC cable.[6]

Transverse compressive stress on the critical current and upper critical field of the Nb_3Sn was first studied by J. Ekin. He developed an apparatus, which simultaneously applies mutually perpendicular components of the field and current and transverse compressive stress to a single strand [15],[16]. Fig. 1.18 shows the two stainless steel anvil heads. Two halves of the anvil conform to each other's flat surface. One is fixed, bottom while the other one compresses the wire via the pivoting anvil head. Voltage taps are soldered in the region of the compression region, which ensured that the electric field was measured over the region where the stress was uniformly applied.

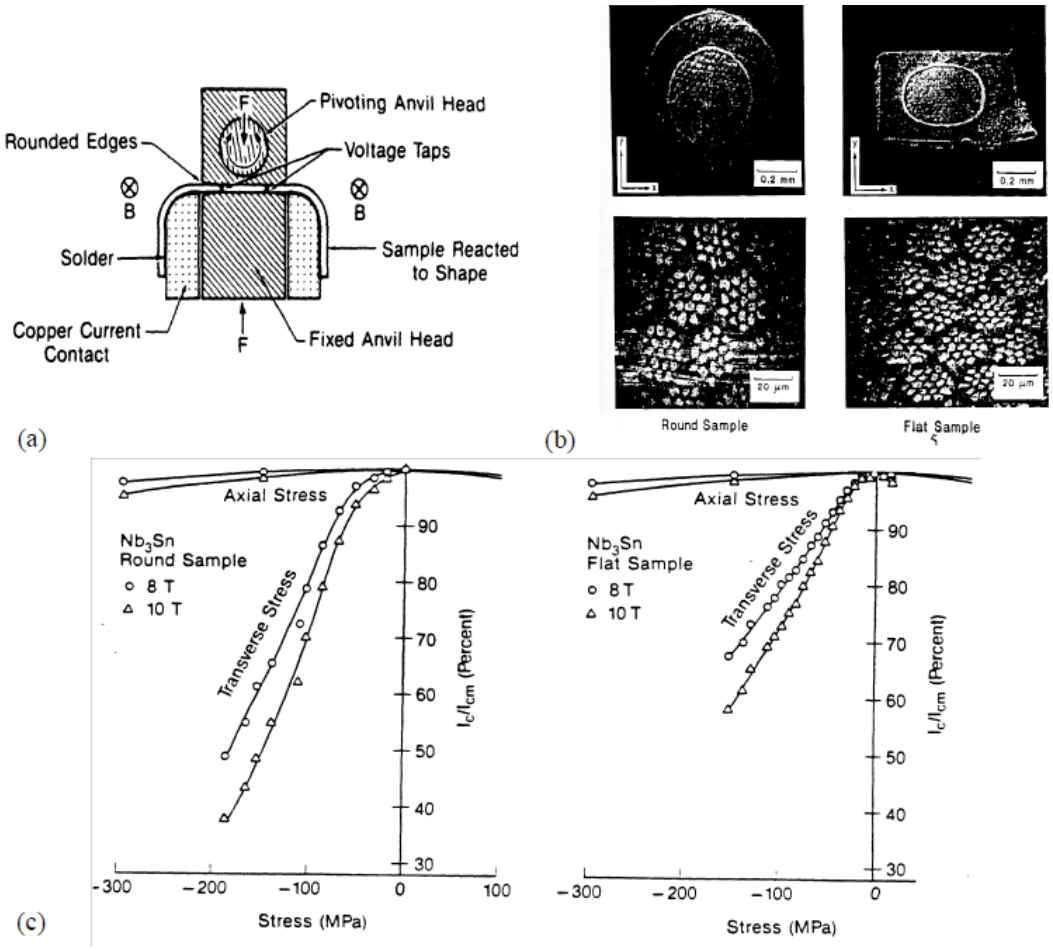

Fig. 1.18 (a) Schematic view of the test setup. (b) Cross section of two samples used (flat and round). (c) Critical current degradation for transverse and axial compressive stress for round sample. (d) Critical current degradation for transverse and axial compressive stress for flat sample [15],[16].

The results showed that the strands showed strong degradation due to the transverse load, much greater than in the uniaxial strain. The explanation offered by Ekin was that, under axial strain, the axial force is apportioned among the various composite materials because they occupied parallel load-bearing paths, while, in the transverse case, all the components of the composite experienced the same stress which was transferred from one material to the next in a serial load chain [6]. A possible explanation for the difference provided between the axial and the transverse stress could have been due to the preferred crystal growth orientation in the Nb_3Sn

layer. Since Type II superconductors have flux-lines which can be prevented from moving, by lattice imperfections, controlling the crystal growth structure will therefore affect the axial stress more than transverse stress.

A similar experiment was later performed by Specking [17]. He found that the transverse stress effect was not highly dependent on either grain morphology or strand fabrication process.

Few subsequent tests were performed on a cable comprised of more than 2 strands. The showed sufficient data to conclude that there was not significant degradation caused by natural electromagnetic load up to 50 MPa which is higher than the average Lorentz load effect expected in the ITER cable (~ 20 MPa). The result of negligible electromagnetic effects on a full size CICC cable was convincing enough to abandon any further research. This result assumed nominal pressure over the diameter of the full cable, while disregarding the localized contact pressure among strands which could be potentially much higher, thus greatly degrading the performance of the magnet.

Only after the ITER CSMC test results came into view, which showed higher degradation of the magnet than the expected, did the transverse strain issue rose up to awareness. The explanation of the degraded magnet seems to point back to the transverse load effect of the accumulating Lorentz load across the cable cross section [18].

The lack of experimental results motivated L. Chiesa and M. Takayasu to dedicate time and effort into developing a device that's capable of applying transverse load on a sub-sized cable to simulate the loads in a full size cable. Two

experimental setups were developed to measure cables of various configurations. Different strands types and sizes were tested.

The first experiment, single turn experiment, was set out to measure the critical current of a 36 strand superconducting cable. The load was applied by the expanding collet when the linear actuator was moved vertically. The forces were applied uniformly due to the cylindrical shape of the collet. Load cell, mounted outside the dewer measured the vertical load, from which the force was calculated from.

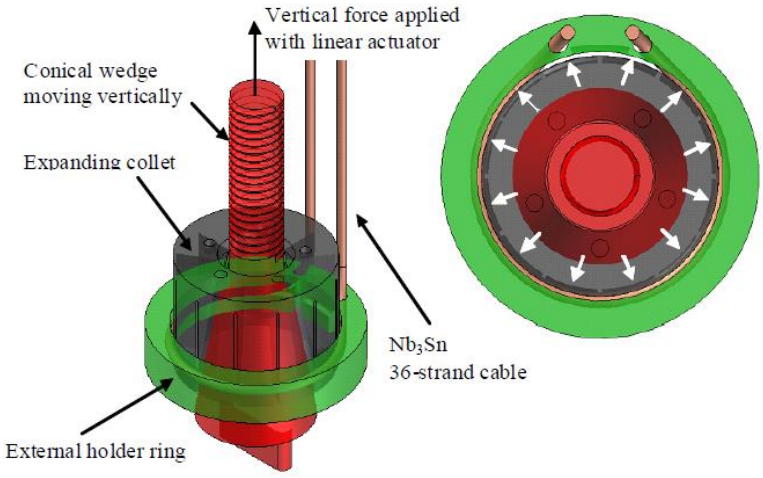

Fig. 1.19 Schematic view of the single turn test rig used inside a 20T, 195mm diameter bore magnet: main parts (left), expected load distribution during the experiment (right) [6].

The results exhibited significant initial degradation even before applying any load. This was much greater than expected and was attributed to the difficult fabrication process for the experiment.

Learning from the single turn experiment, a Hairpin experimental setup was developed, which proved to be more fruitful than the first setup. As before, the goal

was to measure the effect of transverse load on the critical current of a superconducting cable.

The load was applied by vertically pulling a metal rod with multiple wedges machined on opposing surfaces. By pulling on the wedge, it forces the pressing plate toward the cable holder, thus compressing the cable laid inside the groove.

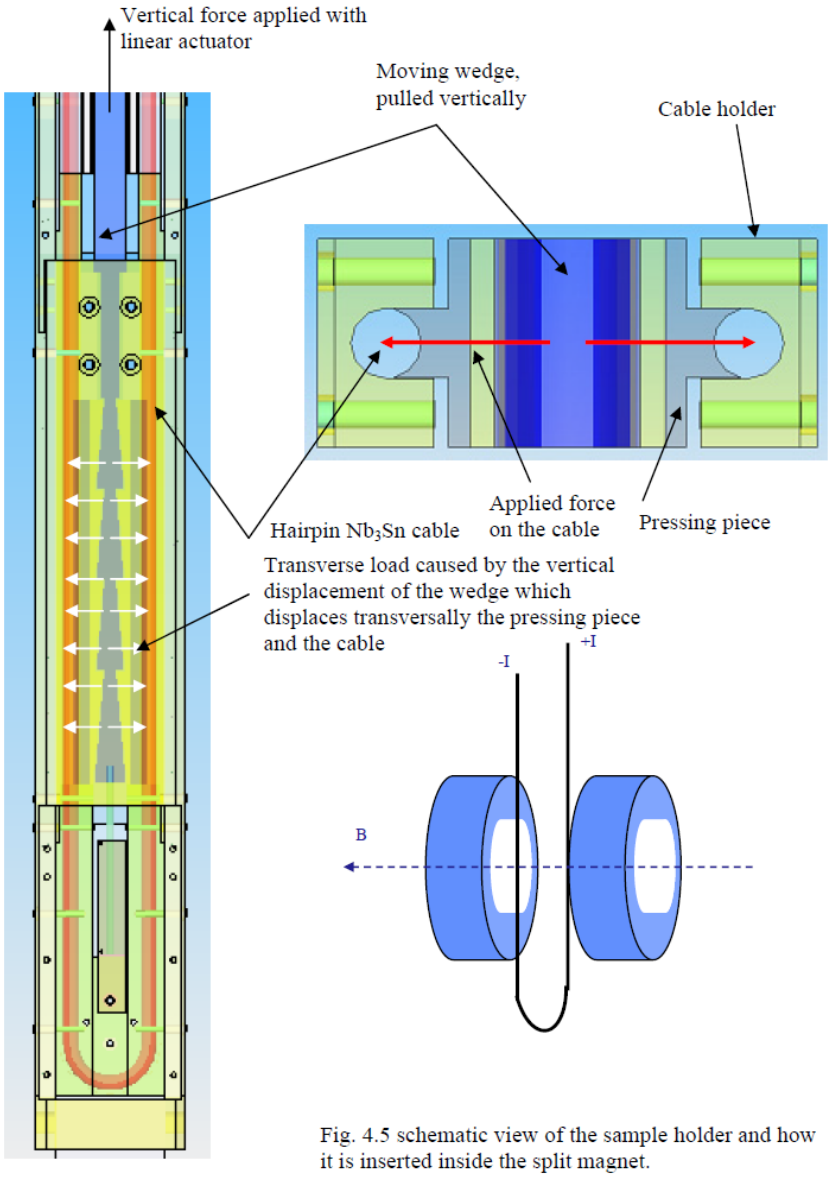

Fig. 1.20 Schematic view of the sample holder and how much it's inserted inside the split magnet [6].

The advantage of a setup such as this is the simplicity of the design, which makes the handling and fabrication much easier than the previous experiment. Another advantage is a much longer sample of roughly 1.45 m long. This experiment tested a single wire as well as a triplet and a 45-strand Nb_3Sn cable. This experiment yielded positive results; it showed significant transverse load degradation for the single and 3-strand cable. These results could not be explained by a recent bending model indicating further work in this area is really crucial to the understanding of large CICC [6].

1.8 Difficulty in Modeling

Modeling large superconducting cables and magnets is valuable as it provides the ability to understand physical phenomena without the exertion of the real experiment. Multiple scenarios could be quickly tested and adjusted, potentially providing invaluable understanding. The downside to this approach is the numerous uncertainties that modeling introduces. Modeling requires very accurate initial and boundary conditions to solve the problem correctly. Additionally modeling Nb_3Sn accurately is challenging due to uncertainty in the non-heterogeneous material properties. Modeling results are important as much as a validation done through experiments and a continuous feedback between the two will allow a better understanding of these complex systems.

1.9 Thesis objective

The scope of this work is to continue the transverse load work of L. Chiesa. Although positive results came out of the previous experiments [6], changing the

samples was time consuming and the cost was rather significant. The cost of the previous experiment was roughly $100,000, with three samples per experiment. A new mechanism is needed which will allow measurements of the critical current degradation during transverse strain loading on a 3-strand cable.

This thesis work focused on the design of a three strand transverse load experiment, designed to simulate the Lorenz force artificially by applying mechanical transverse stress to the three strand cable. The goal is to have a well thought design, have the necessary parts machined and finally verify the mechanism under a room temperature test simulating the experimental conditions. The reason the 3-strand configuration was chosen, is because that is the first step toward building the CICC cable, talked about in Section 1.6. An important goal of this design is the reduction of the experiment cost as well as providing greater flexibility in different diameter setups. The added flexibility would give the option to test from small size strands and up to 3-strands at a fraction of the cost of previous experiments.

The goal is to perform this experiment in cryogenic conditions, to evenly apply a known transverse pressure to the cable in the tested section of the cable. Future work will perform experiments using this design at the National High Magnetic Field Laboratory (NHMFL) in Florida and investigate any degradation of the superconducting cable properties, particularly the degradation of the critical current.

While this thesis is being written, the experiment setup was successfully tested for the first time at the NHMFL facility.

Chapter 2 Design of Transverse Load Mechanism

2.1 Experimental Design

Chapter 1 gave an overview of background of superconductivity, types of superconductors and what they are used for, as well as experiments performed in the past. It briefly discussed the benefits and the results of models as well as its limitations. Experiments offer real data which to be analyzed, while modeling is only as accurate as the initial conditions. The benefit of modeling is the insight which can be extracted from them, such as strain in superconducting elements. Performing real experiments is one of the few ways to directly verify whether the experimental data is reasonable and the created model is representative of reality.

This thesis covers the design, assembly and analysis of a new experimental device to test electromechanical behaviors of 3-strand superconducting cable samples under transverse loads applied to simulate the Lorentz load the strands would feel in a large CICC. The working principles of the new device are based on an experiment designed in [6]. The transverse experimental assembly is illustrated in Fig. 2.1. It comprises of three major assemblies, cable assembly, load cell assembly and the gear mechanism assembly. This experiment simulates the real operating conditions, felt by a CICC in cryogenic state when it's under the influence of magnetic field. The 3-strand Nb_3Sn cable runs through the cable assembly, illustrated in Fig. 2.2. The cable is being compressed in two areas, illustrated by test section cable holder.

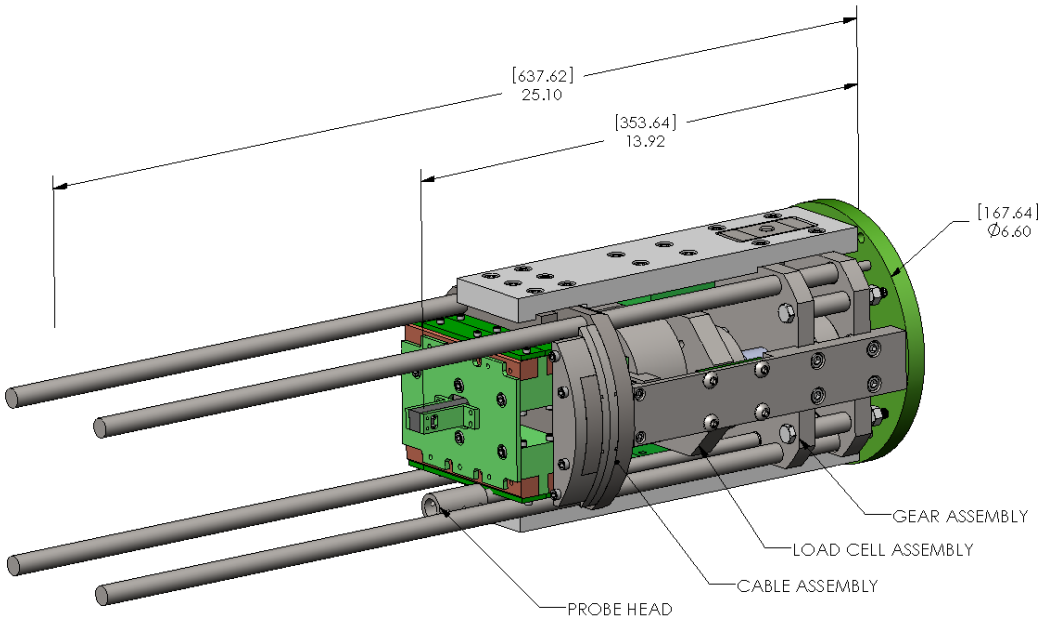

Fig. 2.1 Transverse Experimental Assembly

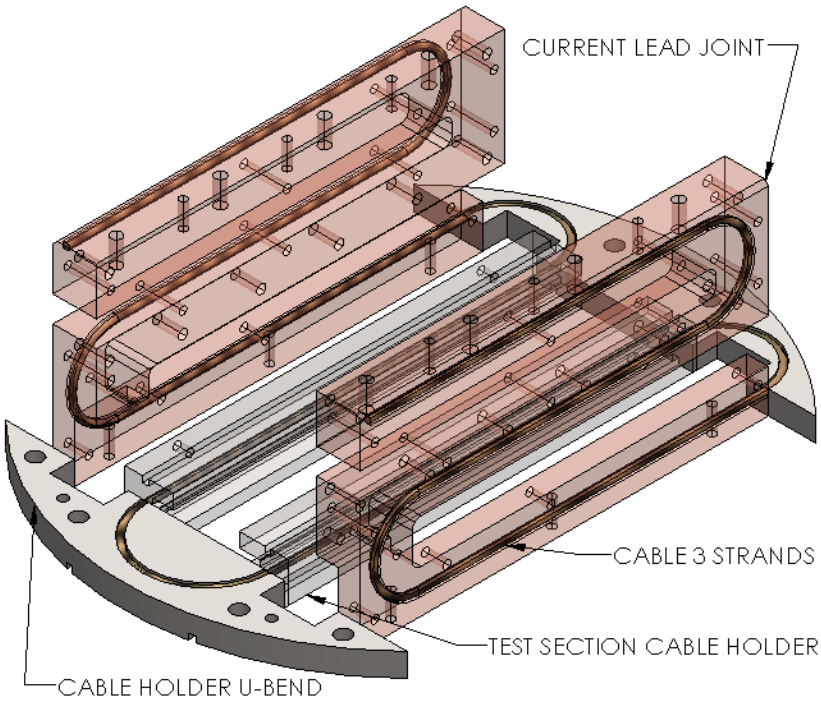

Fig. 2.2 Cable routing within the Cable Assembly.

This transverse experimental assembly is mounted to an existing probe, designed by D. Harris, illustrated in Fig. 2.3. This probe is then lowered inside a cryostat positioned in the bore of a 20 T magnet at the National High Magnetic Field Laboratory (NHMFL). The upper assembly was originally designed to be mated to the bending mechanism, designed to analyze a single strand under true bending conditions.

With few minor changes, the upper assembly was converted to operate the transverse experimental assembly. The flange plate creates a seal with a magnet cryostat and the G-10 plates provide electrical insulation. The current lead tubes encase the current leads which terminate near the bending mechanism. The helium fill tube allows the cryostat to be filled with liquid helium from the bottom.

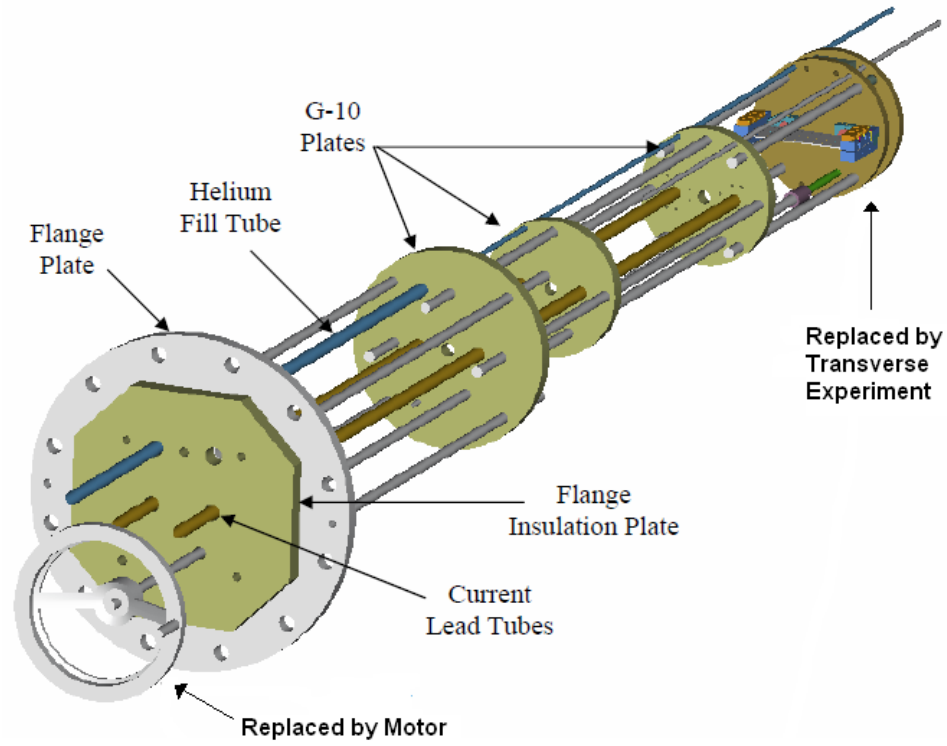

Fig. 2.3 Partial Probe Illustration. [9]

This chapter discusses the practical mechanism for transversely loading of the Nb_3Sn cable for the critical current testing. It will cover the operating conditions considered in the design followed the construction considerations that went into the principal components. It will then covers the overall transverse load assembly from a system level point of view discussing the types of magnet and facility required for this test. Detailed sections will consist of the three major assemblies, gear mechanism assembly, load cell assembly and the cable assembly.

2.2 Operating Conditions and Requirements.

Transverse load critical experiment of the Nb_3Sn superconducting cable will be performed in the Ø195 mm (7.68 inch) bore, 20 T, Bitter magnet at the National High Magnetic Field Laboratory (NHMFL), Florida State University in Tallahassee, Florida.

The NHMFL magnet is an Iron-free, water cooled electromagnet, improved from the original design by Francis Bitter [4]. Bitters magnet design was put together with stacked copper annular plates with a slit, separated by a thin sheet of insulation except for where the plates overlapped. The slit allowed pressure contact with the bare area of the next stacked circular plate, enabling the current to go up the magnet in a spiral. The cooling of the magnet was done via cooling holes in the plate through which water was passed a very high velocity. The major improvement to the Florida-Bitter magnet over the traditional Bitter magnet is the magnet's efficiency. One of the ways the magnet was optimized was the improvement of the cooling channels, replacing them with slits instead of holes.

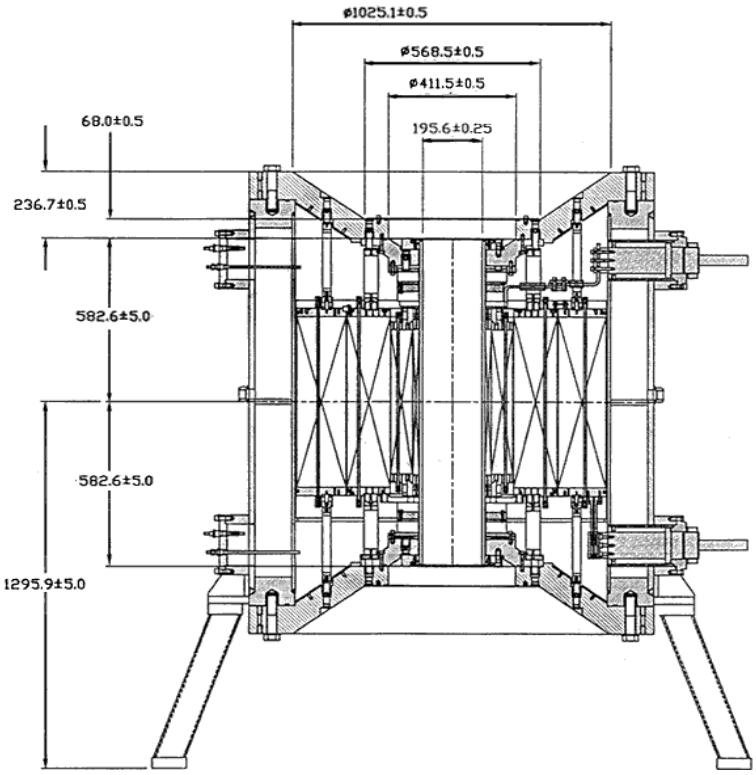

Fig. 2.4 Drawing of the 195mm bore, 20T Bitter resistive magnet and cryostat at the National High Magnetic Field Laboratory (NHMFL) in Tallahassee, FL [3.1].

Fig. 2.4 shows an illustration of the cross-section of the magnet as well as its cryostat. [19]. The cryostat has two chambers. The outer chamber, filled with liquid nitrogen, acts as an insulator from the magnet, reducing the radiating heat loss generated by the magnet. And the inner chamber, filled with liquid helium to maintain the 4.2 K test temperature. The diameter of the cryostat at the experimental magnet level is called cold-bore and is 170 mm (6.70 inches) in diameter.

The center of the magnet, where the field is most uniform and highest, is 188.3 cm (74.13 inches) from the top flange of the cryostat. Hence, it is critical that the transverse loading mechanism is designed to be flexible and to accurately be positioned at this location. This experiment is using the frame of the probe used previously in the bending load experiment. The frame serves multiple uses. It's

structurally resisting the forces generated during the test as well as providing the support for the electrical wiring and instrumentation.

2.2.1 Operating Conditions and requirements

1. The entire experiment will be submerged in liquid helium, a temperature of 4.2 K. This temperature ensures that the Nb_3Sn cable is below its critical temperature. A stable temperature will ensure the safety of the mechanism as well as stable operating conditions. Materials must withstand the differences in coefficients of thermal expansion (CTE). Wires must be electrically insulated to prevent shorting. Dry lubrication should be used for moving parts, either graphite or molybdenum disulfide. If the mechanism cold welds itself, it would stop the experiment or worse, damage the facility.

2. Materials cannot be ferromagnetic due to high magnetic fields. The sample cable needs to be supported throughout its length. Unsupported cable could be damaged, via breakage due to the brittle nature of the Nb_3Sn, if it is not supported.

3. The 3-strand cable used in the experiment will be made using 3 separate individual Nb_3Sn strands, roughly 0.8 mm in diameter, twisted together. Different twisted pitches will be explored, as the length of the pitch is believed to be an important factor in the critical current degradation.

4. The transverse mechanism shall be mechanically stable at total load of 60 kN applied to the cable of ~215 mm in length.

5. It is critical to apply the load evenly throughout the test area of the cable. Even distribution will ensure that no one area has localized compression and avoid local damage of the samples.

6. The cost to build the transverse mechanism is to be kept to the minimum. All of the design constraints have to be thought through ahead of time as the budget does not allow extensive rework. One way to minimize the cost is to specify tight tolerances only for critical components. In non-critical components the tolerances can be relaxed to give the machine shop the maximum flexibility on cost. Another way is to create a mechanism which shares components with multiple experiments, thus reducing the need to machine extra parts.

7. Maximizing the compression length of the cable assembly, thus maximizing how many twist pitches the cable will exhibit. The bulk cable characteristics will be represented more accurately the more pitches there are. The experiment must fit inside the 170 mm (6.70 inches) diameter restriction of the dewar in this particular magnet of the Florida Facility.

8. Maximizing the current lead joint length to ensure proper current transfer from the current leads to the sample. The transition from the superconducting cable to the copper current lead joint area has been maximized by allowing the cable to run multiple lengths back and forth. Additionally the joint has four holes to solder the thick copper cable that will carry the current from the current leads to the sample passing through the joint. Those components will be described in details in later sections.

9. Mechanism capable of loading the sample reducing its diameter from 1.78 mm (0.070”) to 1.16 mm (0.046”). This corresponds to a diameter reduction of ~35%.

10. The current flowing in the sample should be perpendicular to the magnetic field for the duration of the transverse loading procedure. This is a standard procedure for critical current measurements but also allows for the natural Lorentz load produced by the sample to be in the same direction as the mechanical load applied. This condition resembles what a Nb_3Sn cable will experience in a fusion magnet.

11. The apparatus should be able to cyclically apply transverse load through duration of a single experiment. This represents the power cycling of the ITER central solenoid magnet sees throughout its lifetime. This cycling may cause fatigue degradation in the superconducting strand. [9] Having cyclical data would be helpful in understanding fatigue of Nb_3Sn conductors.

12. Experimental setup has to be designed in such a way as to cause no damage to the facility at NHMFL or any of the surrounding personal.

2.3 Transverse Experiment Assembly

This experiment is using a similar gear design to the bending experiment to convert rotational torque to vertical load, which displace some components horizontally, which ultimately applies the load to the sample.

The transverse load experimental setup consists of three main assemblies, cable assembly, load cell assembly and the gear assembly as illustrated in Fig. 2.1.

The mechanism which transforms the rotational torque to the transverse compression of the cable is driven by a motor placed outside the cryostat and connected through a long shaft to the probe head.

The motor drive replaces a hand crank, as shown in Fig. 2.5 is located roughly 100 to 110 inches above the experimental setup outside the cryostat. The torque from the motor allows for remote application of the transverse loading mechanism without being close to the current leads and for a better control of the applied force [6]. It should be noted, the input shaft has to be rotated counter-close in order to engage the mechanism.

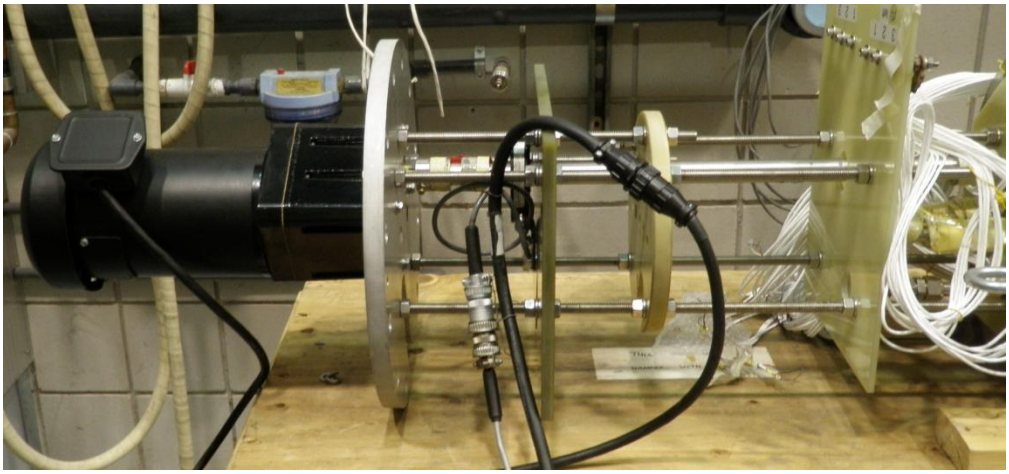

Fig. 2.5 Motor drive above the top flange.

Fig. 2.6 shows the schematic for the transverse experiment as it would look like right before it's inserted into the cryostat. The goal is to position the transverse loaded cable around the center of the magnet, 74.5 inches from the top of the cryostat flange.

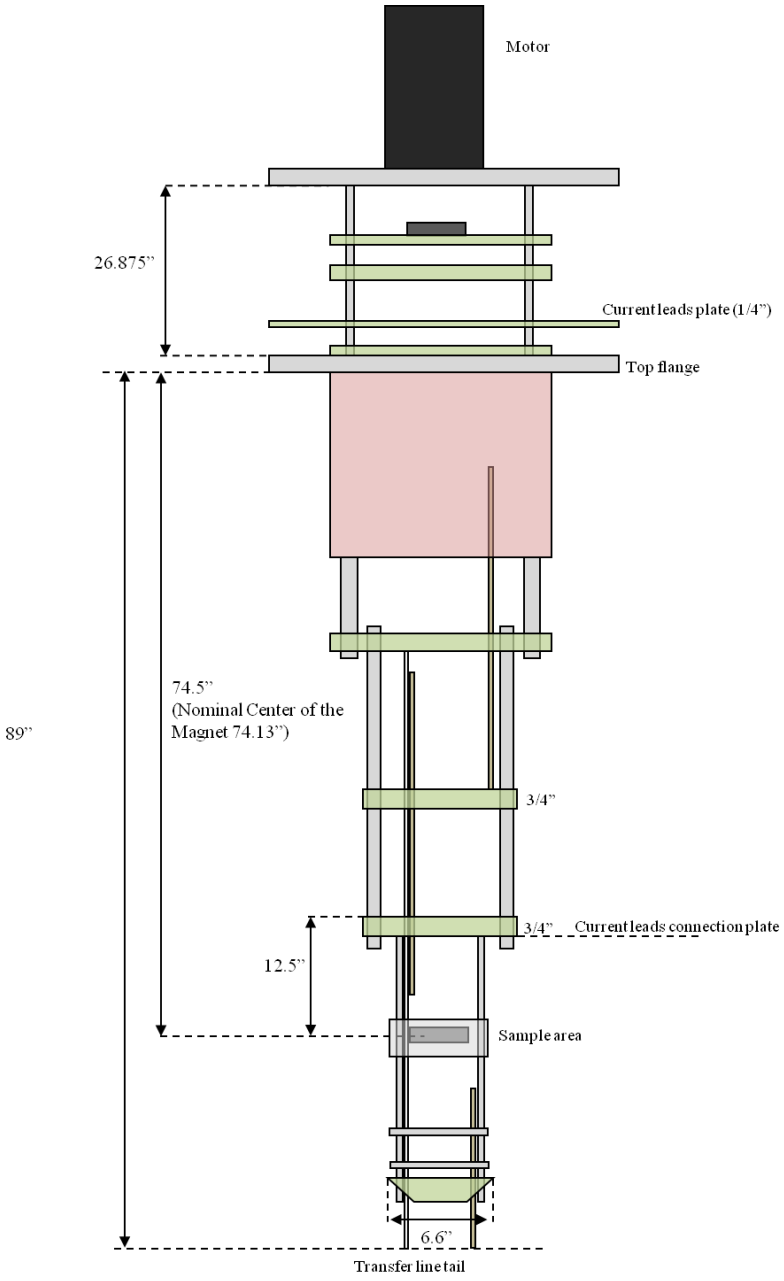

Fig. 2.6 Schematic of how the transverse experiment is loaded into the cryostat.

The assembly shown in Fig. 2.7 is the driving force for the experiment. This is the place where Nb_3Sn 3-strand cable is compressed. Designing this area is critical to the success of the experiment.

The final configuration of the transverse load design is illustrated in Fig. 2.7. Both pressure plates apply transverse load onto the cable when the wedge is displaced vertically. The cable is being held by two test section cable holders. Each pressure plate applies the load to approximately 108 mm long cable section. The design underwent through numerous iteration and modifications to maximize the ease of machining, assembly and strength of the experiment.

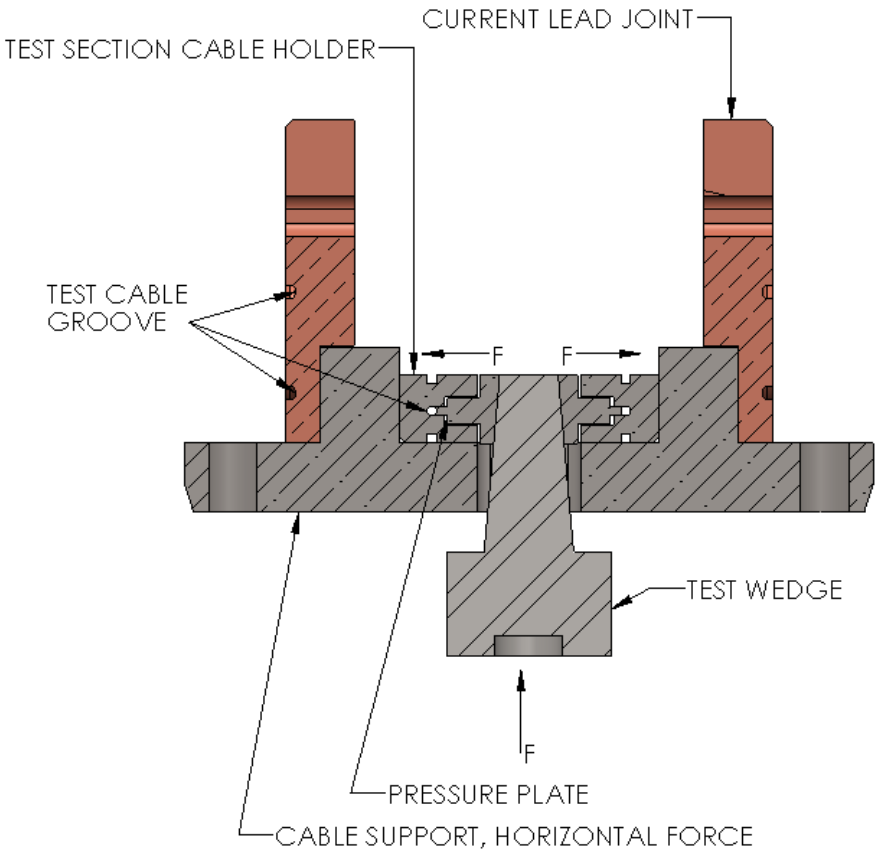

Fig. 2.7 Transverse Load cross section with Test Cable Groove

The experiment is assembled with components made out of different materials. The critical parts of the cable test section are made with Ti-6Al-4V, which has similar coefficient of expansion as the Nb_3Sn cable so any axial pre-strain caused by the cooling process can be avoided. The structural components are made with

stainless steel 316, which exhibits non-magnetic properties, required for experiment where a high magnetic field environment will be experienced. Some components in the cable assembly, such as lead joints, are made out of copper to allow for optimal current transfer and ease of soldering. Some parts are made of G10, which provides electrical insulation in some instances and being an insulator it does not add to the boil off of liquid helium as a normal metal would. G10 was used in multiple places of each assembly.

Designing this experiment was a complicated and long process. It was important to visualize, understand and analyze how all the parts will be assembled, interact with each other as well as make the structure strong enough to withstand the high forces throughout the experiment. A mistake in the design could lead to catastrophic disaster during the experiment.

As illustrated in Fig. 2.4, and per experimental requirements, the maximum diameter of the probe head is under the 170 mm in diameter. Like in the bending experiment, the transverse experiment set a maximum diameter of 167.6 mm (6.6 in) with the length being roughly 350 mm (13.9 in).

This chapter covers design of three major assemblies, gear mechanism, load cell and cable assembly. After a brief introduction of each section, each assembly and its components will be discussed in detail.

2.3.1 Gear mechanism assembly

The gear assembly and the support structure for the transverse experiment are shown in Fig. 2.8. The gear assembly is essentially designed as a modification of the

pure bending experiment setup described in Chapter 1. Most of the structure was design anew in order to suit the different requirements of this experiment. The vertical support is bolted directly to the gear assembly and serves as the support for the transverse experiment. Notches in the upper section of two of the vertical supports react against the cable assembly.

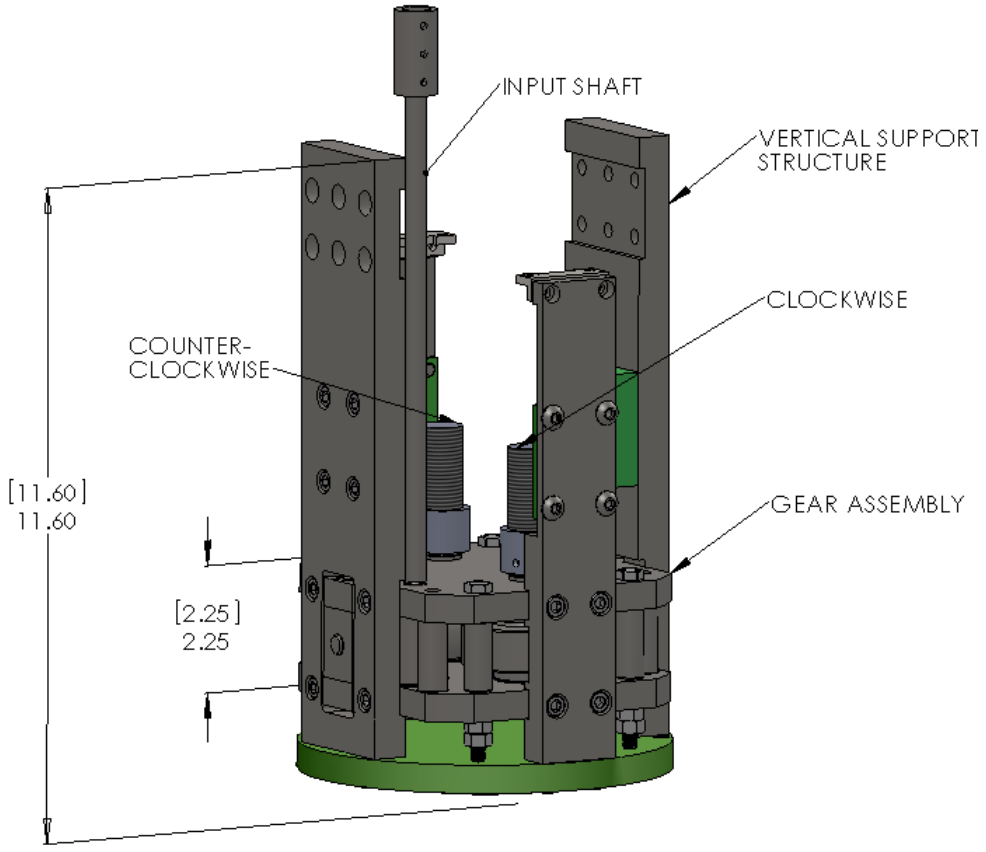

Fig. 2.8 Gear assembly and vertical support

2.3.2 Load cell assembly

The load assembly connects the gear mechanism to the cable assembly. This assembly, illustrated in Fig. 2.9, performs multiple functions. It takes the threaded screws, each one moves in the opposite direction, shown in Fig. 2.8, and converts the rotational movement into a vertical linear movement via the mounting flange. The

transfer plate provides a strong platform for the load cell to vertical react against. The test wedge, threaded into the load cell, pushes on the pressing plates which press directly on the three-strand cable.

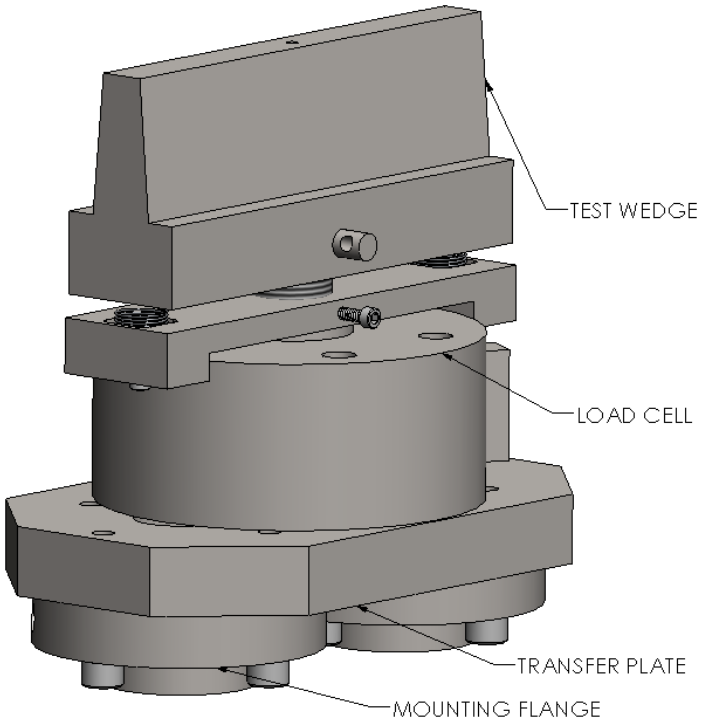

Fig. 2.9 Load Cell Assembly

2.3.3 Cable assembly

The cable assembly shown in Fig. 2.10 has a diameter of 167 mm, and the height of the main body is roughly 73 mm. This section contains the transverse load mechanism and the mechanical structure that reacts to the high forces produced during operation. Naturally, this is where the cable is positioned as shown in Fig. 2.2 and the current lead joint, to which the Nb_3Sn is soldered.

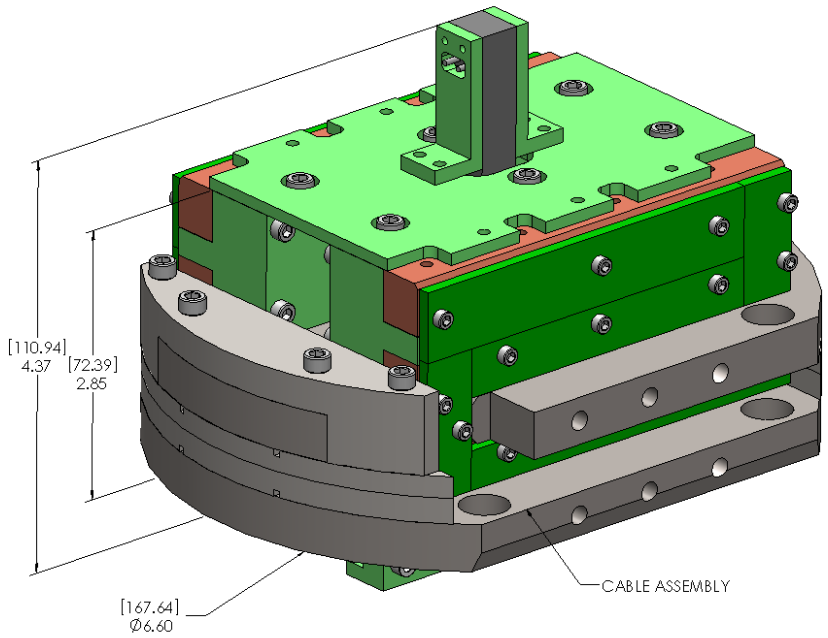

Fig. 2.10 Cable Assembly

2.4 Gear Mechanism Design

The gear mechanism has been designed previously for the 20 T Bitter resistive magnet and used in bending experiments by D. Harris and other [9],[6],[13]. In this design the rotational motion of the gears was converted to bending motion of the support beam, used to investigate the critical current behavior of Nb_3Sn wires under pure bending loads.

The input shaft is connected via the input shaft coupler which is then connected via a 208 cm long shaft the motor drive above the experimental setup. The input shaft coupler allows the probe head to be easily separated from the probe supporting structure. The major benefit of the decoupling is the ability to assemble the transverse experimental assembly as one unit and when everything is ready connect it to the supporting structure before being inserted in the cryostat.

When the input shaft, Fig. 2.11, is rotated via the motor, it transfers the input torque to the gear assembly that will be described in detailed later. The gear assembly in turn is applying a vertical displacement to the load assembly, also described later, which ultimately is what applied the load to the sample. 90 degrees to the drive shaft wormgear. The wormgear motion causes the two torque gears that are connected directly to the torque arms to rotate in the opposite directions.

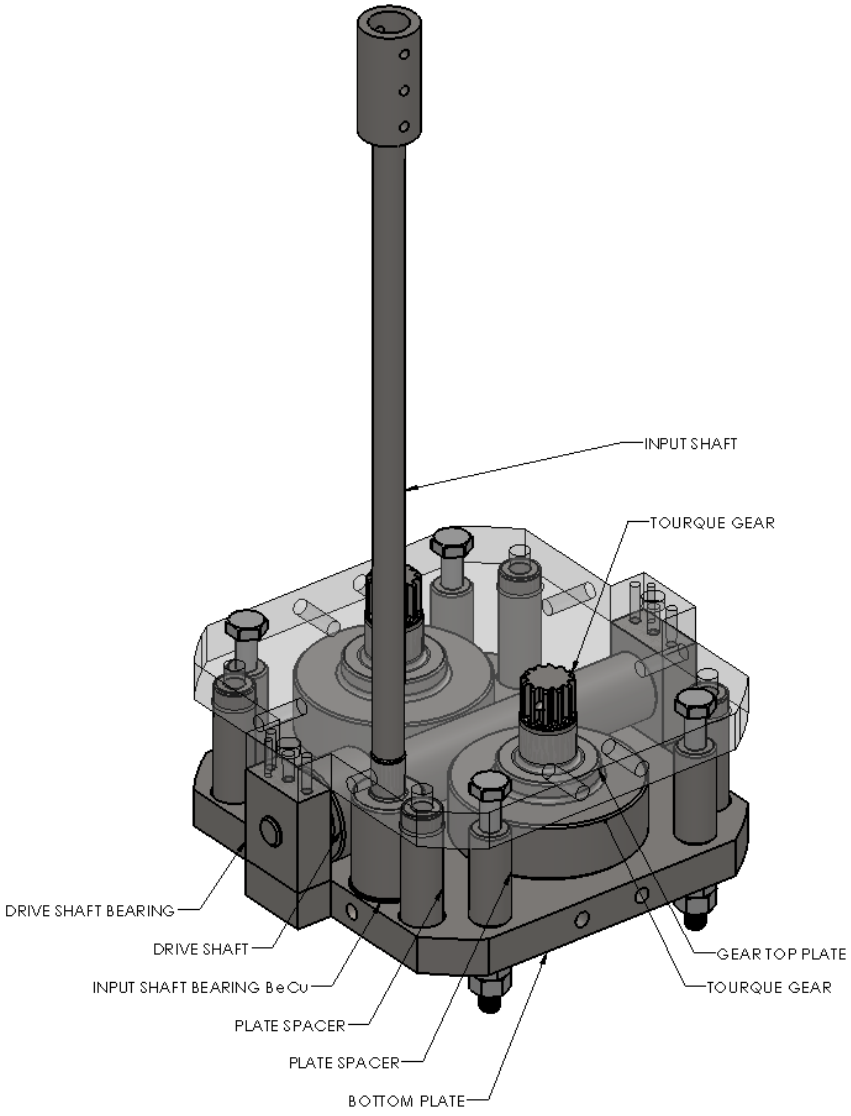

Fig. 2.11 Gear Mechanism view of the internal components.

There was one improvement made to the gear box that should be mentioned. In previous experiments, the gear mechanism exhibited galling of the gears with the bottom cover. To reduce galling, the gears have been coated with Balzers Balinit C (WCC). In addition, a metal bearing in the form of a Beryllium Copper shim has been incorporated into the design, illustrated in Fig. 2.12. This shim was placed under the input shaft, and under the two wormgears. This will reduce the friction coefficient between the metals and eliminate the galling.

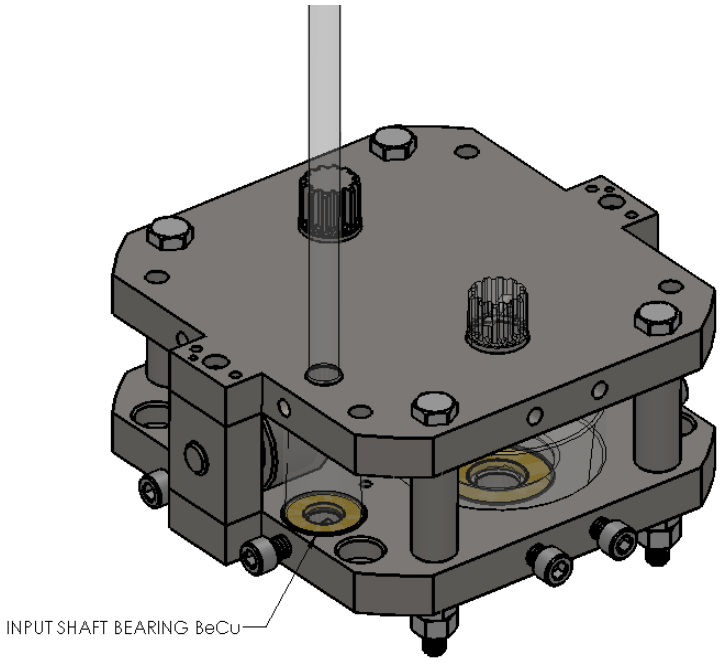

Fig. 2.12 Gear assembly with the illustration of the BeCu shims.

Additional support is created to keep the top and bottom plates level parallel to each other through the use spacers shown in Fig. 2.11. The plate spacers also act as alignment mechanism to square up the gear assembly. To provide a solid structure, that reacts against the wedge, four rectangular support beams are designed and bolted to the side of the gear assembly, shown in Fig. 2.8

Additionally a G10 bottom cover has been designed, shown in Fig. 2.8. The plate, being circular, eases the insertion of the probe into the dewar avoiding that any sharp corners of the assembly touch the dewar and cause damages. The bottom cover is attached via the support structure that holds the whole experimental assembly.

2.5 Load Cell assembly design

The load cell assembly plays a major role in the experimental assembly. It connects the gearbox assembly and the cable assembly. The load cell assembly has two purposes. It converts rotational torque from two worm gears into a vertical movement. It also, allows measuring of the load, that the gearbox is applying vertically to the cable assembly. It enables the wedge to be moved vertically via a load cell, which measures the total vertical load applied to the wedge.

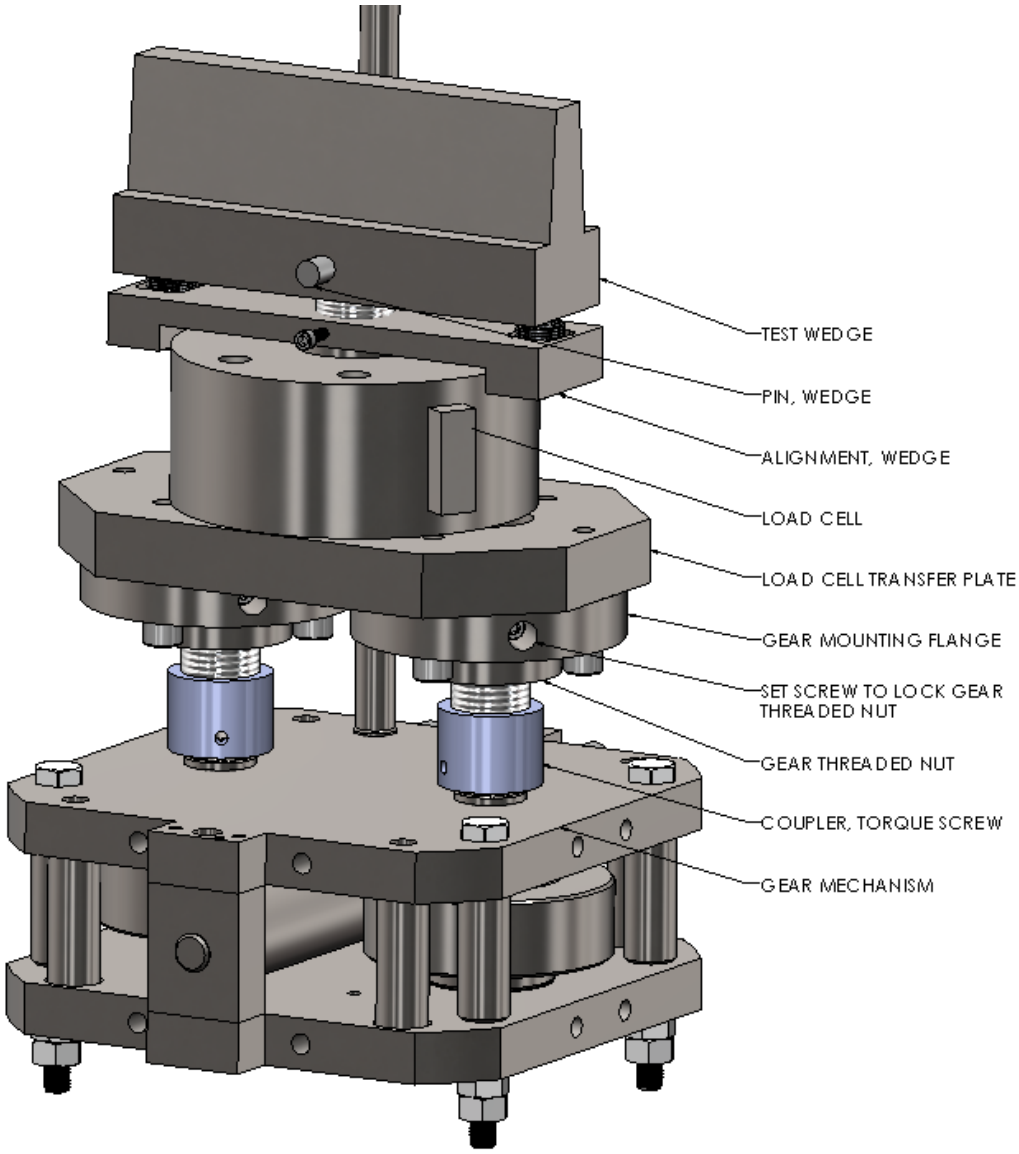

Fig. 2.13 Load cell assembly on top of gear mechanism

2.5.1 Rotation to Linear movement

In order to use the existing gearbox, a way to convert the opposite rotation of the torque gears into the linear vertical movement needed to be developed. Initially, the design was being developed with off-the-shelf components. Quickly design progressed to using mostly custom parts with a few off-the-shelf components.

To convert the rotational to vertical movement, two torque gears from the gear mechanism are used. Two threaded coupler screws were developed, Fig. 2.15. When the gear mechanism is rotating, the stationary gear threaded nuts are able to move vertically. Since the torque gears are rotating in the opposite directions, the connecting screws are machined with left and right threads to accommodate this movement. The gear mounting flanges as well as the gear threaded nuts are modified off the shelf components. Together, they allow the load cell transfer plate to move vertically.

It would be almost impossible to machine the threads on the coupler to match them in such way as to have both of the tops of the mounting flanges to be flat and parallel relatively with each other when they are bolted to the transfer plate. To allow the adjustability, the gear threaded nut can rotate independently inside the gear mounting flange. When the transfer plate is flat and parallel, relative to the gear mechanism, two set screws are used in each of the mounting flanges to lock the threaded nut. Now, when the gear mechanism rotates the torque screws, the transfer plate would move up and down evenly.

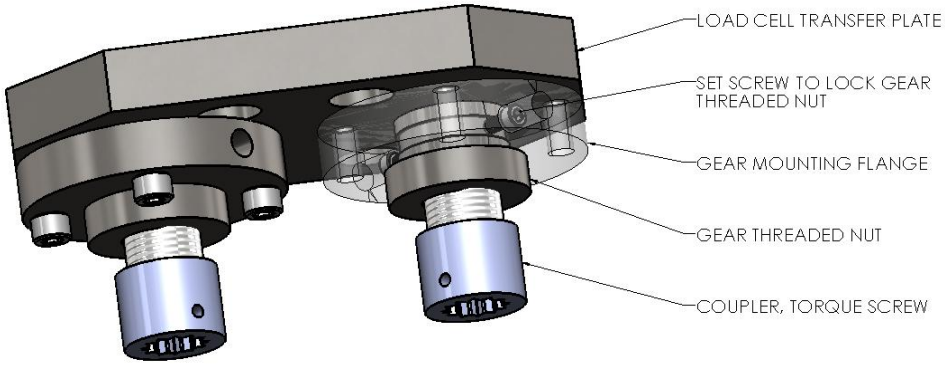

Fig. 2.14 Load assembly mechanism to convert rotational to vertical movement.

2.5.2 Load cell

A load cell is used to measure the force applied by the gear mechanism below the wedge. A custom load cell had to be designed for this application, as it had to adhere to our mechanical and electrical specifications and be able to withstand cryogenic temperatures. The load cell was bolted down to the table from the bottom using the outside threaded holes.

A local company, specializing in load cell manufacturing was outsourced to help design and manufacture a load cell to meet all of our constraints. The load requirements were the following: it is made out of Beryllium copper, 3.5 inches in diameter and 1.5 inches in height. The maximum designed load is 2000 lbs (8896 N).

2.5.3 Wedge design

In order to apply the force to the cable, horizontal load was necessary to be applied on the pressure plate. The vertical load is coming from the transfer plate through the load cell. This load is then transferred to a wedge, which accomplishes the horizontal load, Fig. 2.15.

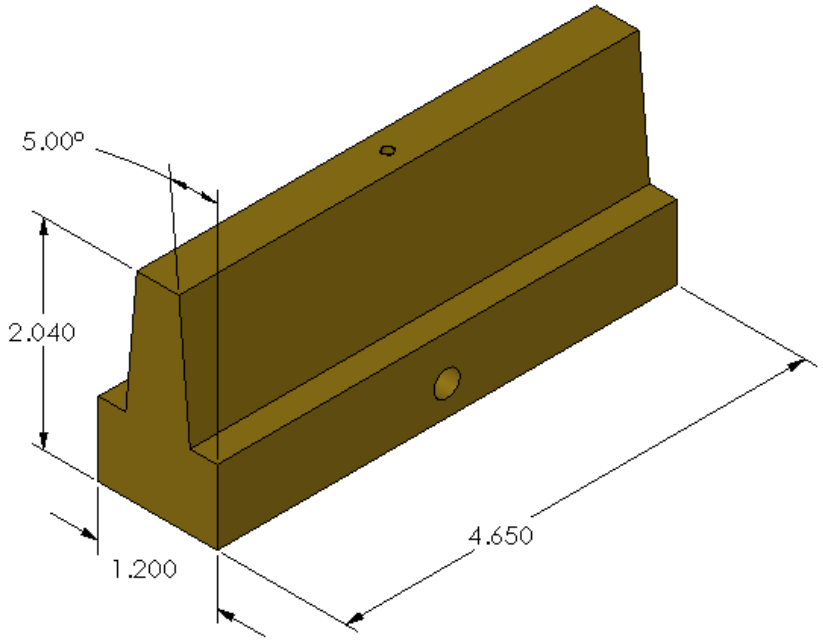

Fig. 2.15 Test wedge used for the experiment with 5° draft.

The wedge converts the vertical load to horizontal force via the use of geometry, illustrated Fig. 2.16and Fig. 2.17. The wedge pushes both pressure plates in the opposite direction. The total load applied by the wedge is split in half. Vertical load $F_{vertical\text{-}load}$ is being recorded by the load cell, mounted below the load wedge and vertical displacement $L_{vertical}$ is recorded by the extensometer, it is mounted directly to the top of the wedge. The transverse load $F_{transverse}$ and transverse displacement $L_{transverse}$ is calculated based on the geometric analysis using Eq. 2.1 and 2.2.

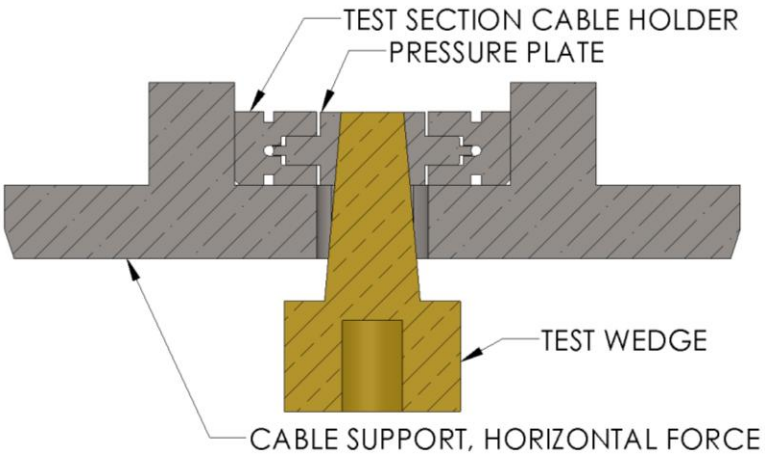

Fig. 2.16 The mechanical design of the transverse load components.

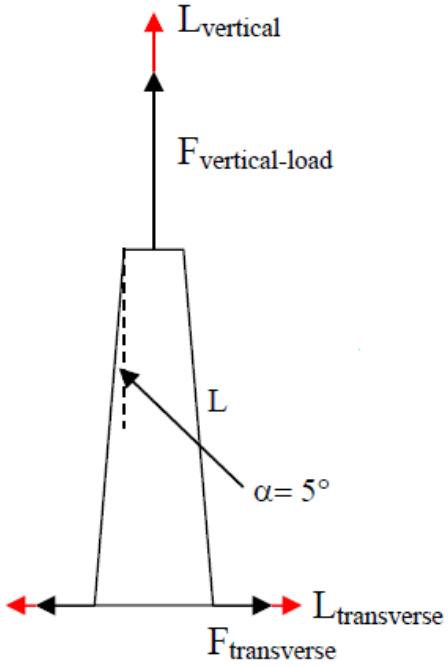

Fig. 2.17 Geometrical schematic of the forces, design of the wedge [6].

$$F_{vertical-load} * L_{vertical} = 2 * F_{transverse} * L_{transverse} \quad (2.1)$$

$$F_{transverse} = \frac{F_{vertical-load} * L_{vertical}}{2 * L_{transverse}} = F_{vertical-load} \frac{1}{2 * \tan(\alpha)} \quad (2.2)$$

In addition to mechanical measurements, electrical measurements will be taken using voltage taps. The voltage taps are mounted on the 3-strand cable and measure the voltage across the sample. There will be three sets of voltage taps, one for each section of the cable that is being transversally loaded. Another one

measuring the voltage for the length of both sections combined. As the current is driven into the sample initially a zero voltage will be recorded showing the superconducting state. At a certain current the voltage will start rising exponentially indicating the transition from the superconducting to the resistive states. Using this voltage-current curve it will be possible to determine the critical current of the sample for each applied load conditions.

2.6 Cable Assembly Design

Designing the Cable Assembly, Fig. 2.18, was a dynamic process. A change in one part affected the design of other parts as well.

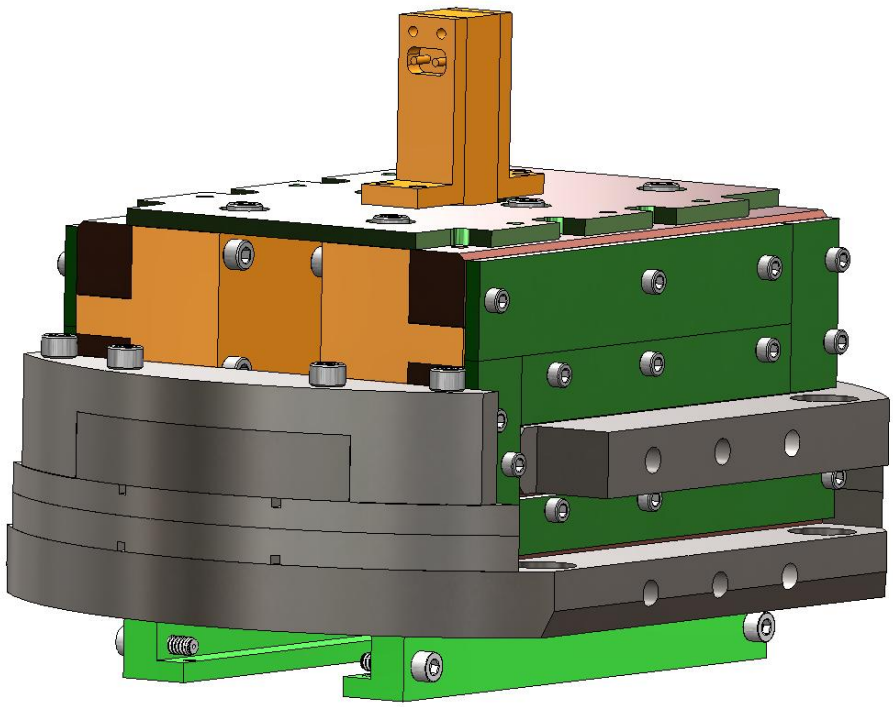

Fig. 2.18 Final Experimental Assembly with extensometer attached to the top plate.

Cable assembly comprises of three similar configurations: Heat Treatment configuration, Transportation configuration, and Experimental configuration. While

sharing the major structural components, they have some parts unique to a particular task.

The purpose the heat treatment configuration, Fig. 2.19, is to condition the test cable using the right heat treatment recipe in order to get the cable ready for the experiment. A heat treatment with temperature up to 650 °C is necessary to allow for the formation of the superconducting filaments. Additionally after heat treatment Nb_3Sn becomes brittle so it cannot be removed and manipulated so that is necessary to design the heat treatment assembly so that only few parts need replacement after this process. The replacement of those components has to be done without moving the sample. Due to high temperatures and long heat treatment duration, only high temperature metals are permissible in this design. Some of the cable covers were made of stainless steel instead of G10. Some of the components were made with metal for structural consideration, as at high temperatures, the copper current joints could become soft and would not be able to support the structure, thus its shape could inadvertently be compromised. Some additional parts were also designed in order to solder the cable to the current joint. Heat treatment shims were required in order to prevent the pressure plates compressing the cable during the heat treatment and possibly cause damage before the experiments.

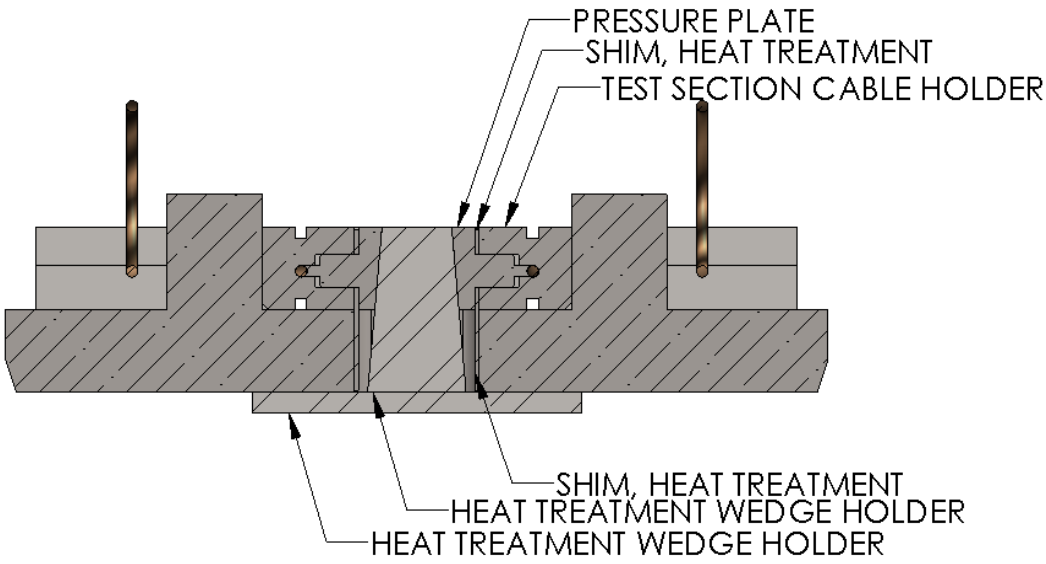

Fig. 2.19 Heat treatment configuration of the cable assembly.

No special parts were required for the transportation configuration. The concern is that after heat treatment the 3-strand cable is very brittle and all possible means should be taken in order to protect it. To do this a combination of parts from both heat treatment as well as the experimental configuration are utilized. Heat treatment shims stay in order to prevent the pressure plates from engaging the cable. The heat treatment wedge (also made of stainless steel) stays as it is and it is bolted to the bottom of the horizontal force support. The wedge is placed in position during the heat treatment to maintain the necessary space between pressing piece and cable holder to achieve the desired void fraction. This wedge is then replaced with a brass wedge during the tests. In the final configuration G10 components replace the stainless steel covers. The top cover is replaced with G10 cover as the current leads get soldered with copper cables that are connected to the current leads carrying the current to the sample from an external power supply.

In order for the cable assembly to be ready for the experiment, the heat treatment shims, shown in Fig. 2.19 are removed. These shims were put in place to protect the wire during the heat treatment. Also, the covers, illustrated in Fig. 2.20, are replaced by similar covers made out of G10, shown as the final configuration in Fig. 2.18. Although solder should be sufficient to keep the cable-current joint together, these covers are put as a precautionary measure. Another component that is installed in the experimental configuration is the extensometer. It will be used to measure the vertical engagement of the wedge. The extensometer is supported by the top cover made out of G10. The extensometer measurement is made via the connection to the experimental wedge.

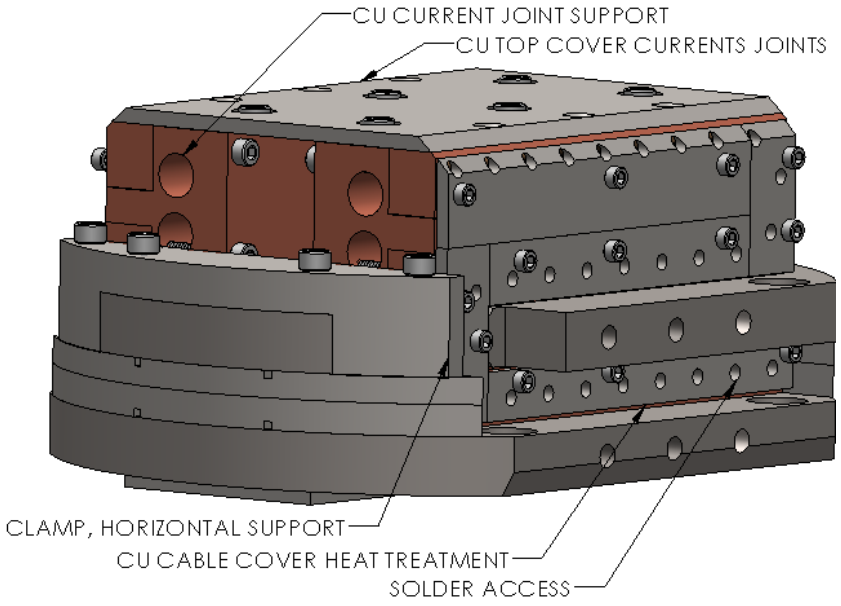

Fig. 2.20 Heat treatment cable assembly.

There were a few hard constrains that were set. One of them, mentioned earlier, is the 6.6 inches diameter throughout the vertical length of the experiment. The other constraint is the heat treatment oven, into which this experiment will be loaded into had a restriction of 5.2 inches. Before going into the oven, the

experiment needs to be wrapped up with special nickel rich steel blanket to avoid contaminations of the furnace. Taking all those constraints in consideration, the experimental front diameter could not exceed 5.2 inches in diameter, Fig. 2.21. This is the reason why some of the parts have a chamfer in unusual locations.

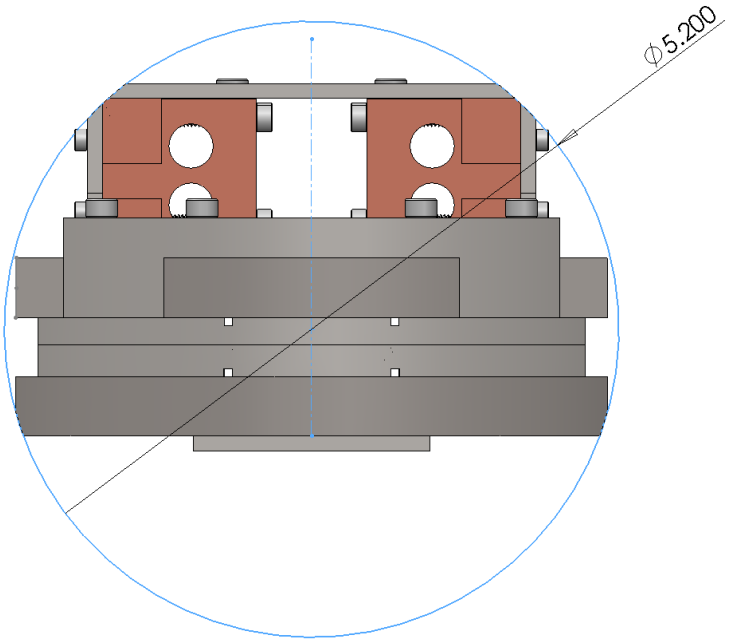

Fig. 2.21 Front view of the cable assembly with chamfers shown.

2.6.1 Current lead joint

To carry all the current coming from the power supply to the superconducting test sample, an electrical joint needed to be designed. The current lead joint will carry the current and provide the rigid section that will support the strand against the Lorentz forces. The current lead joint was designed not to interfere with the sample length; therefore, the length of the electrical joint was independent from the test section length and it was increased as much as possible to ensure good current transfer.

The current lead joint, shown in Fig. 2.22 picks up the three strand cable from the cable holder and runs parallel to the experimental sample. At this point it makes a 180 degree turn and runs parallel the initial groove. This repeats once more until it is terminated at the top of the current joint lead. The cable undergoes heat treatment operation while it's installed in the groove to avoid the damage that would occur with trying to bend it if the cable was heat treated prior to installation. After the heat treatment the cable is soldered with continuous solder operation throughout the length of the groove of the current joint support. On top of the current joint support there are four holes for soldering of flexible cables that are connected to the current leads carrying the current from the outside, not shown. This cable runs up to the outside of the experiment where it receives current from the power supply. All four cables from each side of the current joint support are joined together to a thicker cable, which is able to carry the high current supplied to the sample.

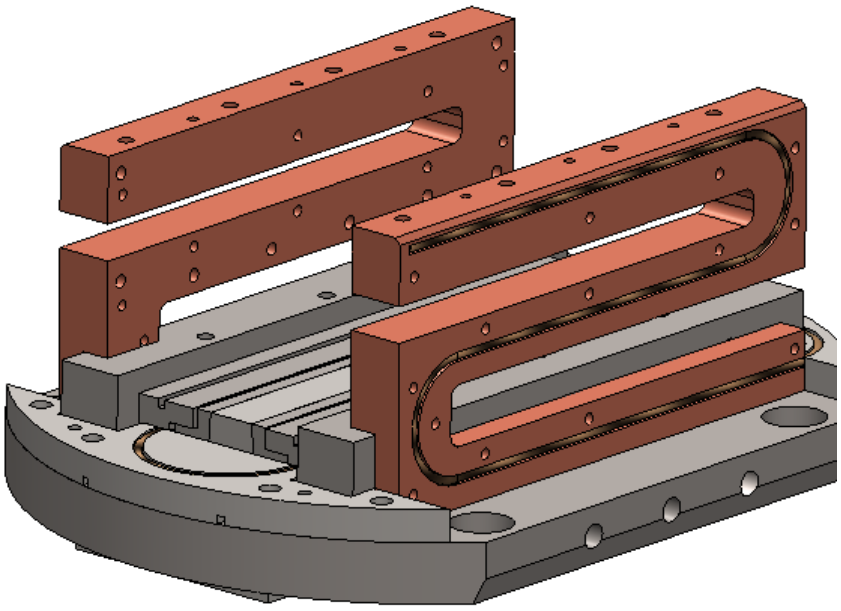

Fig. 2.22 Current lead joint with 3 strand cable routed through it.

One question would arise, rightfully so, is whether there is a concern for a short circuiting in the assembly, since clearly there is no insulating material. Because of the large relative resistance of the surrounding components compared to the superconducting sample, this is of a little concern. Mounting a superconductive sample to a metal support system has been used in a majority of the strain-behavior current experiments [9].

One might notice that the current lead joint groove is long, making the assembly larger. In prior experiments, [6], it was though that poor electrical contact caused the superconducting wire to raise its resistance and ruin the experiment. For this reason, and from the current transfer standpoint, it was important to increase the joint to be as long as possible. The increased length the additional distance needed to transfer the current between the copper wires and the test strand.

2.6.2 Cable routing

Design of the cable assembly was highly influenced by maximizing the length of the test cable section area. As previously mentioned, the longer the transverse load cable length, the more uniform the current distribution will be and it will be possible to apply the load to at least one twist pitch length, the length of the pitch of the 3 superconducting strands twisted together. In Fig. 2.23, the routing of the 3-stranded cable within the cable assembly is shown. The cable makes a u-bend in the cable run of the cable holder u-bend piece. It is then routed through the test section cable holder. The pressure plate, not shown and discussed earlier, compresses the cable during the experiment. The distance between two pressing sections of the test cable is roughly 1.41 inches center-to-center. The cable is then routed through the cable

holder double u-bend. The radius of this bend was smaller at 1.030 inches. After the cable holder double u-bend run, the cable is terminated along the current lead joint as it snakes all the way to the top. Because the cable is relatively fragile, it is beneficial to keep the cable radius as large as possible at in the areas where the cable had to change its location.

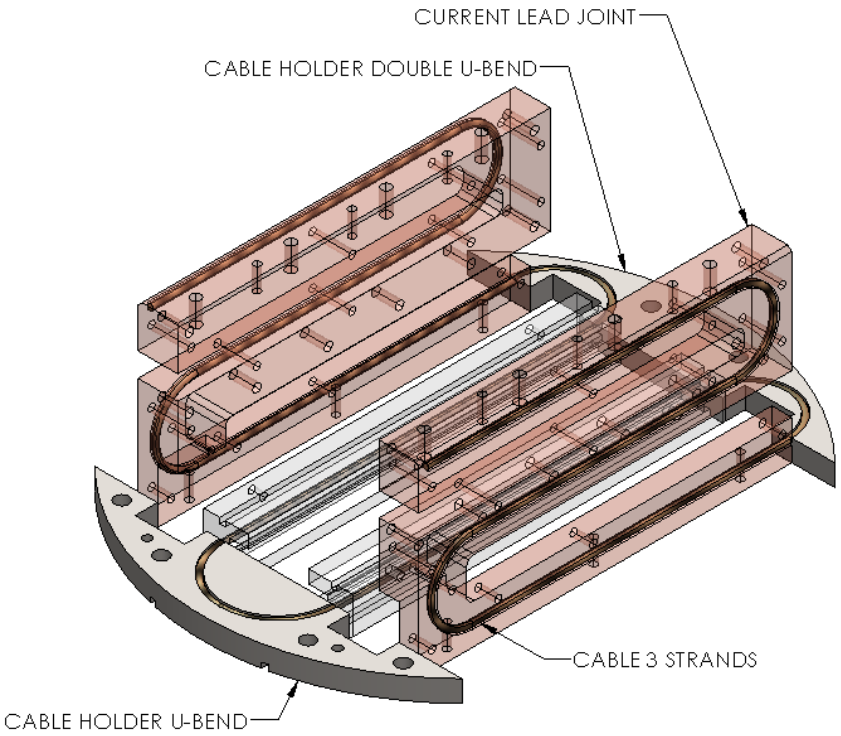

Fig. 2.23 Cable Routing within the Cable Assembly

After the heat treatment, the current lead joint along with the 3-strand cable is filled up with solder. There are two reasons for this. To maximize the contact with the current lead joint increases the current distribution. Secondly, maximizing the current distribution in the current lead will minimize the resistance of this transition between the Nb_3Sn cable and the copper current lead. A poor contact will cause increased resistance would significant degradations of the critical current by localized Joule heating and poor current transfer from the power supply outside to the sample.

2.7 Cable Assembly Structural Design

The cable assembly structure needed to serves two main purposes. It resists the vertical forces created by the vertically moving wedge. It also has to resist the horizontal forces created when this wedge transfers the force onto the horizontally moving pressure plates. Although it's best to design a mechanism where a component has a singular purpose, it was not always possible to do so in the design of this experiment.

The structural system is comprised of two main components. Horizontal Force as well as Vertical Force support as described in the following sections.

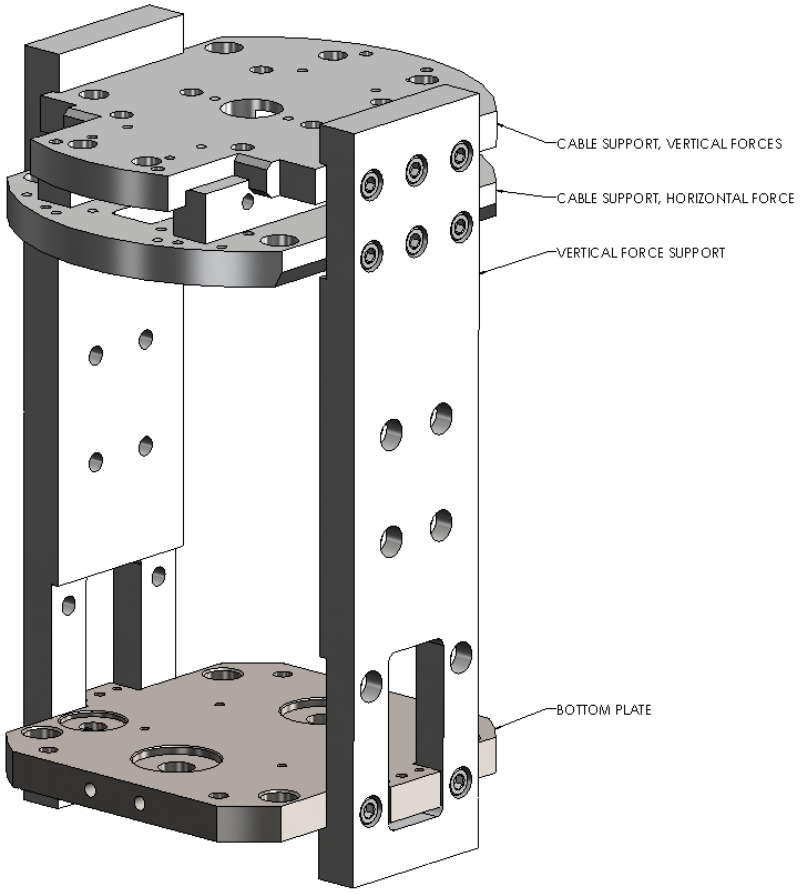

Fig. 2.24 Main components of the structure.

2.7.1 Cable Support Vertical Force & Vertical Force Support structural design

The purpose of the cable support vertical force, Fig. 2.25, and the vertical force support, Fig. 2.26, is to resist the vertical forces that the wedge is applying to the cable assembly during the duration of the experiment. The area responsible for resisting the force is the notch in the vertical force support.

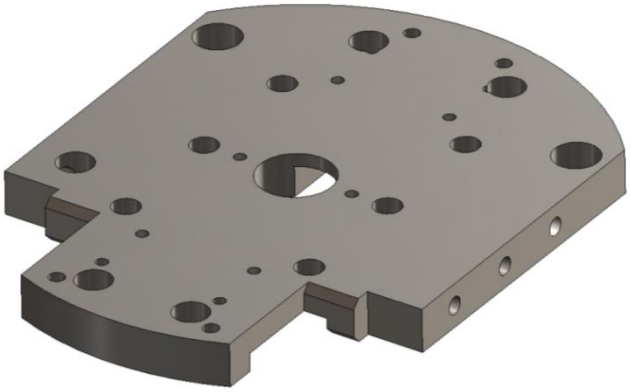

Fig. 2.25 Cable support, vertical force part

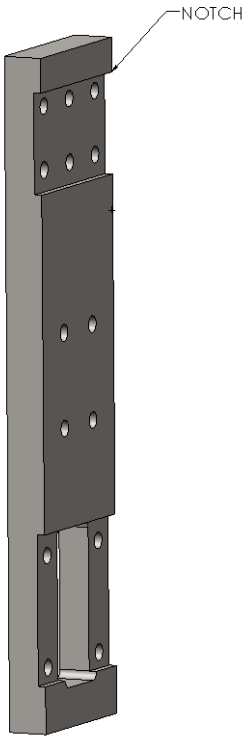

Fig. 2.26 Vertical force support part

In addition to the notch, the structure will be secured to the cable vertical support, using six ¼ inch bolts. When bolted together with screws, Fig. 2.27, the assembly provides a solid connection from the gear assembly to the cable assembly as well as the tensional structural stability for the whole experimental assembly.

Secondary, as shown in Fig. 2.28, cable vertical force interlocks with the cable horizontal force support. When bolted together, this creates a solid structure, which will be discussed in the horizontal force support section later in this chapter.

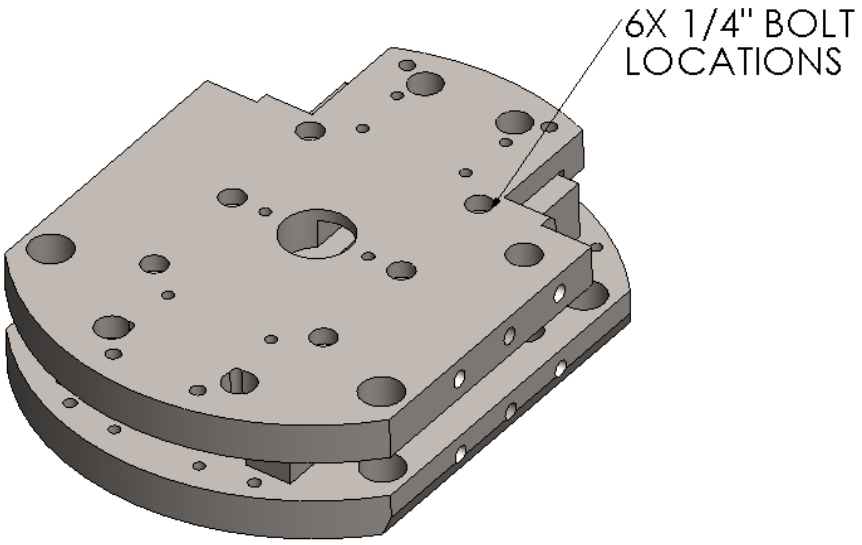

Fig. 2.27 Cable Assembly main support structure

Fig. 2.28 Cable Assembly main support structure. Both parts interlock together to form a solid assembly.

2.7.2 Horizontal Force Support structural design

The horizontal force support, shown in Fig. 2.29, acts to resist the forces transferred to it by the wedge during the experiment. As mentioned in Section 2.7.1 it was designed both vertical and horizontal support parts to interlock. Together, they create a solid structure that can withstand the forces applied to it. The horizontal force support have 4 holes for the vertical rods that connect the whole experiment to the upper supporting structure, as well as the hole for the input shaft which drives the gear assembly.

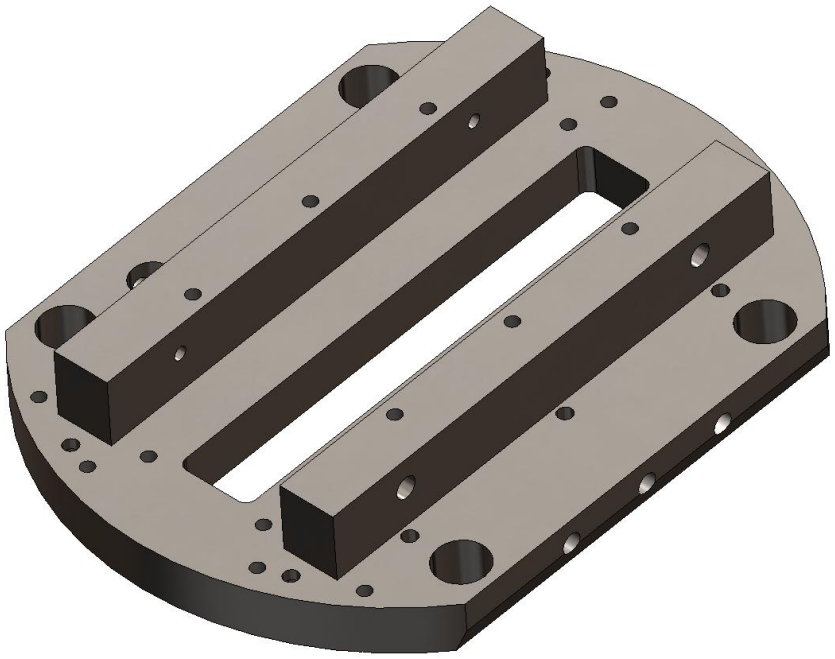

Fig. 2.29 Support, Horizontal Force.

The horizontal force support also gets bolted to the side vertical force plates, but this is not its primary role in the experiment. The decision to bolt both the vertical and the horizontal support is to keep the whole assembly more stable throughout the movement of the motor drive. The opening in the middle of the component is the opening for the wedge.

There are many holes that appear in the horizontal support. Some serve a role of preventing a part from moving around during the assembly, test cable section holder for example, Fig. 2.32. There are also threaded holes which bolt the vertical and the horizontal support together, making it a more solid structure. The vertical support would have a matching through hole for a bolt to go through.

2.8 Transverse Load Operation

The final configuration of the transverse load design, shown already in Fig. 2.7, is illustrated in Fig. 2.30. The design underwent through numerous iteration and modifications to maximize the ease of machining, assembly and strength of the experiment.

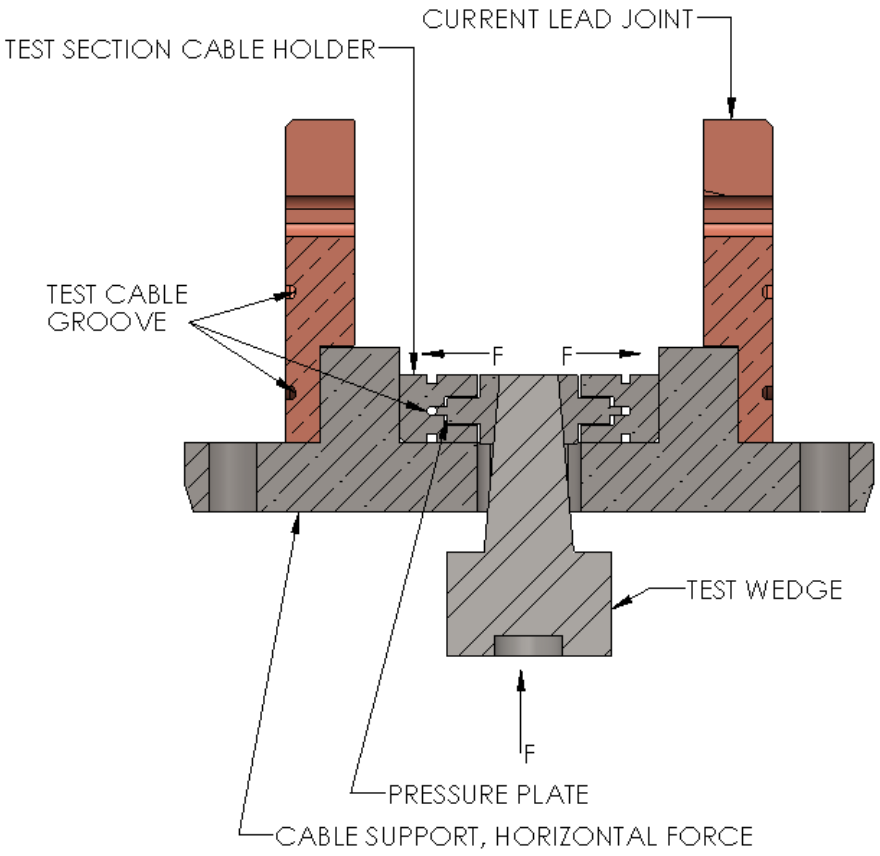

Fig. 2.30 Transverse Load cross section with Test Cable Groove

The 5 degree test wedge slides vertically against the pressure plate, which is also machined with the same five degree draft. As the wedge moves vertically, because of the draft, both pressure plates move horizontally inside the groove of the test section cable holder. The cable is laid in a groove in the test section cable holder. The groove in the test section holder, Fig. 2.31, is designed with 1.79 mm diameter

groove. It will accommodate three-strand cable. Each strand having a diameter of roughly 0.8 mm.

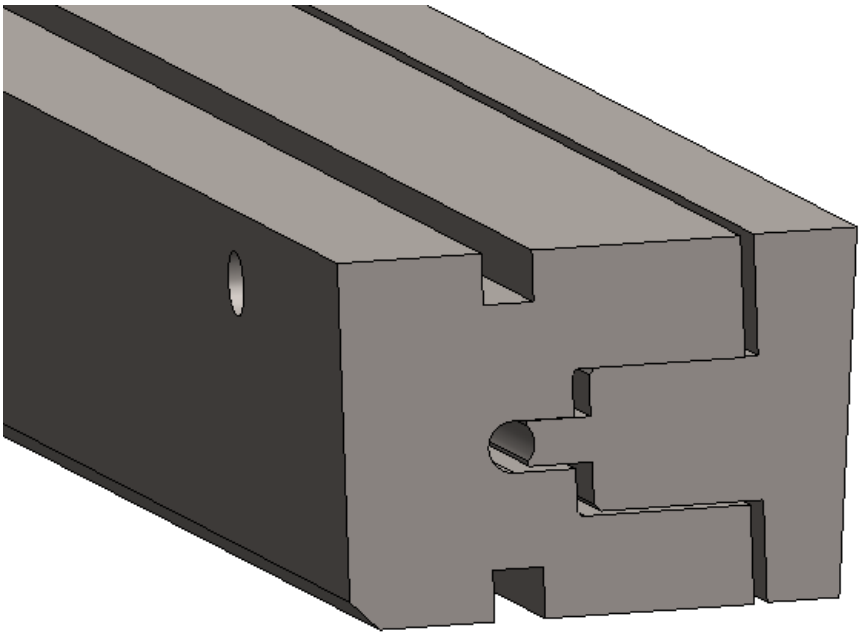

Fig. 2.31 Cable Run Cross-section

Shims have been designed to be inserted in the space between the pressure plate and the test section holder. When shimmed, the pressure plate and the test section holder will not compress further than a diameter of 1.79 mm. This creates a circular envelope in which the test cable should not exhibit any undue pressure. This is beneficial in two ways. First, it is done for heat treatment of the cable, to prevent compression of the cable during heat treatment. Second, the shims will protect the cable during transport to the NHMFL Facility. When the shims are taken out, the pressure plate is designed to compress the cable from 1.79 mm to 1.17 mm. This equates to roughly 34% from the nominal diameter.

The movement of the wedge is approximately 7 mm, significantly more than the movement of the pressure plate. The uncompressed state of the mechanism is illustrated in Fig. 2.32 and compressed state in Fig. 2.33.

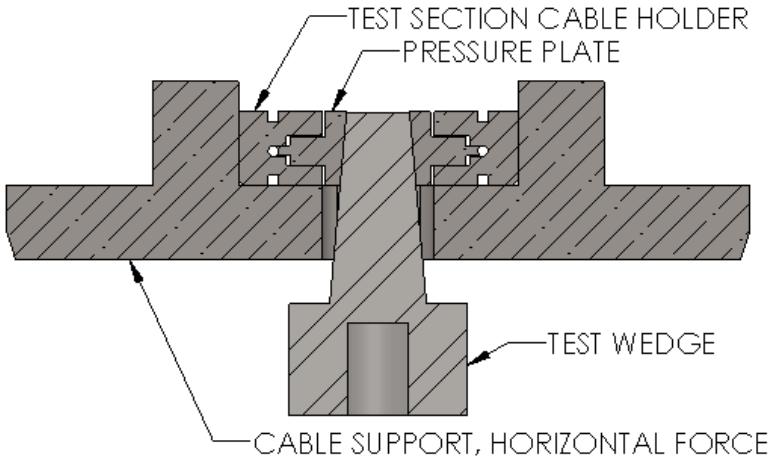

Fig. 2.32 Uncompressed state of the mechanism

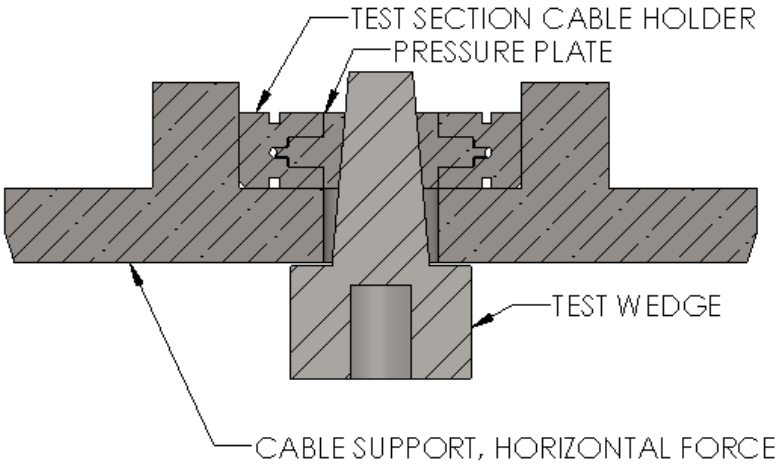

Fig. 2.33 Compressed state of the mechanism

It was important to limit the movement of the pressure plate, thus not to damage the test section cable holder. This was achieved with a separate design feature of the pressure plate. The distance from the cable radii to the section where the heat treatment section shims are is constrained. Shown in Fig. 2.34 the pressure plate stops before the cable section hits the cable holder.

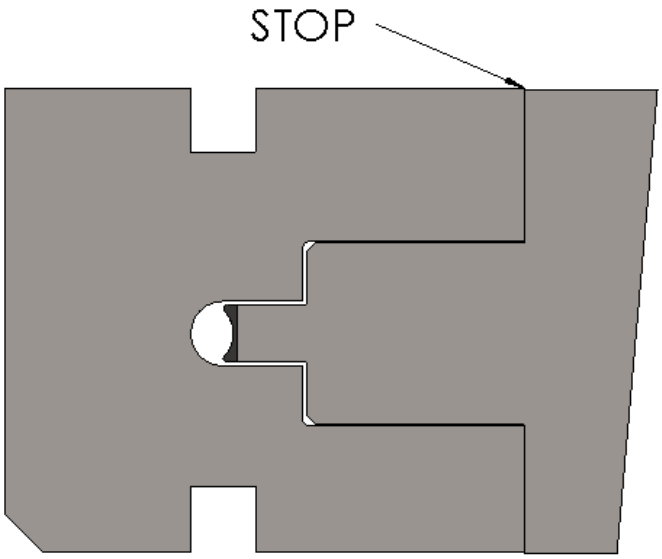

Fig. 2.34 Pressure plates stop when it hits the cable holder.

Chapter 3 Experimental Mechanism Assembly.

The experimental mechanism consists of three different assemblies. The cable assembly, gear assembly and the load cell assembly. Each one requires great care, patience and attention to detail when putting them together.

The cable assembly is the only piece that requires heat treatment prior to the experiment. It needs to be assembled prior to shipment to the NHMFL. The gear assembly as well as the load cell assembly can be shipped and assembled at the facility.

3.1 Mounting Cable Assembly Heat treatment

Assembly methods were considered when designing the cable assembly. The size constraint of the experiment, numerous parts, and tight experimental space as well as heat treatment space, was considered from the beginning of the design process.

The cable assembly was designed and built to take in consideration the fact that the cable cannot be moved after it goes through heat treatment when the brittle Nb_3Sn superconductor forms. The heat treatment is performed with temperature as high as 650 °C, during which no G10 material can be used. After heat treatment only few parts are removed and the replaced by the G10. It should also be noted, to avoid sintering of similar metal parts, the touching surfaces have been covered with a graphite coat.

3.1.1 Test Cable Preparation

Partial cable assembly is performed prior to putting all of the components together. When the test cable in its untreated form, it is rather flexible and it is not brittle as the reacted sample, so that it is possible to bend it to the desired shape. To prepare the sample, a partial shaping of the cable is done in order to ease the positioning of the sample inside the holding structure. The forming helps when assembling the 3-strand cable into the cable assembly for the heat treatment. It should be noted that the cable is covered in chromium to reduce the A/C losses. The chrome is partially removed for the sections of the cable that need to be soldered to the copper after heat treatment.

3.1.2 Horizontal force support & Test Section Cable Holder

The first step in the assembly is to mount two test section cable holder sections to the horizontal force plate, illustrated in Fig. 3.1. Loosely secure the holder section and lightly tighten two screws on each side to prevent the holders from falling out. Leaving the screws loose, gives the adjustability of moving the test sections a bit in order to adjust the cable holders, shown in Fig. 3.1 When the cable holders are aligned, both the test section cable holders can be tightened.

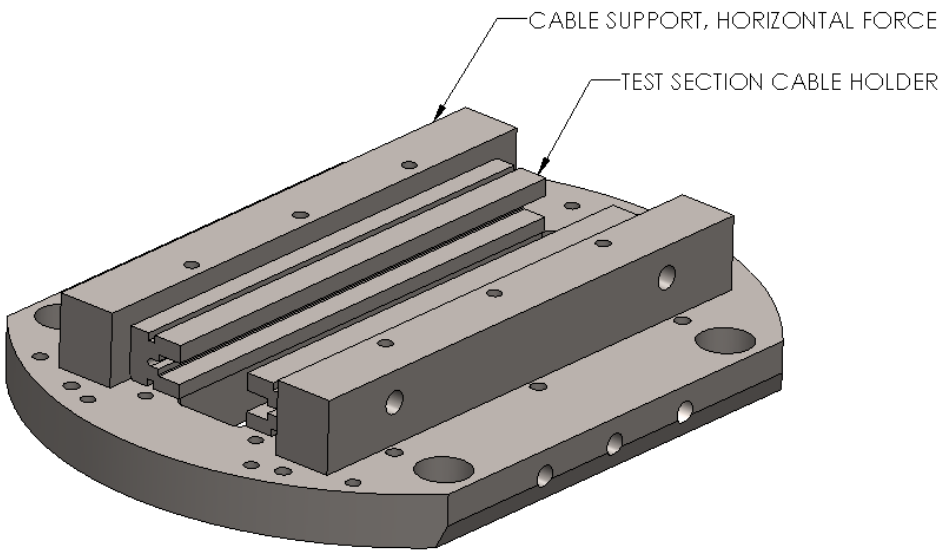

Fig. 3.1 First step to assemble the cable assembly.

3.1.3 Cable holders and cable covers

Prior to attaching the u-bend cable holder to the horizontal force support, lay the formed cable into the u-bend groove as well as the double u-groove holder, Fig. 3.3. This is done as an intermediate step toward the final positioning of the cable in the assembly and has two functions. It will form the cable into the desired shape of the final assembly as well as make it easier to install.

The voltage tap wires need to be prepared prior to the assembly as it would be impossible to install them after heat treatment since it is very difficult to access the cable. Trying to manipulate the cable after heat treatment would cause irreparable damages. The cable has been covered with chromium to reduce the A/C losses. This coating has to come off in the location of the voltage tap to successfully solder the voltage taps after heat treatment. Chromium can be removed by carefully and lightly scrapping the outer surface of the cable with a charge object. In this case a new razor blade. More details on the voltage taps will be given later.

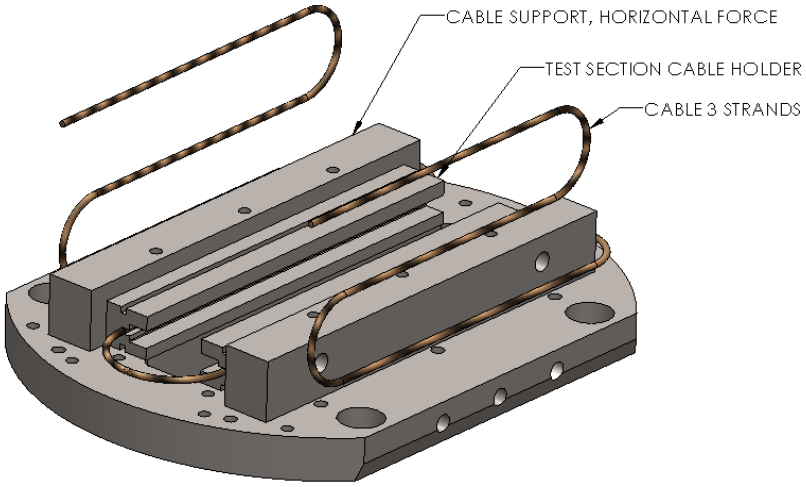

Fig. 3.2 Preparing the cable for the assembly by bending it into its final shape

Once the cable is prepped, it is ready to be installed in the assembly, illustrated in Fig. 3.3. The cable is laid into the u-shaped groove of the cable holder while matching the location of the current lead opening. U-shaped cable holder is then slid toward the test section cable holder, while making sure the cable fits in the groove of the test section holder. When the u-shaped cable holder is snug against the test section on both sides of the test section, secure it from the bottom of the assembly, with screws.

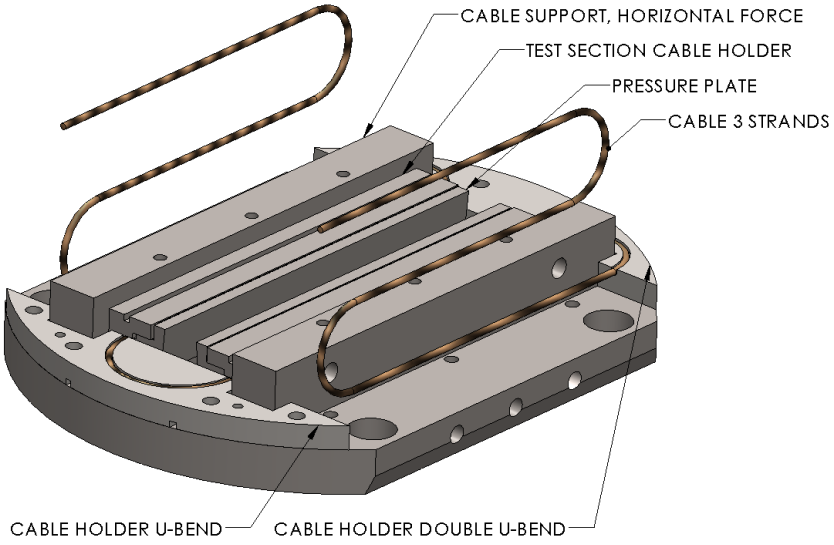

Fig. 3.3 Routing the cable through the pressing mechanism as well as the supporting structure.

With the cable in the grooves it can now be secured with the cable covers shown in Fig. 3.3. Careful attention must be paid to make sure the cable sits completely flush in the grooves of the cable holder. The cable cover can be secured and bolted down until it's flush to the cable holder, Fig. 3.4

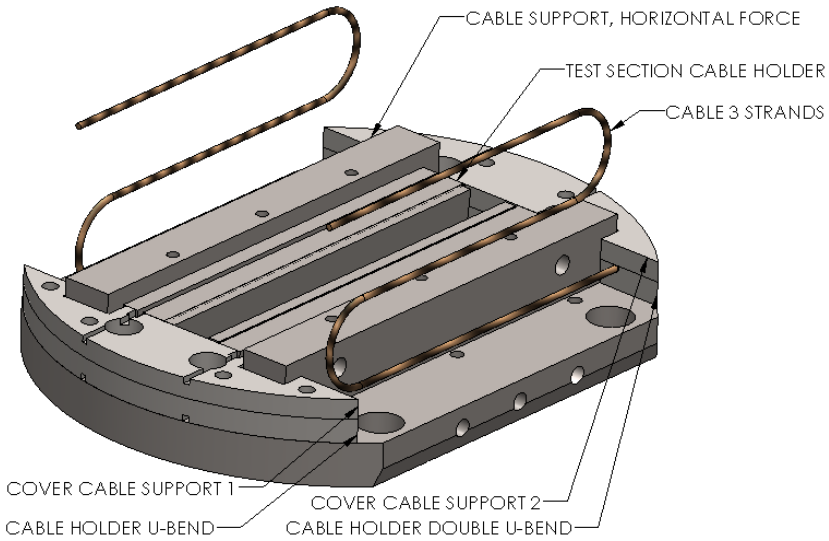

Fig. 3.4 Covering and securing the cable.

3.1.4 Pressure plate and Shims

During the heat treatment, it is important to keep the cable in position and to minimize any undue load applied to it. The amount of transverse movement that the pressing plates will be able to cover during the experiment to apply load to the sample is not allowed during heat treatment when steel shims are inserted in the gaps between the pressing pieces and the cable holders. Those shims fix in position the pressure plates on top and bottom to maintain the exact size of the diameter of the

cable. A heat treatment wedge is then slid in place to keep the assembly secure Fig. 3.5.

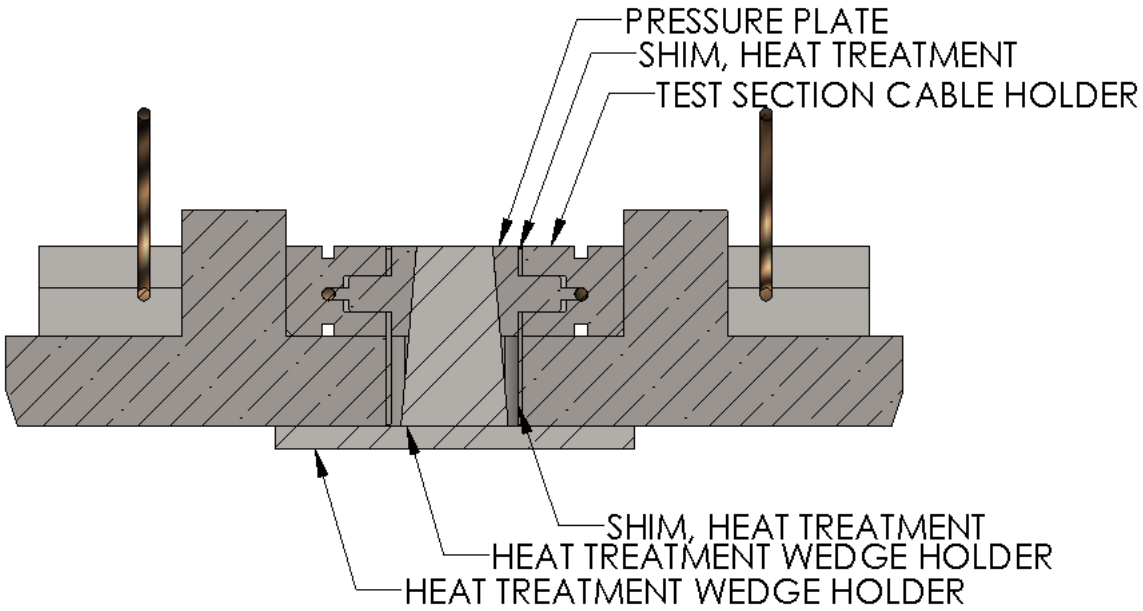

Fig. 3.5 Insert the pressure plates, making sure the cable is secure in the groove. Insert the top and bottom shims prior to inserting the heat treatment wedge holder.

3.1.5 Voltage tap wires

In order to be able to measure the transition from superconducting to normal state during the cable compression test, voltage tap detection wires need to be installed before heat treatment. These wires are wrapped around the 3-strand cable and located close to where the wires come out from the pressing plates, and snaked through the cable assembly. Eventually they are wired up and brought up to the outside for measurement, Fig. 3.6. The voltage taps are thin stainless steel and copper wires, covered with fiber glass sleeve. The fiber glass sleeve is insulting material and will prevent shorts from happening when multiple voltage taps are close

together. The reason it's made out of fiber glass is due to its ability to withstand the high temperature of upwards of 660 °C reached during the heat treatment.

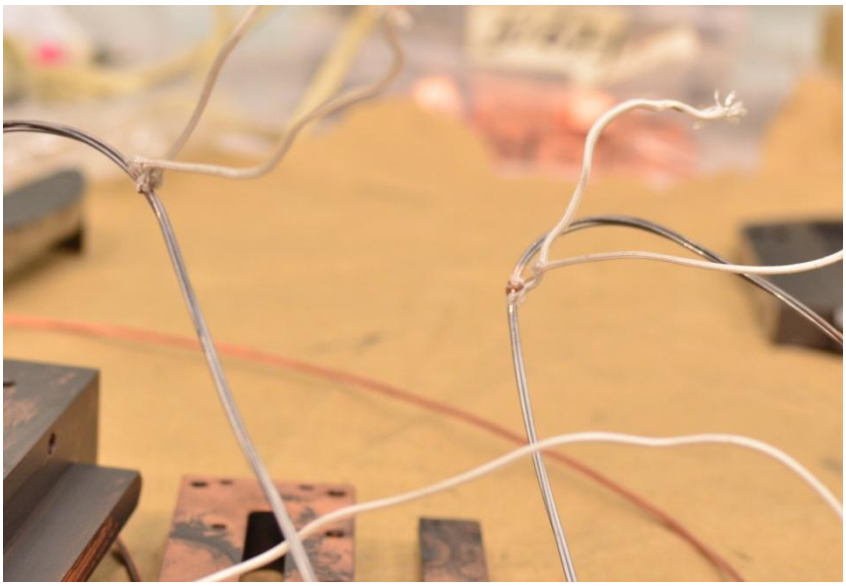

Fig. 3.6 Voltage tap wires are wrapped around the 3-strand cable.

Three voltage taps are mounted on the sample. Two of them are recording the voltage across the two pressed sections of the 3-strand cable and one is recording the total voltage across the entire length of the sample, two pressed legs plus the bend section from one pressed section to the other as illustrated in Fig. 3.7. The current through the samples will be driven so that the natural Lorentz load, the product of current and magnetic field, which is pointing outward as the mechanical force applied to the sample.

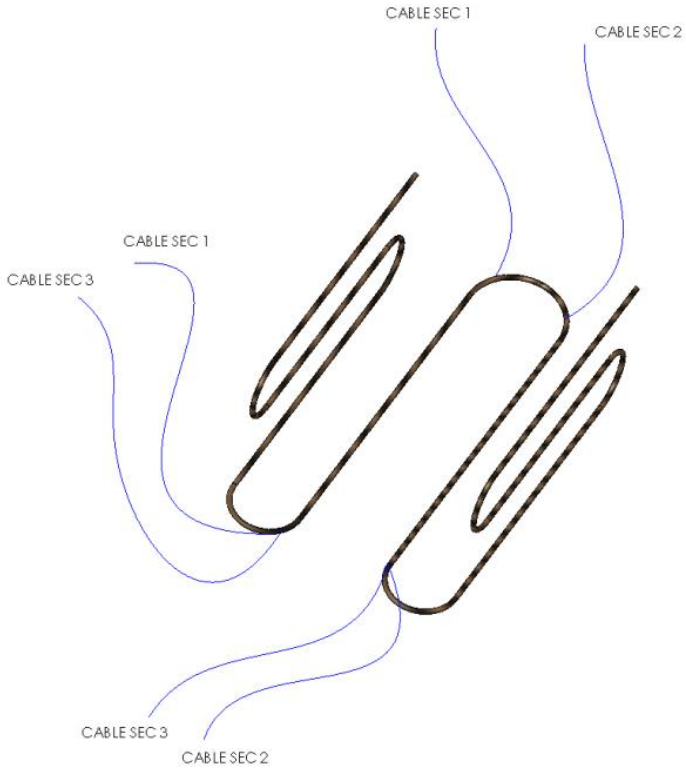

Fig. 3.7 Voltage tap mounting diagram.

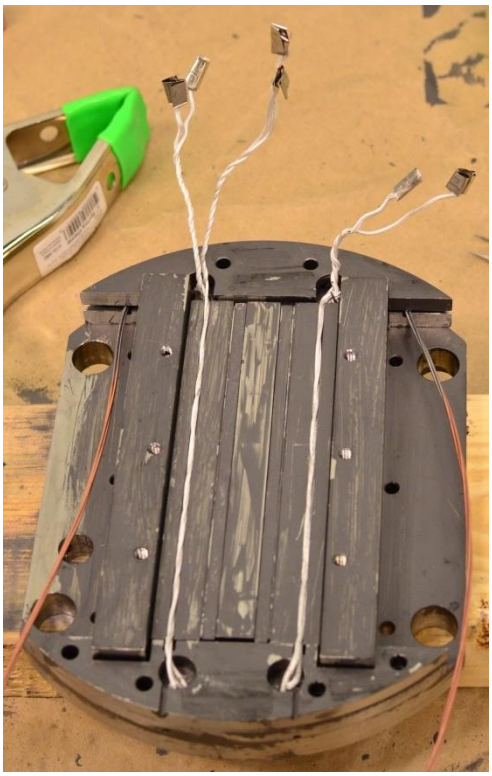

Fig. 3.8 Heat treatment assembly with voltage taps wired.

The voltage tap wires must be routed on through the grooves of the test section cable holder. The current voltage tap wires are springy and do not conform to a shape. One way to keep them together and in the groove is to twist the two wires inside the groove against each other Fig. 3.8. This allows the vertical force support to press flush against the test cable holder.

3.1.6 Vertical force cable support

At this point of the assembly, the current lead detection wires are inside the grooves and ready to for the next step of the assembly. Snake the voltage tap detection wires through the opening of the vertical support force prior to pressing the vertical support Fig. 3.9.

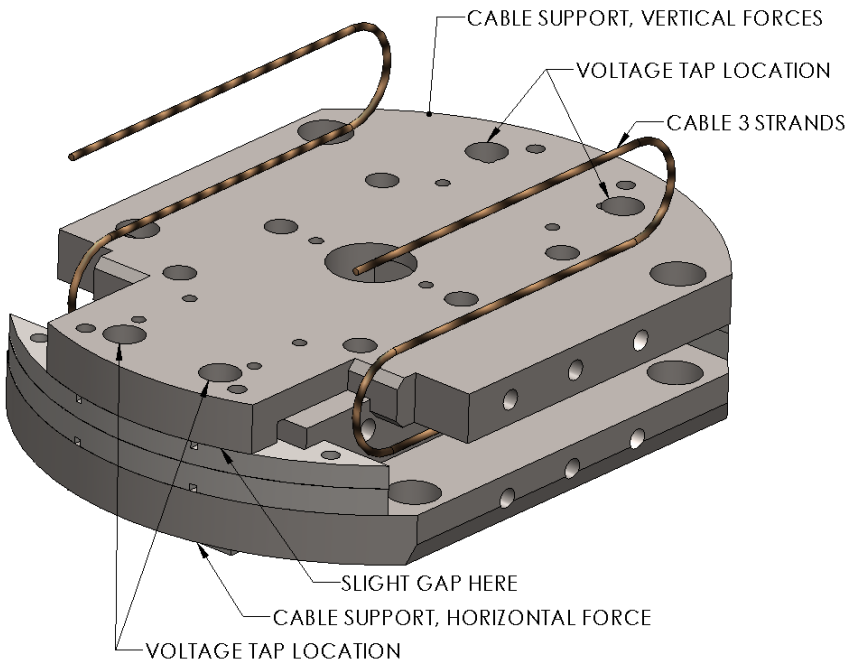

Fig. 3.9 Insertion of vertical forces cable support.

The vertical force support was designed to fit snugly against the horizontal force support. Some pressure from the top of the vertical support is required to

engage the two pieces together. Press the vertical support down until there is a small gap under it. The bolts can be inserted to hold the vertical and the horizontal support structure together. Tightening isn't necessary, as the copper current support will need to be inserted into the assembly and some slack is required for proper insertion.

3.1.7 Copper Current Lead Joint support

It is important to be aware of the wire when proceeding with this step, the copper current lead should slide smoothly, without significant use of force. To install the copper support, the grooved area of the current lead joint goes into the space between the vertical and the horizontal cable support.

As shown in Fig. 3.10, the grooved area that connects to the cable from the experimental area, slides toward the cable first. When the current lead is slid all the way to the cable holder, the back end of the current lead support can then be rotated and pushed toward the cable assembly, until it is pressed against the assembly. The current lead is supported with screws from the bottom of the assembly. They prevent any current lead movement as well as help provide rigidity of the structure.

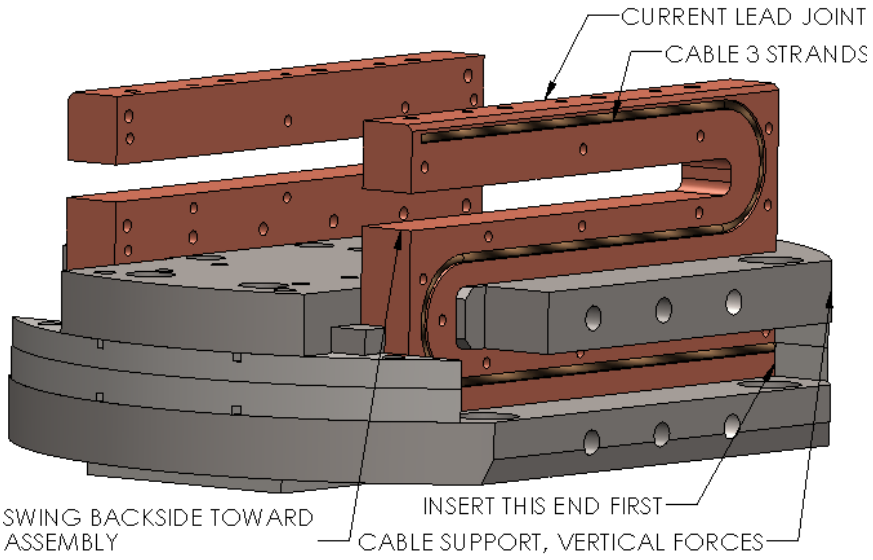

Fig. 3.10 Current lead copper joints are shown. They are already inserted into their respective final location.

The cable is secured in the groove of the copper current joint support with multiple steel plates, shown in Fig. 3.11. Each plate is secured with screws progressively starting from the cable holder all the way to the top of the copper support. The last securing plate of the copper support allows easy cable exit. The copper support installation procedure is repeated on the other side of the cable assembly. Those plates will be changed to G10 after the heat treatment and after soldering the sample to the copper joints.

3.1.8 Horizontal Clamp & Copper Current Joint Support and Top Cover

Before the heat treatment assembly is ready to be heat treated, a few steps need to be completed.

The heat treatment copper current joint support needs to be installed on both sides of the current lead joint. These supports provide structural support to the copper

lead joint and prevent any movement of the current lead joint during the heat treatment. Another function, which the current joint support provides is the access for the cartridge heaters via two through holes. These holes have been machined specifically to the diameter of cartridge heaters that are utilized after heat treatment to solder the sample onto the copper current joints. Solder will be feed through the holes of the cable cover or the covers will be carefully removed to have visual access to the sample and control the soldering process more adequately. During the heat treatment the current joint support is secured to the vertical forces cable support via 3 vertical screws, to keep the current lead joint stable throughout the process, Fig. 3.11.

The heat treatment cover is a stainless steel cover that keeps the assembly stable during the three week heat treatment. It bolts to the top of copper current joint support via three screws on each side.

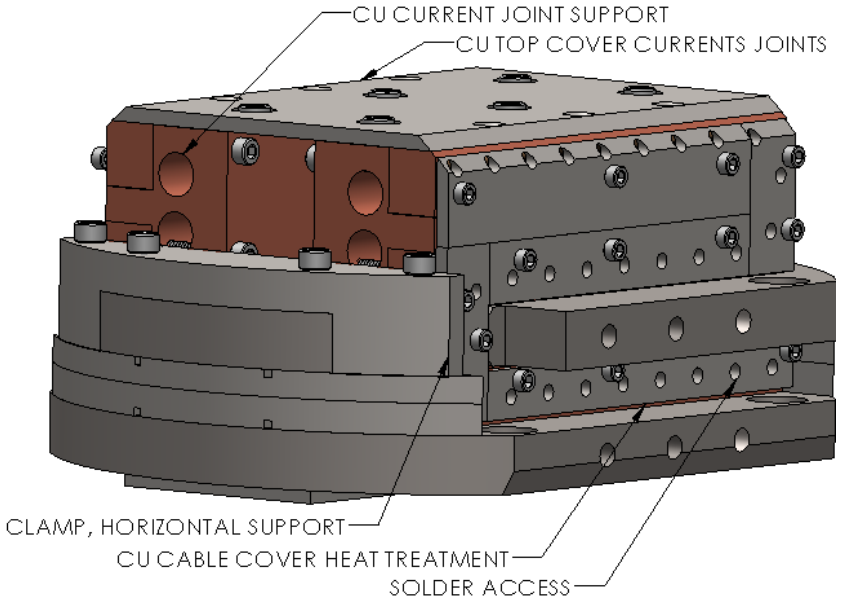

Fig. 3.11 Cable assembly as it should appear before heat treatment.

When everything is put together, bolted and secured, the heat cable assembly should look like Fig. 3.12 before going in the oven for heat treatment.

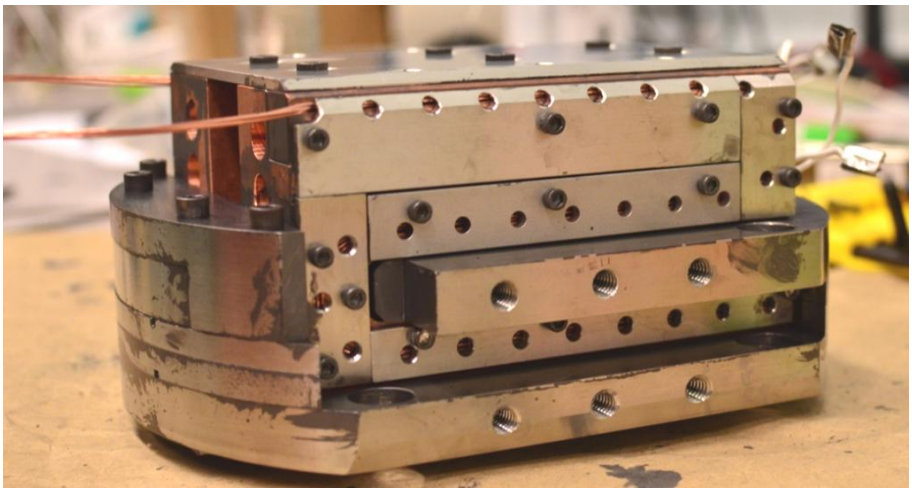

Fig. 3.12 Cable assembly ready to be heat treated.

3.2 Strand Heat Treatment

As described in section 1.5, the cable must be heat treated in order for niobium and tin can react to form Nb_3Sn superconducting filaments. Prior to heat treatment, the 3-strand wire is ductile and can be handled without any concern for damage. After the heat treatment, extreme care must be used in handling the cable as it becomes very brittle during the heat treatment process.

When the heat treatment configuration assembly is ready to go into the oven, it is first placed in the carrier support, which is made to fit into the oven, Fig. 3.13. During the heat treatment, the cable ends extends toward the cold section of the oven. This is done to prevent any material from leaking out when the assembly is heated in the hot section of the oven. Assembly is then placed at the location where it will be roughly in the middle of the heat treatment oven, where the temperature is more uniform than at its ends.

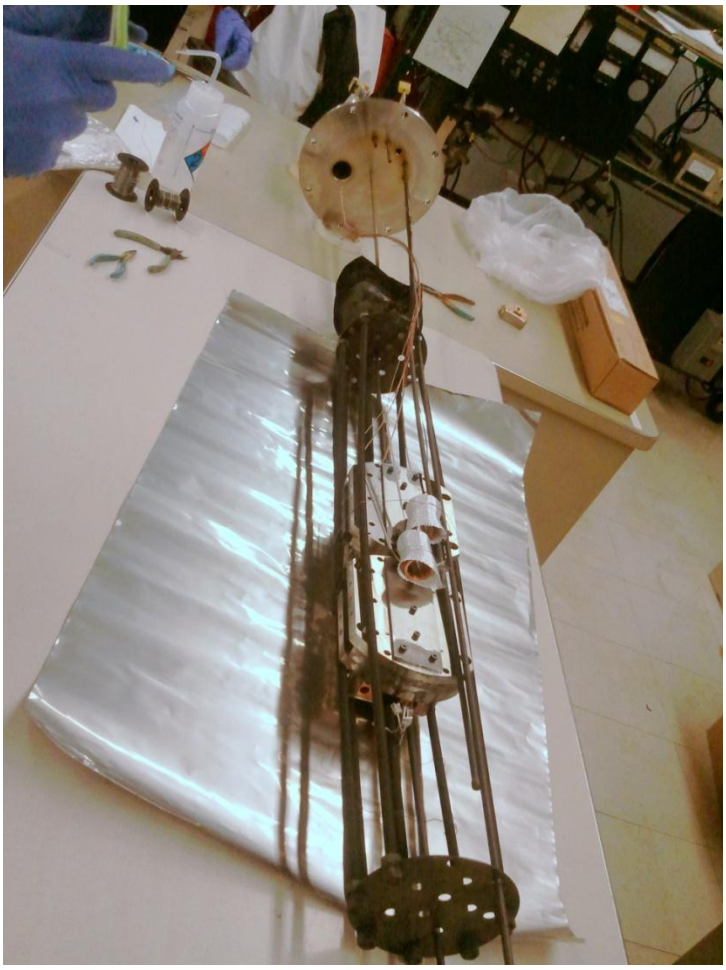

Fig. 3.13 Two transverse experimental assemblies ready to go into the oven for heat treatment. Notice the assembly is up-side down to fit better in the oven holder.

The ends of the voltage taps is clearly marked by covering the ends with a stainless steel foil, shown in Fig. 3.14. The foil is clearly marked by using a engraving pencil. This ensures correct wiring during the experiment, as it is not possible to install the voltage taps or check their locations after heat treatment once the sample cannot be manipulated due to its brittleness. The requirement of not moving the sample from its position after heat treatment is what drives most of the decisions during the design process from mounting, heat treatment to the final assembly for the experiment.

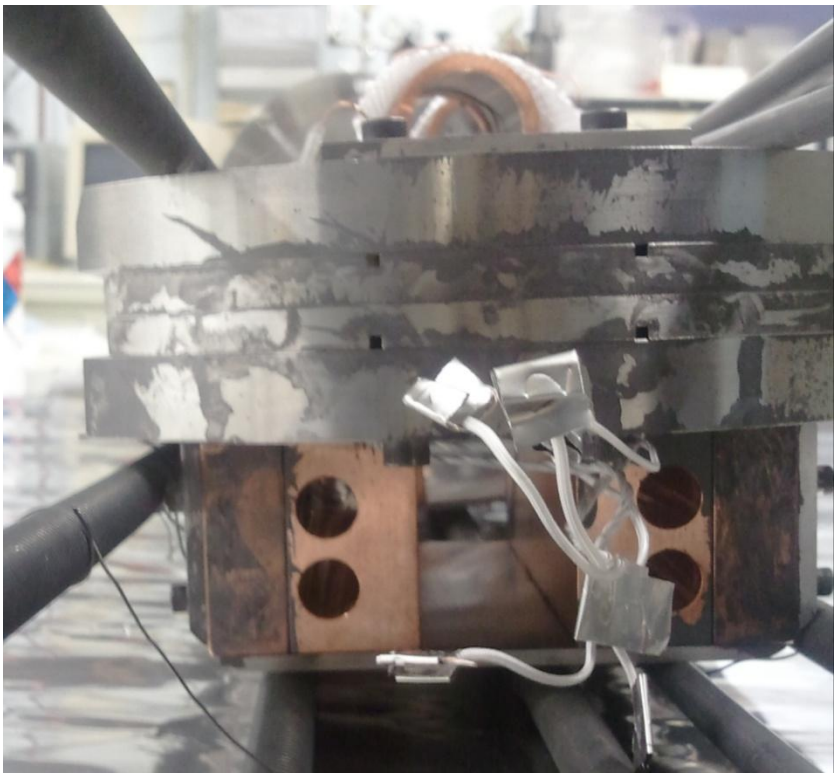

Fig. 3.14 Heat treatment cable assembly in the carrier. Voltage tap are marked with stainless steel foil.

When the heat treatment assemblies are positioned in the correct place in the carrier, they are secured using a stainless steel wire, Fig. 3.15. This prevents their movement during the carrier insertion into the oven.

Fig. 3.15 Two heat treatment cable assemblies secured in the heat treatment carrier.

The sample is wrapped with stainless steel wrap foil prior to placement in the oven, Fig. 3.16

Fig. 3.16 Carrier is wrapped with foil.

3.3 Mounting Cable Assembly Experimental Setup

The assembly is not yet ready for the tests at cryogenic temperatures when the heat treatment is complete. Multiple steps are required in order to convert the assembly from the heat treatment configuration into an experimental configuration where the critical current as a function of the applied mechanical load will be measured. The heat treatment was done at very high temperature for three weeks. Because of the high temperatures, no prior soldering could have been done and a few components will require soldering prior to the experiment. Some of the supporting plates used for during the heat treatment will be replaced with a lighter and just as supportive G10 material. Illustration Fig. 3.17 shows the final configuration of the experimental cable assembly.

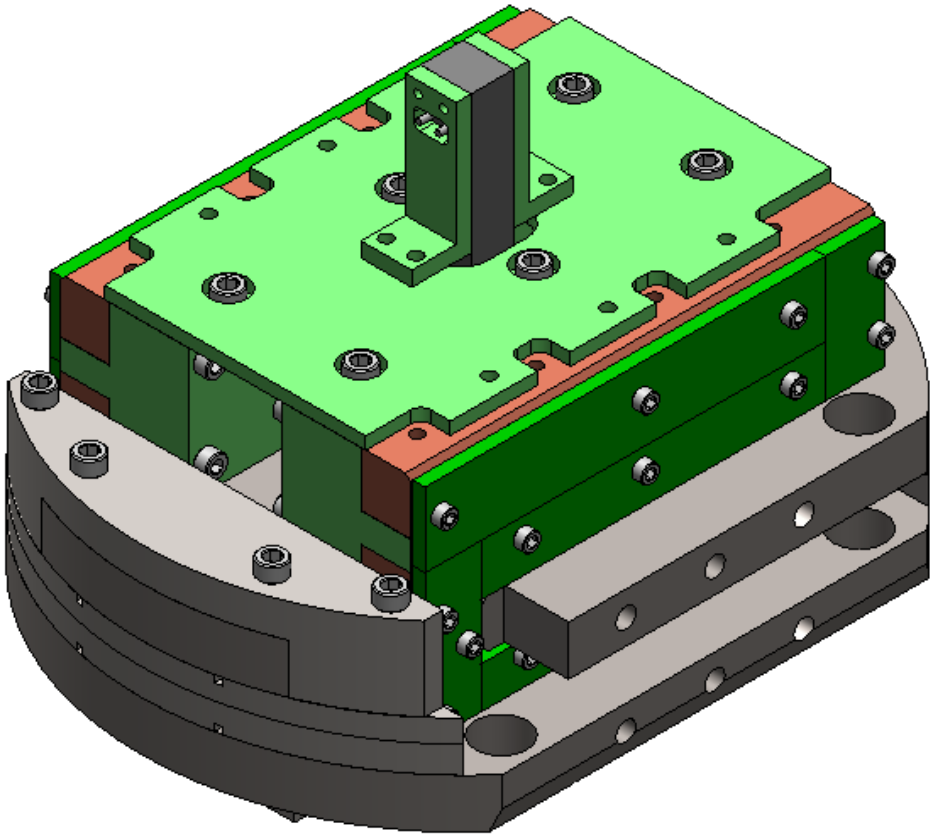

Fig. 3.17 View of what experimental assembly should look like when it's fully assembled.

3.3.1 Current joint support soldering

There are a few steps that are required in order to get the experimental assembly ready for the tests after the heat treatment. Soldering the cable to the copper current lead is critical. This connection will carry all the current and thus must be done with extreme care, making sure the solder makes positive contact with the cable. Cartridge heaters are required for this step. Each side of the assembly will be soldered separately by orienting the desired cable side vertically. After one side is soldered, cartridges will be moved to the other side of the assembly to solder the cable on the other side.

3.3.2 Voltage tap soldering.

In order to accurately measure critical currents, a good contact with the cable is desired. After soldering the cable to the copper current joint, the voltage taps leads must be soldered as well. The voltage taps leads were already wrapped around the cable prior to the heat treatment. There are two access holes, big enough for accept of a small soldering tip. If the soldering step fails it will be possible to read the voltages across the sample anyway even if the signal might be noisier.

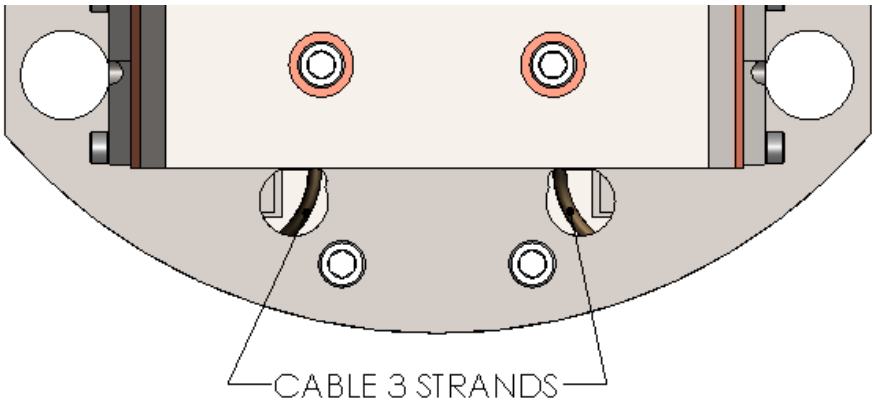

Fig. 3.18 Voltage tap cable access.

3.3.3 Replacing heat treatment Stainless Steel for G10 components.

After the soldering is complete, some of the parts that were used for heat treatment must be replaced with lighter and non-conductive G10 material, illustrated in Fig. 3.19.

The copper joint support that was used for stability as well as providing access for the cartridge support will be replaced with a G10 replica. The only difference is this current joint support is solid, without the cartridge holes. During

the experiment in Florida it will be used for mechanical support of the current lead joint.

The stainless steel cable covers are also replaced with its G10 equivalent. Although the cable is supported in the current lead joint by the solder, the G10 will provide an added factor of safety during the extreme experimental conditions.

The stainless Steel cover that was used to support the structure during the heat treatment will also be replaced with G10. This cover has additional feature. It has an opening as well as support to mount the extensometer. This will tell us precisely how far the wedge has moved vertically and it turns this will provide the transverse displacement of the pressing plates.

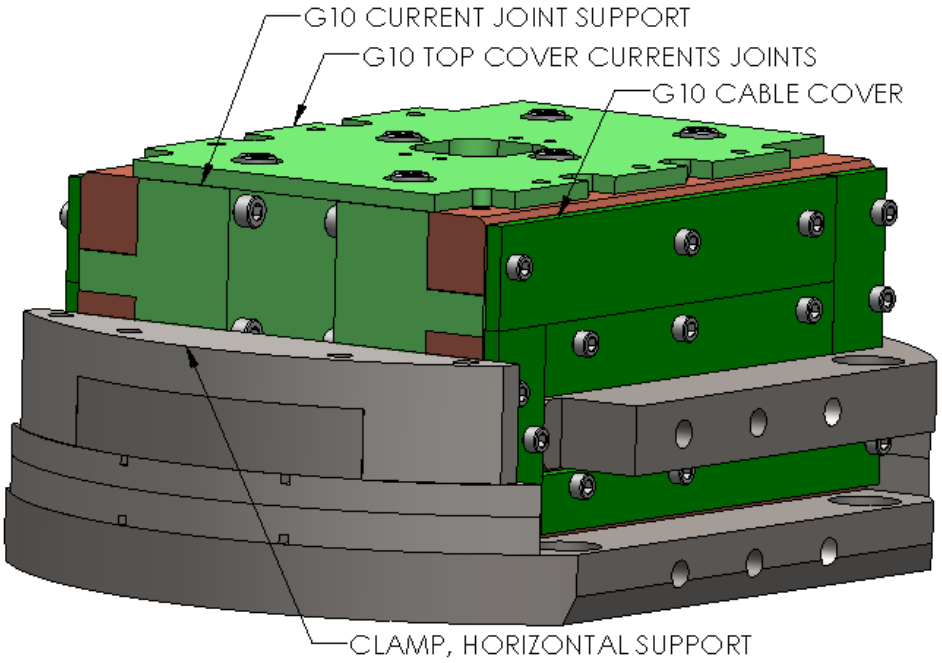

Fig. 3.19 View of the G10 top cover and horizontal clamp support, as well as current joint support

3.3.4 Extensometer mounting

To measure the vertical displacement of the wedge, extensometer must be installed. In order to do this, the heat treatment wedge must be disengaged and the test wedge inserted in its place. The shims that prevented the heat treatment wedge from compressing the cable are removed with the heat treatment wedge. The test wedge should be inserted with care to prevent any pressure put onto the cable, illustrated in Fig. 3.20.

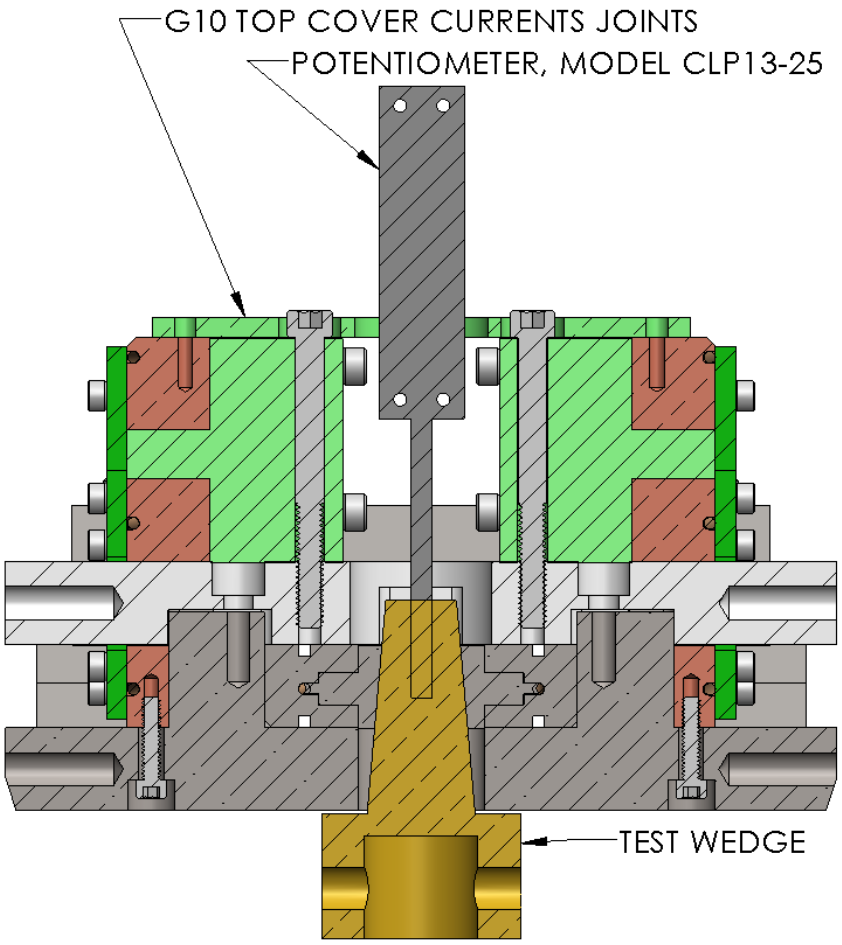

Fig. 3.20 Installation of extensometer and the wedge.

The assembly will be unstable at this point due to the test wedge being rather narrow and might have a tendency to tip over. It's a good idea to place support on opposite side of the wedge to keep the assembly stable. This will also prevent the compression of the test cable by limiting engagement of the test wedge into the assembly. When the test wedge is installed, insert the extensometer through the opening of the G10 cover. The extension rod will then thread into the test wedge. Thread the extensometer until you can't spin the rod any longer.

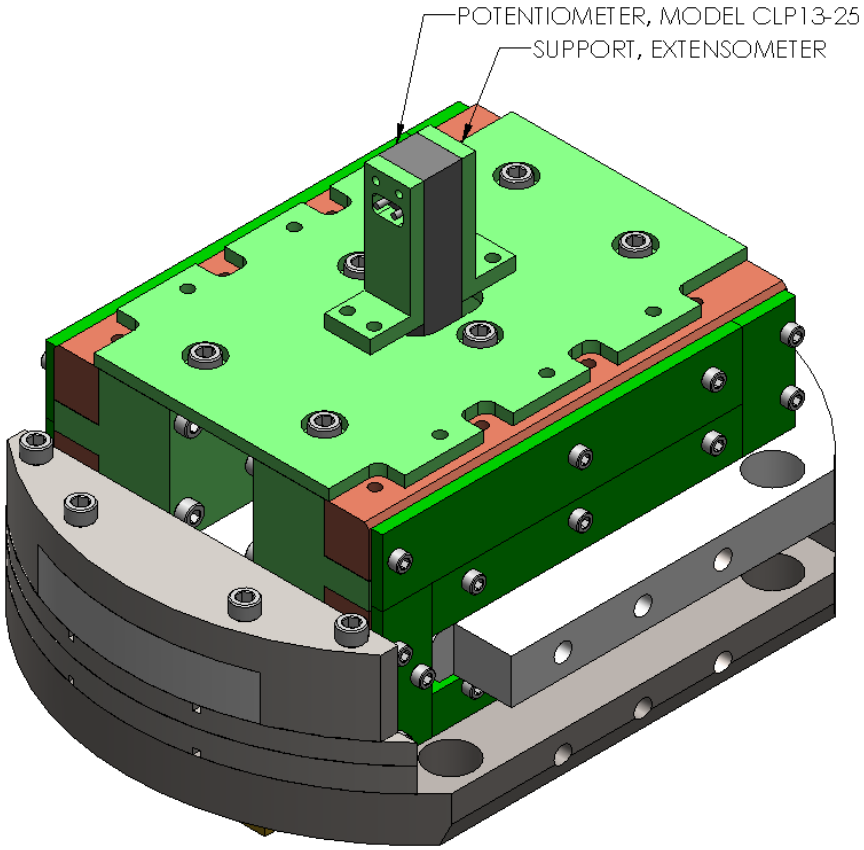

Fig. 3.21 Cable assembly ready for the experiment.

Shown in Fig. 3.21, the cable assembly is complete. To further continue the assembly, the gear assembly as well as the load cell assembly must be prepared.

Each moving piece must be coasted with the graphite to prevent galling during the experiment and reduce friction.

3.4 Mounting Gear Assembly

The gear assembly is put together in the similar fashion as it was put together in the previous experiments, shown in Fig. 3.22. BeCu bearing must be installed during this step under the input shaft and under both torque gears. Careful attention should be paid when lowering the top plate over the drive shaft bearing, making sure top plate is evenly lowered. The gear assembly was designed to be assembled without any significant effort. The joining parts should slide together with ease and do not require excessive force when put together.

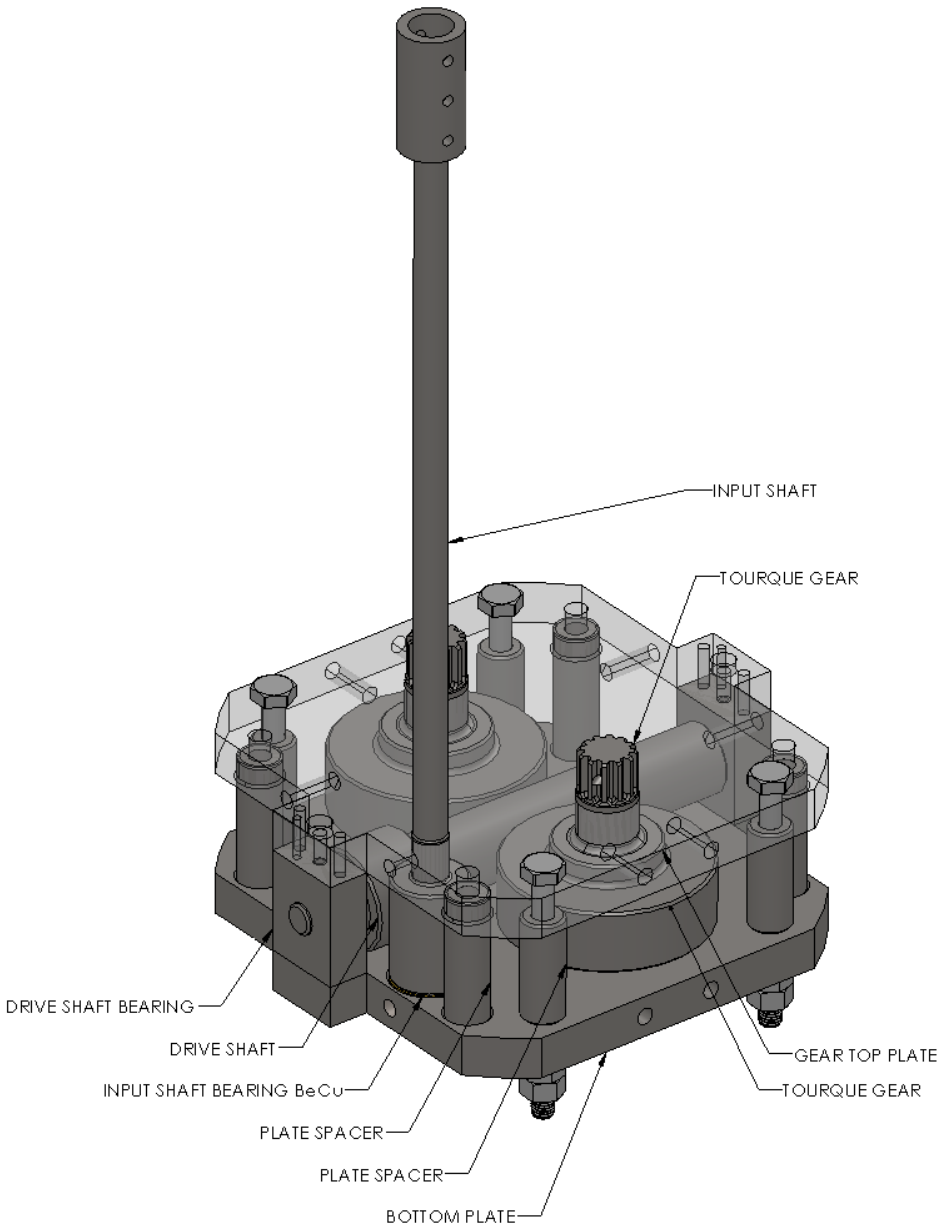

Fig. 3.22 Identification of Gear Mechanism parts.

3.4.1 Torque screw coupler

The torque screw couplers are slid onto the torque gears, Fig. 3.23. There is a left and a right threaded version of each screw. Although it's important to know the designated location of the left and the right screw, the securing holes have been machined in a way that the locking pins, not shown, will not slide all the way through

if the wrong screw is installed. The pins are installed to prevent movement the torque screw movement in the vertical direction.

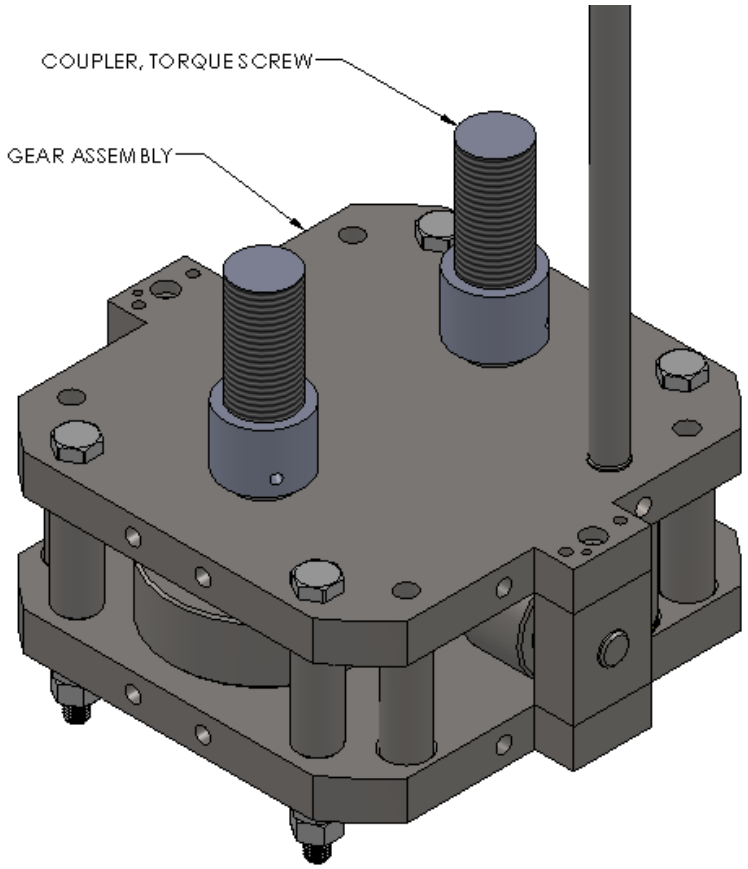

Fig. 3.23 Torque screw are custom designed with right and left threaded ACME threads.

3.5 Mounting load cell assembly

It is important to install and align the load cell assembly correctly. The load cell assembly was designed with a lot of flexibility for the user. This flexibility is important in order to fine tune the assembly.

The load cell is first mounted to the transfer plate by four large screws from the bottom of the transfer plate, shown in Fig. 3.24. The two mounting flanges are also secured to the transfer plate, from the bottom of the mounting flanges. The

ACME threaded nut was designed to slide into the mounting flanges and screw is threaded into the holes but not locked. In order to alignment the system, the threaded nuts are turned on the coupler torque screw. The distance from the four bottom corners of the transfer plates are measured to the top of the gear assembly. When the height between each side is identical or close, the locking screw can be tightened inside the threaded nut.

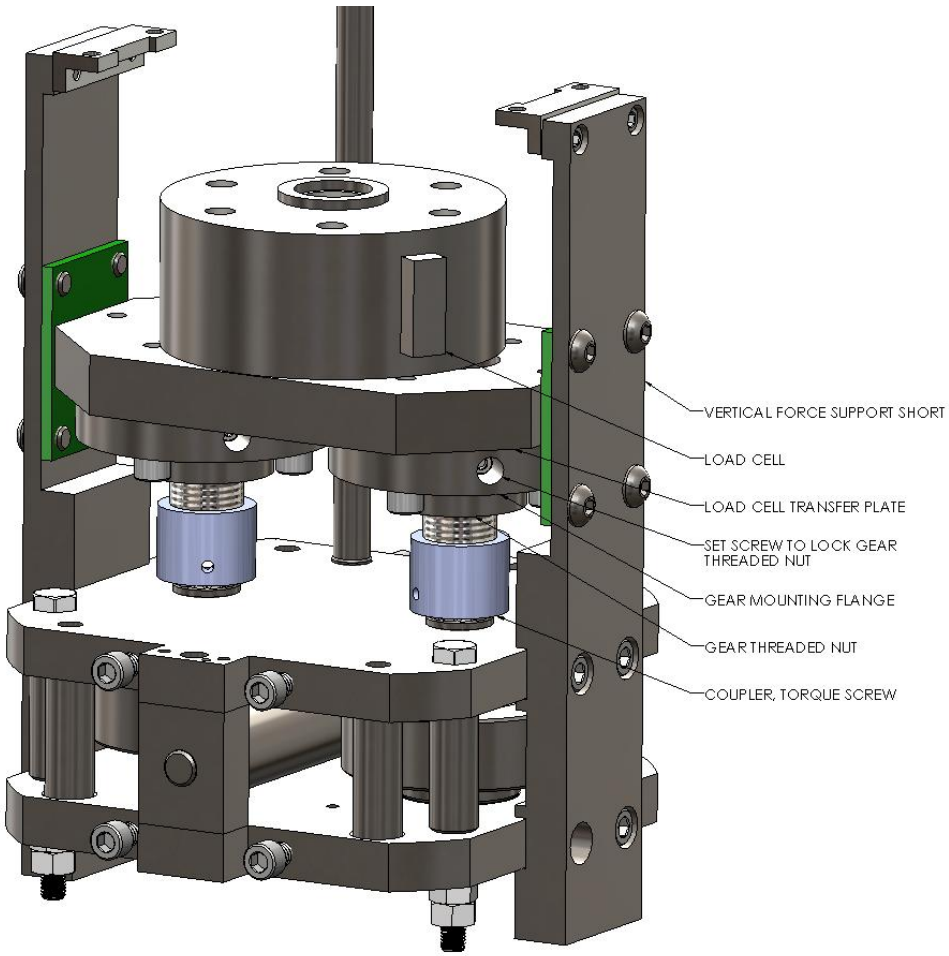

Fig. 3.24 Illustration of the Load Cell assembly and its components.

Before the set screws can be locked against the threaded nut, the transfer plate must be leveled. Four corners of the assembly were measured using calipers to verify

equal distance from the gear assemblies' top plate to the bottom of the transfer plate. Vertical support can also be installed at this point as well.

3.5.1 Wedge mounting and aligning

The wedge is installed after the load cell is installed and secured, illustrated in Fig. 3.25. The threaded rod screws into the load cell. It slides into the wedge without any threads in the wedge insertion area and is secured via a pin. The threaded rod allows height adjustability in the vertical direction.

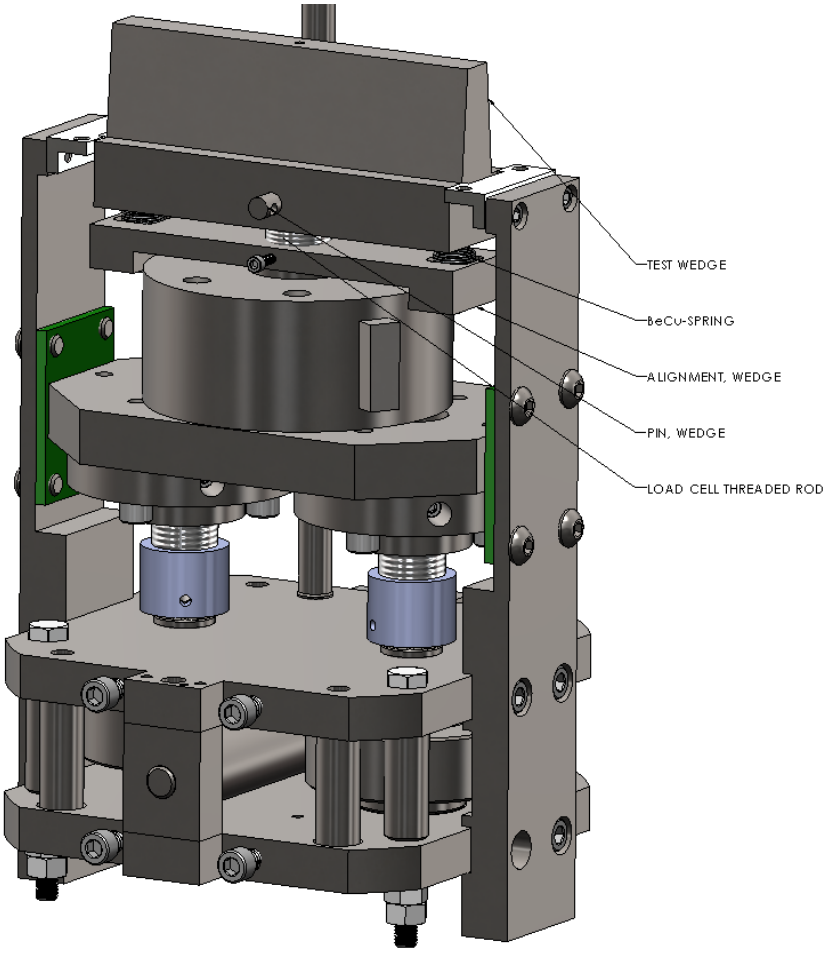

Fig. 3.25 Wedge installed on top of the load cell.

Before the cable assembly is lowered on the wedge, it needs to be aligned. The wedge alignment also shown in Fig. 3.25 was created for this purpose and it sits below the test wedge. The aligning works via two adjustable springs. The wedge is aligned to be as horizontal as possible to equalize the force across the whole area of the pressure plate.

3.6 Experimental design gear and cable assembly

The last step of the mechanical assembly is the lowering of the cable assembly onto the wedge. The short vertical force support, Fig. 3.26, will support and balance the assembly during the installation. The long vertical force support can now be installed, mounting it to the gear mechanism and the cable assembly. The last step is to install the vertical rods, when mounted; they connect the experimental assembly to the support structure of the probe shown in Fig. 2.3, which will be lowered into the cryostat.

Although electrical assembly is not covered in this thesis, the current leads have to be connected to both of the current lead joints. The voltage tap wires, extensometer and load cell wires also have to be brought up to the top of the probe and outside the cryostat in order to make all the necessary measurements.

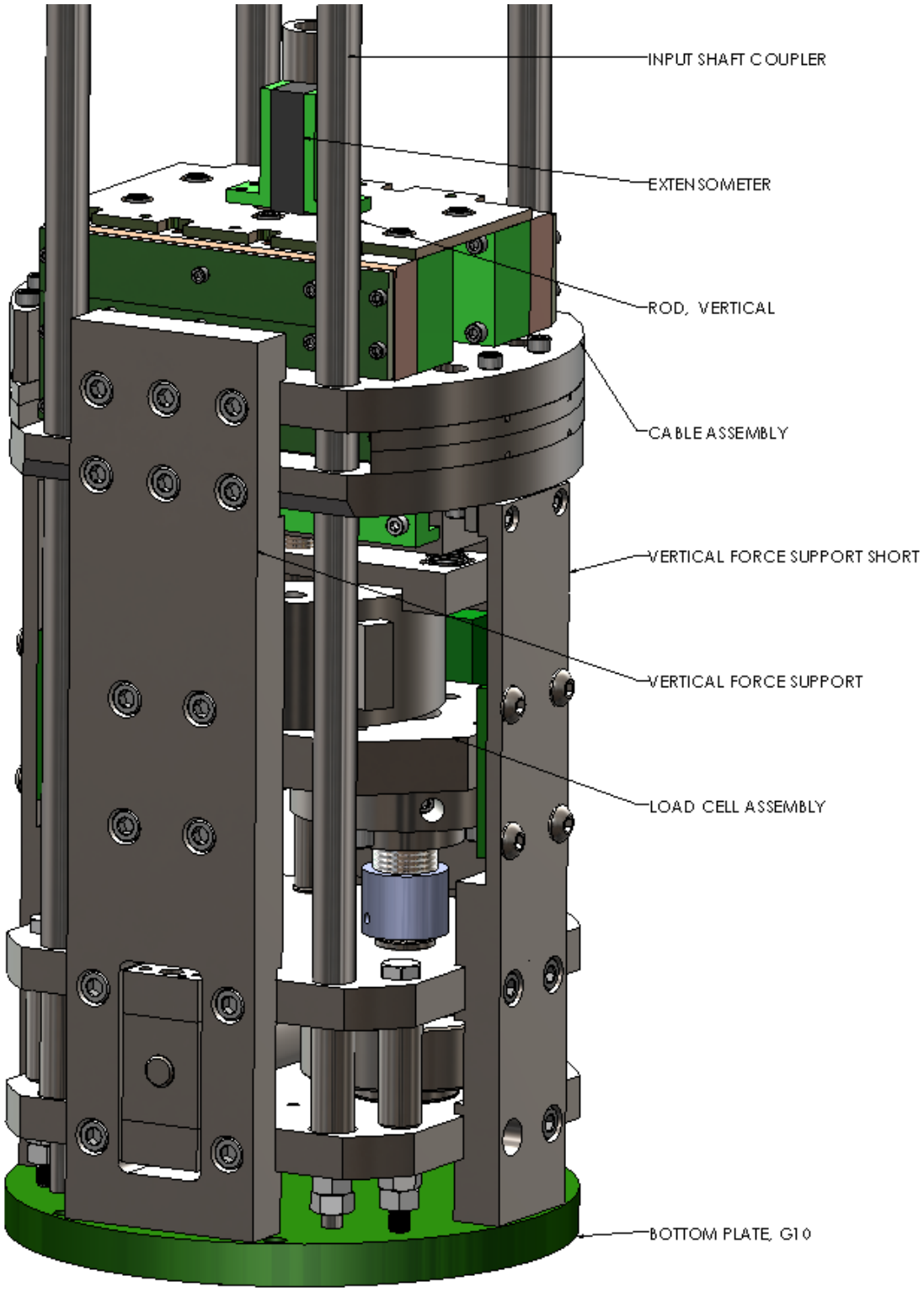

Fig. 3.26 Final Experimental Assembly

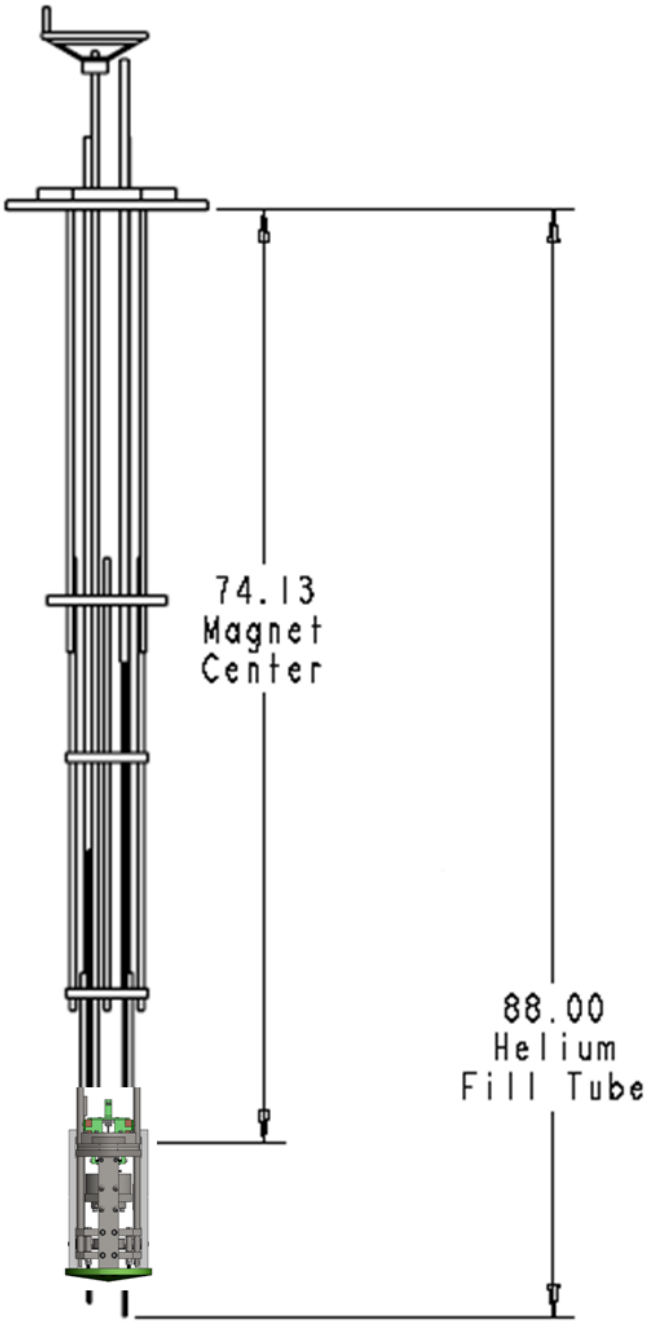

Fig. 3.27 Schematic of how the transverse experiment is loaded into the cryostat.

Chapter 4 FE Analysis

Finite Element Analysis (FEA) was used to check the structural integrity of the design. When performing experiment in a cryogenic environment, it is important to make sure that the design meets and exceeds the structural factor of safety.

The design was created using Solidworks 2010. The FE analysis was performed using an add-in in Solidworks called Solidworks Simulation. This software package allows the user to perform FE analysis of the system to verify a design. Although the simulation package has a build-in library of materials, www.matweb.com was used to verify the material properties and when appropriate the built-in properties were updated.

For practical reasons, simulation studies were broken up into smaller sections consisting of the integral parts relevant to the analysis. This speed up the meshing of the parts and reduced the number of elements each mesh contained. In some instances, where the simulation had trouble meshing, some component features such as small holes were suppressed.

Starting a simulation in Solidworks is straight forward. Start by creating a new study. There are options of different types of studies to create. For these cases all the studies created are static simulations. Other options include frequency, thermal, vibration analysis, etc., these simulations are not of interest in this work. Each body in the simulation can have different physical properties and can interact with other bodies in different ways. If the model is too large to simulate but is

symmetrical, simulation can take advantage of the symmetry. Reducing the number of bodies in the simulation can also simplify it.

In order to run the simulations, initial conditions must be defined. First, a face of a model must be fixed. These points will have zero displacement during the FE analysis. The load must be applied, in this case, a force applied to a particular part of the model. Appropriate material must be applied to each of the components.

It should be noted that the material properties tend to get better as the temperature decreases. These simulations assume room temperature initial conditions and do not account for the cryogenic temperatures. Partly, the reason for this is the difficulty to acquiring accurate material properties at these cryogenic temperatures.

4.1 Pin to wedge connection

It is important to analyze the wedge to pin connection, illustrated in Fig. 4.1. This creates a double shear connection. The pin has a small diameter, 0.250 inches, fits into the threaded wedge and is being held at ends by the test wedge. The pin is made of stainless steel 316 material while the wedge is brass.

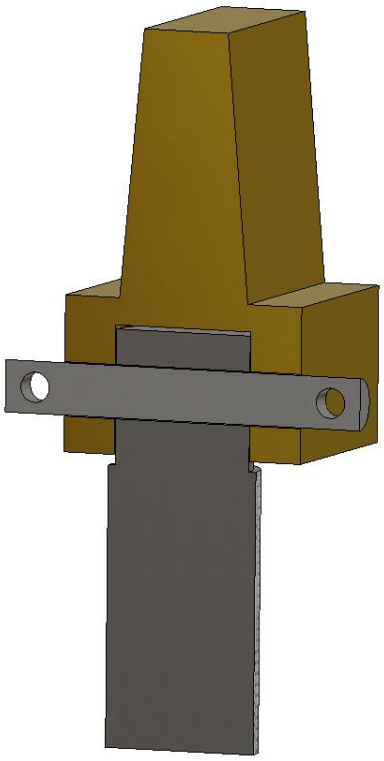

Fig. 4.1 Wedge to pin experimental setup.

This setup is putting the pin in a double shear tensile stress. Using Eq. 4.1, the tensile strength can be calculated. The diameter of the pin is 0.25 inches. The results are shown in Eq. 4.2.

$$\text{Tensile stress per side } \sigma = \frac{F}{A} \tag{4.1}$$

$$\sigma = \frac{4000\ N}{\frac{\pi d^2}{4}} = 126.3\ MPa \tag{4.2}$$

The tensile stress per side is 126.3 MPa. The total stress that's being applied to both surfaces is 252.6 MPa. Doing this hand calculation helps to check the results given by the FEA analysis.

To run the simulation on this assembly, it was necessary to simplify the model. The model was split into two halves and the back of the wedge. The back of the wedge was also removed, since the force applied to the system is right around the

area of the threaded component. This simplified the mesh, shown in Fig. 4.2, and made the simulation run quicker. In areas of interest, a localized mesh control was applied and the mesh size was decreased for better resolution and accuracy of the results. When the mesh is successfully created, the model is ready to be analyzed. Typically three different results are looked at. Stress, represented via Von Mises, displacement in mm for these models and normalized strain, typically in the direction of interest.

The FEA setup constrained the drafted part of the wedge as fixed surfaces, represented as green arrows. The force applied, 6000 N is represented by the purple arrows on the threaded wedge.

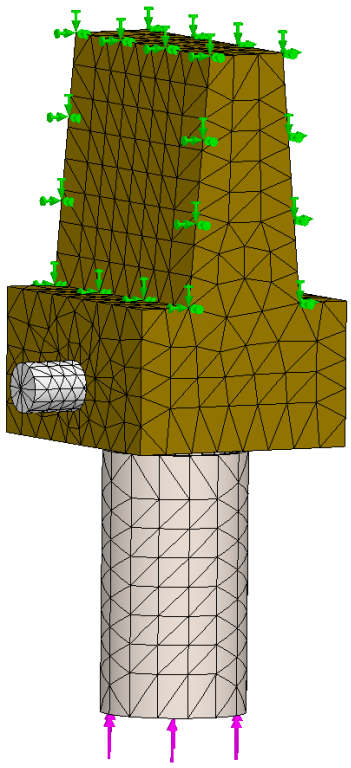

Fig. 4.2 Mesh of the pin to wedge assembly.

The result of the stress analysis is shown in Fig. 4.3. The model shows what was expected. The area where the pin was pressed with the threaded wedge has a higher stress concentration on the bottom. The area that is pushing on the test wedge has a higher stress concentration on the top surface and minimal on the bottom. The maximum stress exhibited by the pin is 262 MPa, compared to a hand calculation of 252 MPa.

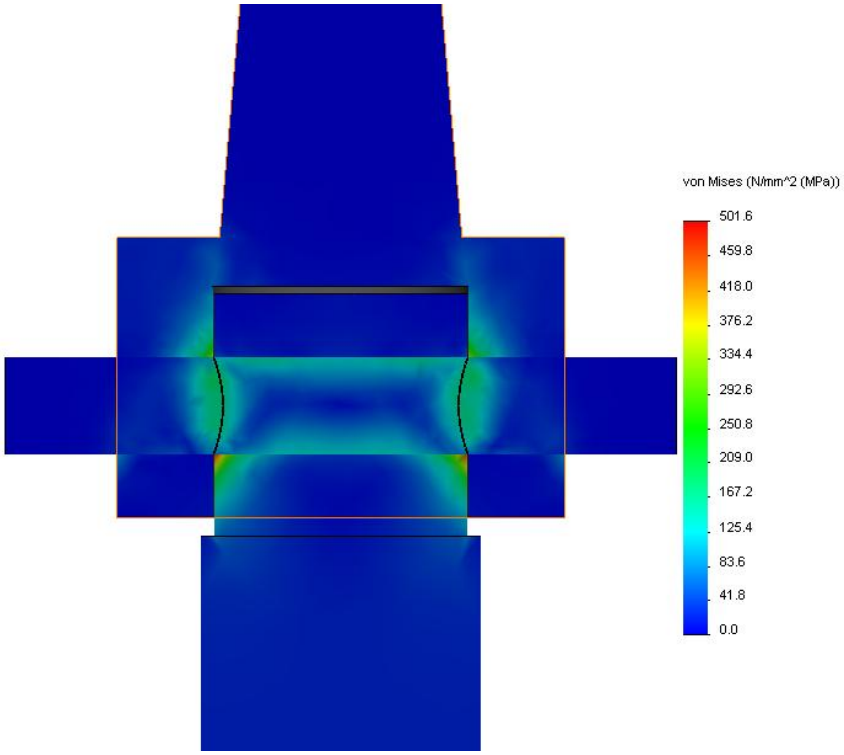

Fig. 4.3 Von Mises pin to wedge assembly.

The hand calculation is relatively close to the FEA analysis. Hand calculation is the ideal case with the average stress over the calculated area. FEA analysis allows deeper understanding by showing localized stresses. One way to isolate the high stressed area is by using a feature in Solidworks called Iso Clipping. This feature shows the stresses at a particular value and higher. Fig. 4.4 shows such a chart at 200 MPa and above. Both the threaded wedge and the test wedge show high stresses in

the of double shear area of the pin. The high stress areas in both parts are under compression, and will be able to withstand the stresses applied to them by the gear mechanism.

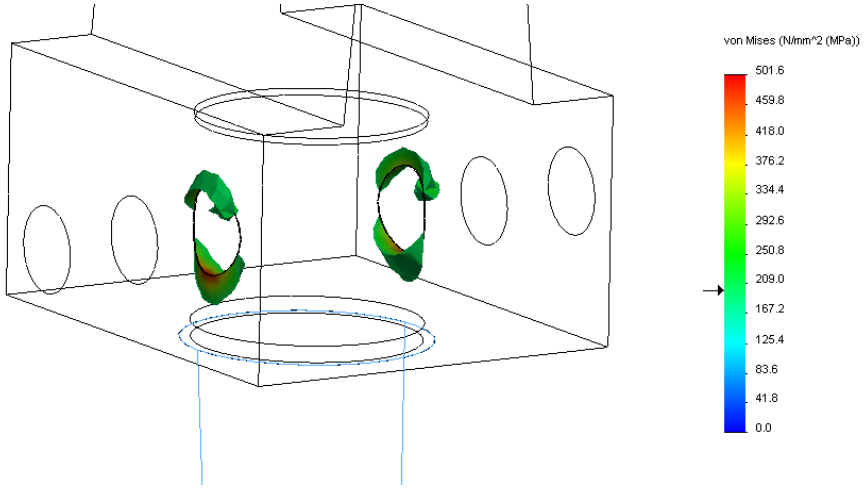

Fig. 4.4 High stresses shown of Iso clipping at 150 MPa.

Total displacement is shown in Fig. 4.5. The displacement of 0.025 mm is small. This will not contribute significantly to the result of the experiment.

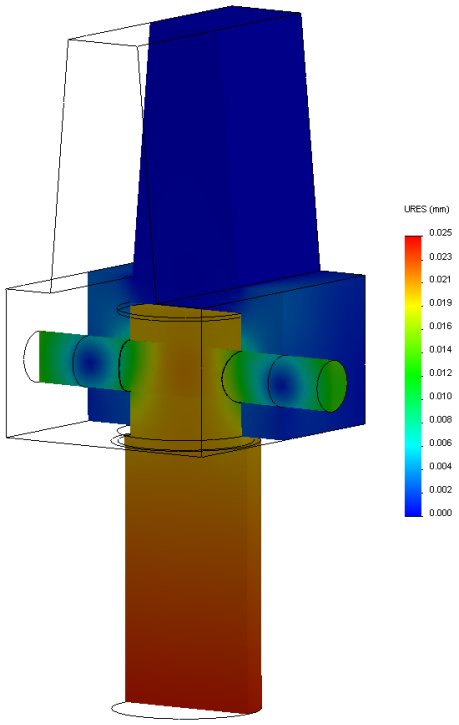

Fig. 4.5 Displacement of the assembly.

Normal strain in the vertical direction is shown in Fig. 4.6. Like the displacement, this should not be a problem for the experiment, with only minimal strain applied to the assembly.

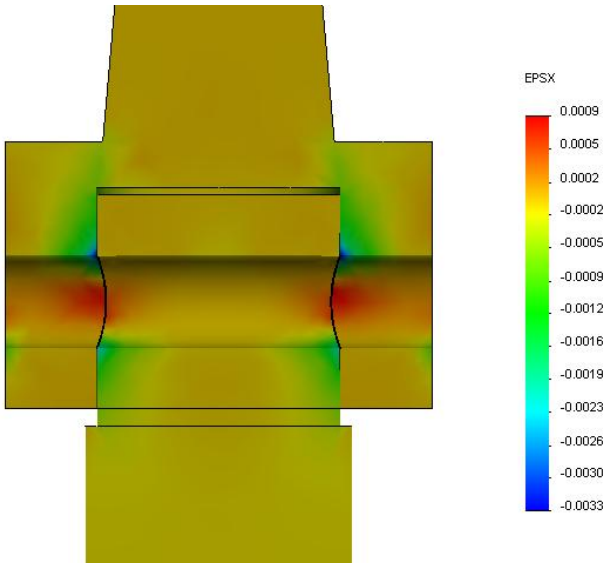

Fig. 4.6 Strain analysis of the pin to wedge assembly.

4.2 Vertical support forces

The vertical support is a structure, connecting the gear mechanism with the cable assembly. When the gear mechanism is engaged, this structure must be strong enough to withstand the forces of the wedge as it pushes against the vertical force support plate. The following section goes over the FEA analysis to verify the structure is sound.

The vertical support is being held by four holes on each of the vertical force support components. This represents how the vertical supports are bolted to the gear assembly in the real experiment. The fixed surfaces are seen on the bottom and illustrated with green arrows. The force applied and its direction is shown with purple arrows, illustrated in Fig. 4.7. These would be the surfaces to which the forces will be applied against. The external vertical force applied is 6000 N applied to the bottom surface of the cable support horizontal force plate. 6000 N was used based on the experimental results gathered from previous experiments on the force requirements to obtain the desired mechanical load on the cable [6]. The applied force accounts for range of forces that are necessary in order to compress the 3-strand cable. The vertical force support will be bolted to the cable support using three ½ inch bolts. The material for cable support vertical force was set to be titanium, Ti-6Al-4V, and the vertical force support to Stainless Steel 316.

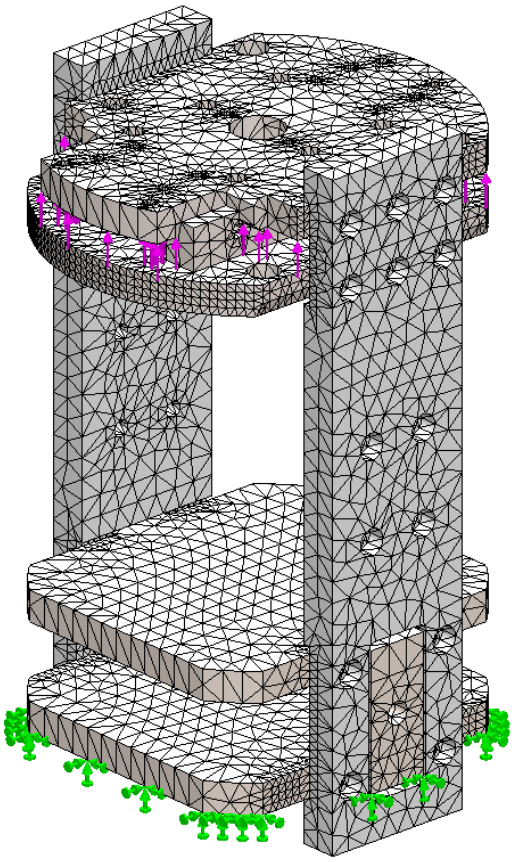

Fig. 4.7 Vertical force assembly FEA connections and loads with mesh used to analyze the model. The load is distributed on the entire bottom surface.

The mesh for the vertical support is illustrated in Fig. 4.7.

The results of the FEA stress simulation are shown in Fig. 4.8, the maximum von Mises felt by the system is 59 MPa. This value is well below the yield tensile strength of Titanium Ti-6Al-4V of 880 MPa indicating the structure will be strong enough to react the vertical forces.

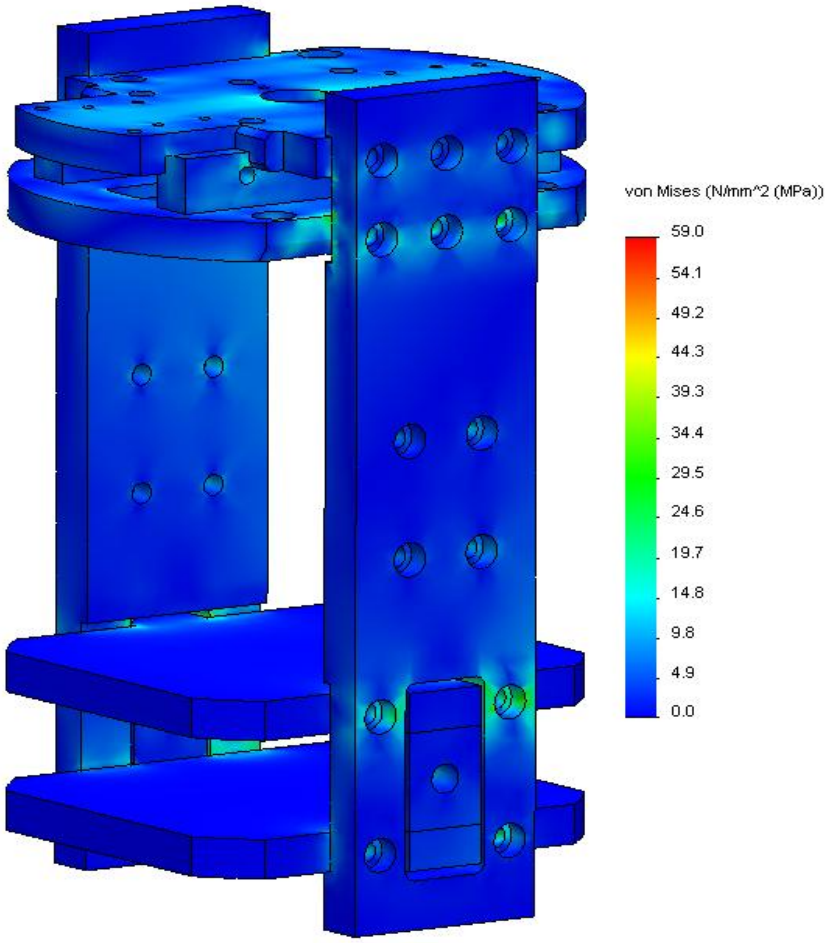

Fig. 4.8 Von Mises Vertical Force Stress Simulation of the vertical support assembly

The displacement of the assembly is shown in Fig. 4.9. The highest displacement in this limited model is 0.032 mm. It should be noted that the vertical support brackets exhibited limited displacement. The area of the highest deflection is in the cable support for the vertical forces.

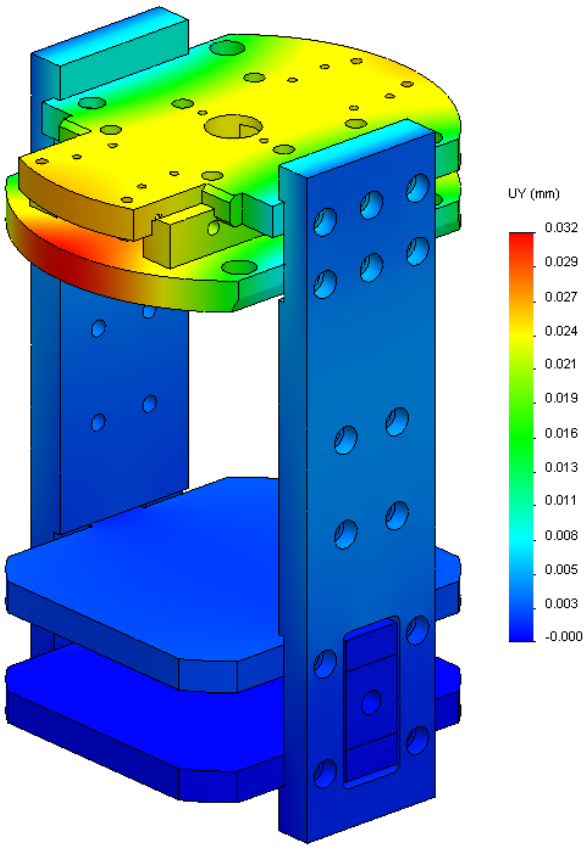

Fig. 4.9 Resultant Displacement showing the maximum change of 0.188 mm.

The strain of this assembly is shown in Fig. 4.10. The maximum strain observed of .0003 is insignificant.

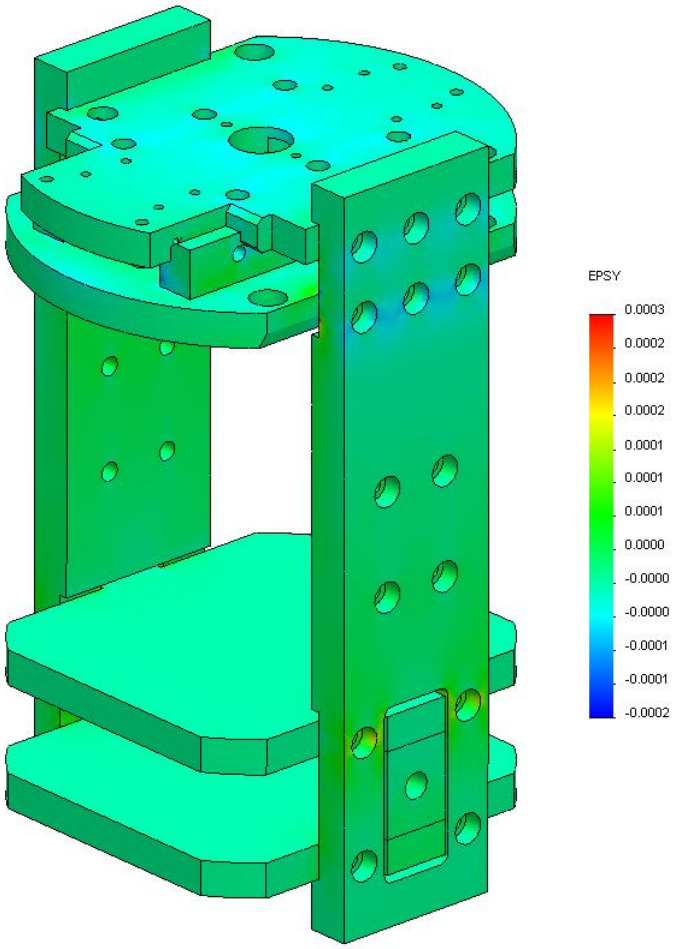

Fig. 4.10 Strain in vertical axis

4.3 Horizontal support forces

The horizontal support reacts with the test wedge when the wedge is being vertically engaged. This structure must be strong enough since the forces felt by this assembly are significantly higher than in the vertical support structure. The horizontal support structure consists of both the vertical support plate engaging over the horizontal support plate. When bolted together this structure will resist the forces applied to the cable. To strengthen this structure, another piece was added, a support clamp. The clamp helped equalize both sides of the assembly, as the vertical support plate isn't symmetrical.

The structure with two plates and the clamp support is analyzed for the stress, displacement and the strain, and is illustrated below. Fig. 4.11 shows the mesh applied to the part. It should be noted that, to improve the mesh, small holes cable support horizontal forces and cable support vertical forces have been suppressed.

Setting up the initial conditions for this experiment was more complicated than the previous one. The wedge moves vertically and thus applies its forces to the pressure plates equally to both sides of the structure. Thus to represent this phenomena, the structure is divided in half as shown in Fig. 4.11. The total load is expected to be around 60,000 N, based on results from previous experiment [6] as well as previous equations Eq. 2.1 and Eq. 2.2. Given the vertical load of 6,000 N, a transverse of roughly 30,000 N per side is then calculated. The surfaces that are in the middle are both symmetrical and the fixed structure against which the forces will be applied too, representing with green arrows. Since symmetry is utilized, half of the total load, 30,000 N is applied to the vertical area that resists the forces of the wedge, represented below with purple arrows. The surfaces where the top and bottom plate connect, a slide connection was applied, representing the physical phenomena.

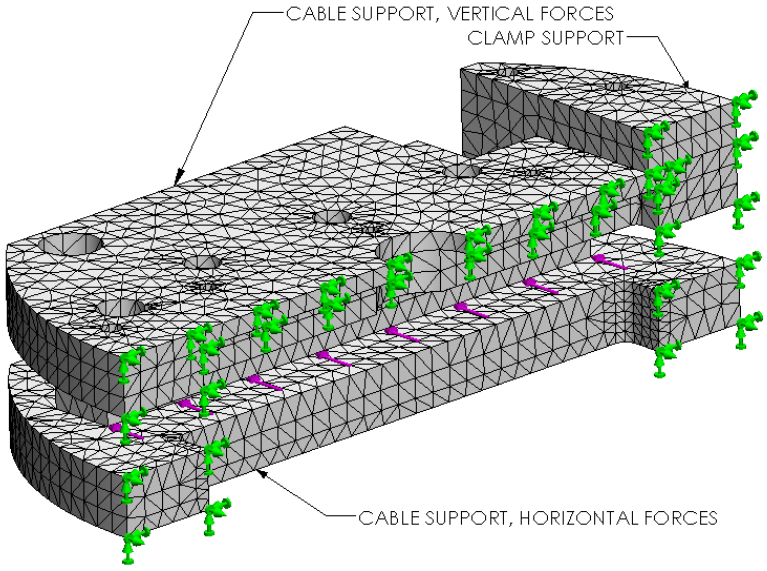

Fig. 4.11 Horizontal force mesh.

The stresses of the assembly are relatively low compared to the tensile yield of the titanium material. Fig. 4.12 and Fig. 4.13 illustrate the stresses, the maximum stress, at the corners of the area where the wedge will be engaging the assembly, is 81 MPa.

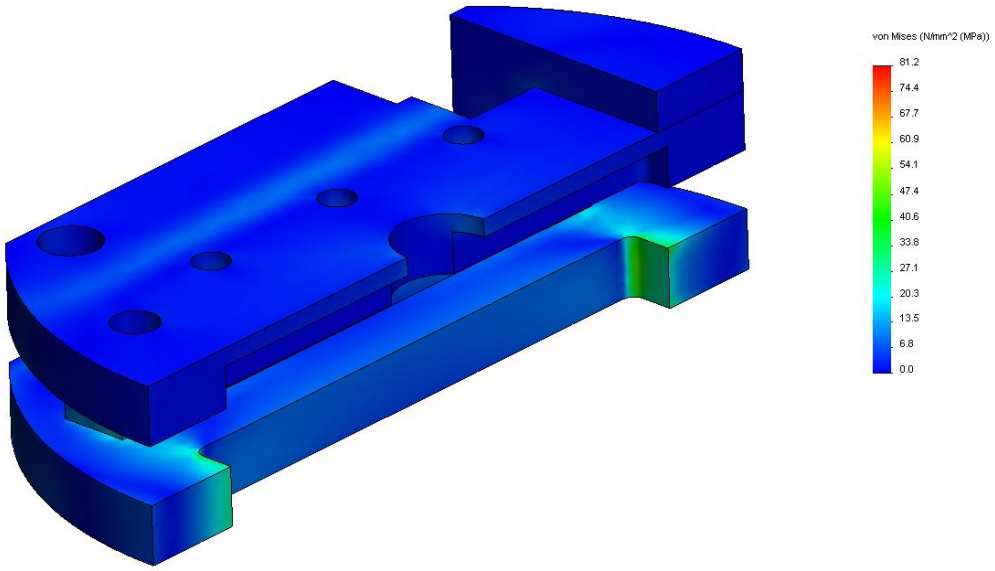

Fig. 4.12 Von Mises vertical force stress simulation of the horizontal support assembly.

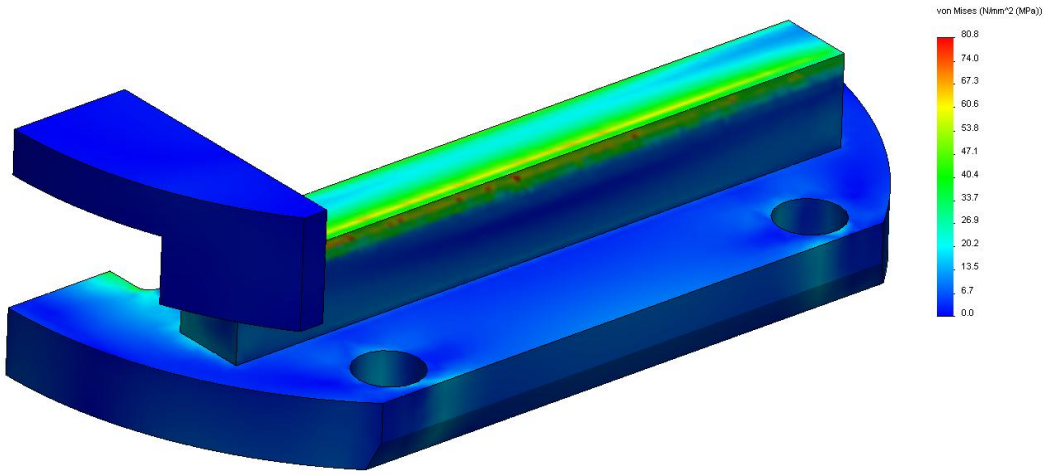

Fig. 4.13 Von Mises stresses with top plate removed. Maximum stresses are shown in the corner, as expected.

A cross-section of the assembly is shown in Fig. 4.14. The third principal stress illustrated in the corner is the maximum compression of the system.

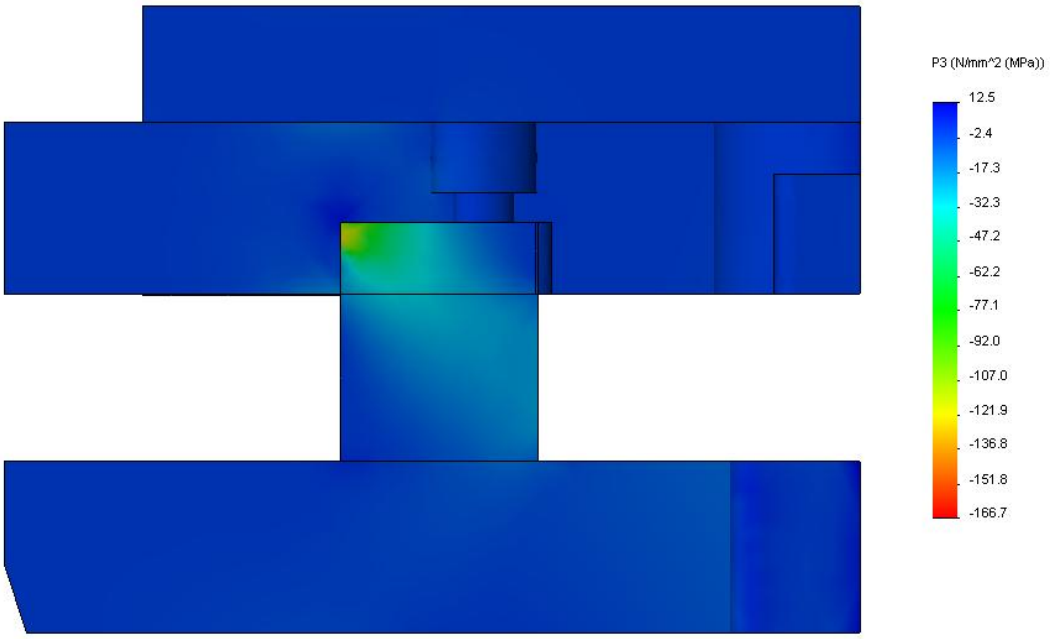

Fig. 4.14 Third principal stress shown in MPa.

The displacement shown in Fig. 4.15 shows the maximum displacement of 0.013 mm. It should be noted that the area of interest, has relatively low displacement change, which is desired during the experiment.

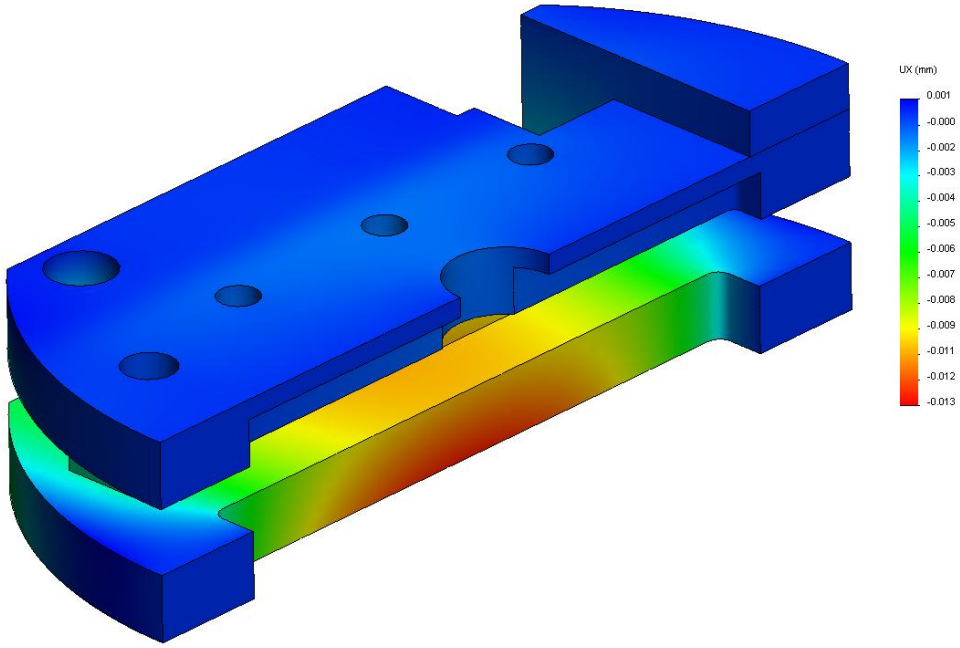

Fig. 4.15 Resultant Displacement showing the maximum change of 0.04 mm. FEA analysis shows that the strain is minimal at .0004 at its maximum point.

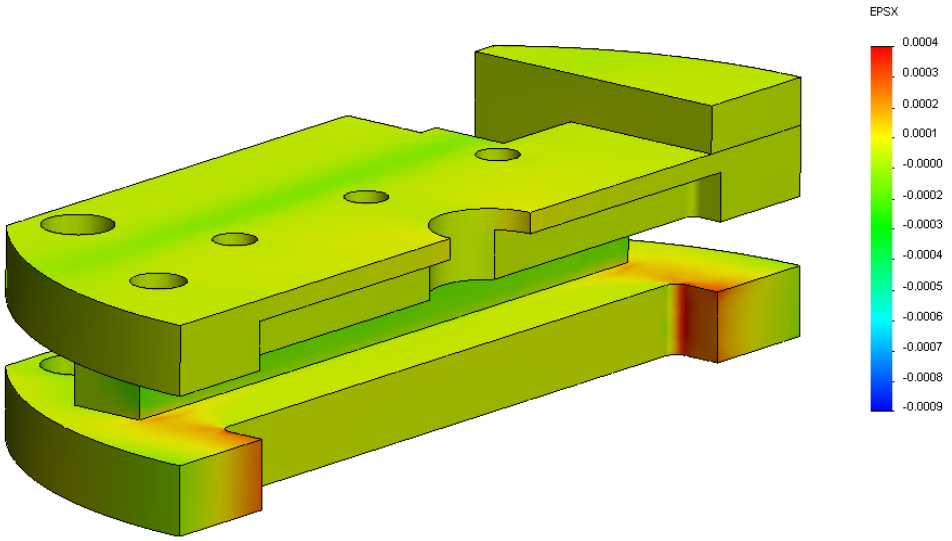

Fig. 4.16 Strain in the direction of the force.

Three major areas of stress have been analyzed to verify structural integrity. The analysis supported that the structural design is sound and will withstand the forces that will be applied to it.

Chapter 5 Room temperature Test & Analysis

When the parts for each assembly have been manufactured and all the hardware ordered, it was time to put the assembly together in steps and start testing the functionality. The gear mechanism and the load cell assembly parts below the load cell were machined by the same machine shop to ensure everything connected and worked together the way it was intended. The rest of the components were manufactured using various machine shops. As mentioned earlier, the tolerances of critical components were controlled to ensure the parts would work together despite being machined in various places.

5.1 Low force room temperature experiment

It was important to test whether the experimental setup, particularly, the cable assembly was working in the way it was intended. The test wedge, which compresses two different pressure plates, needed to be tested for its functionality. The question is whether the pressure plates would apply the same pressure onto the cables when the gear mechanism was engaged.

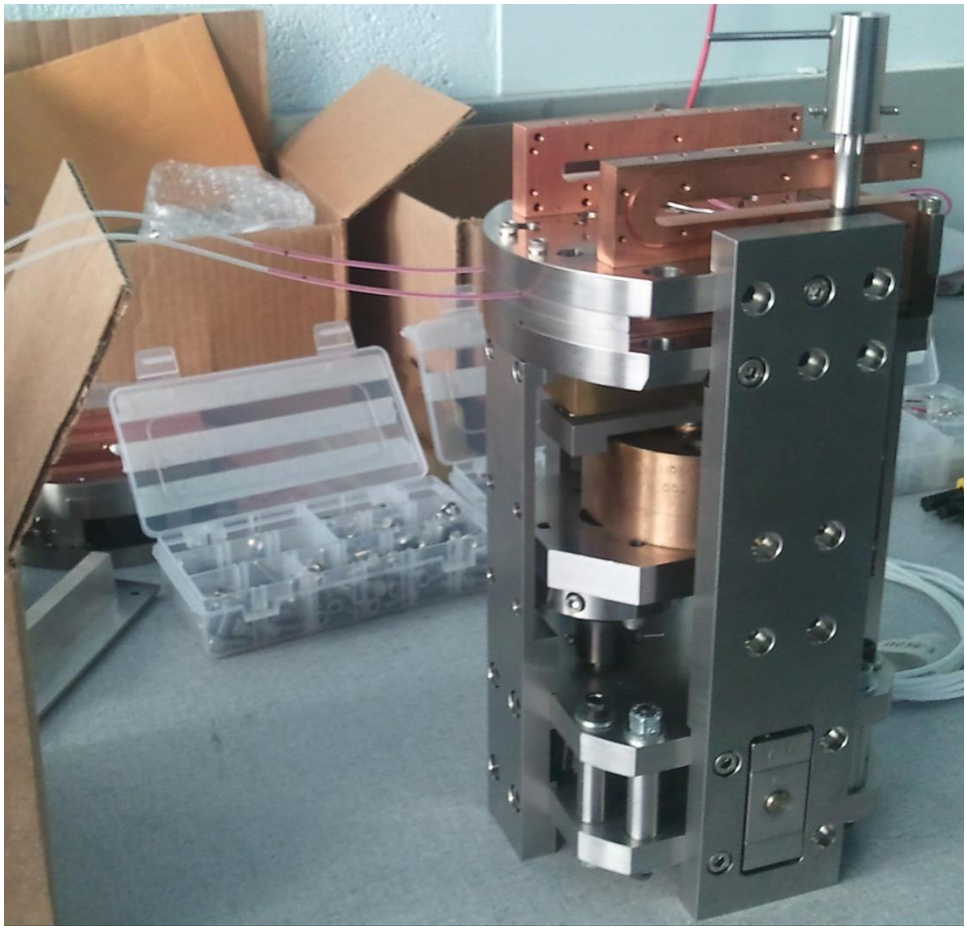

Fig. 5.1 Experimental Design assembled with silicone tube test.

To test the workings of the mechanism, the 3-strand cable was replaced with a same diameter hollow silicone tube, Fig. 5.1. The tube would replace the cable and be filled with colored water. The tube was split into two parts, clamped on one side and open on the other, and when engaged will show whether there was an inherent difference between the force applied to each side of the tube.

The silicone tube was filled with equal amounts of colored water in each tube. Permanent marker was used to mark the edge of the colored water. The black mark is used to see the progression of the silicone tube being compressed as well as relative difference between each side of the experiment. Fig. 5.2 shows the progress after the

gear mechanism has been engaged. The colored water has been displaced equally in the silicone tube.

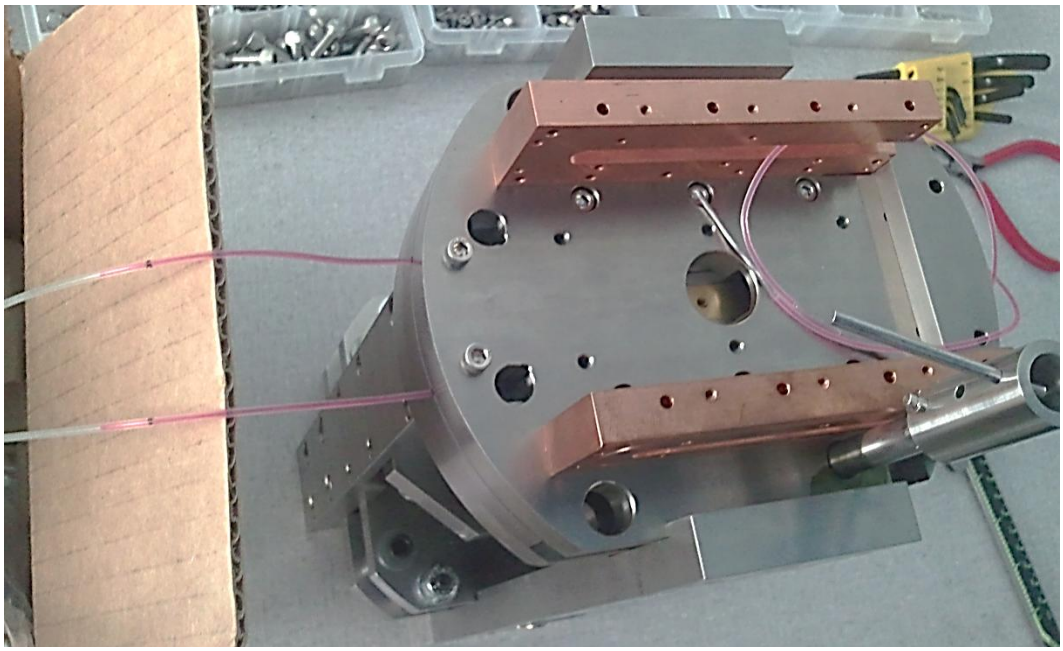

Fig. 5.2 Silicone tube shows equal amounts of colored water is displaced.

This portion of the experiment was a success. It showed that the experiment was working in the way it was designed, under low force condition. It should be noted that since this test was performed to show whether the mechanism was working under low force condition, the load cell was installed but was not taking measurements during this test. The extensometer was not installed.

5.2 Room temperature experiment with non-heat-treated 3-strand cable

The next experiment would be replacing the silicone tube with the 3-strand twisted cable. For this experiment both the load cell and the extensometer would be installed. It should be noted that the extensometer was bought from P3 America, a

San Diego, CA company. The model used for this experiment was CLP13-25. This extensometer is a potentiometer that allows the continuous reading of the resistance of the film element that can be related to the displacement.

The room temperature experiment was put together the same way the real experiment would be. Voltage between strands was recorded to measure the contact resistance between the untreated Nb_3Sn wires. Using a multichannel voltmeter, the load cell and extensometer voltages are measured and recorded using a data-collection system.

The wedge was raised to the expected zero load condition. This happens to be roughly where the top of the wedge is parallel to the pressure plate. When the electronics was ready, the input shaft was rotated counter-clockwise to start engaging the wedge. The input shaft was rotated in 100 rotation increments where the data was checked and also manually recorded. Looking at the extensometer versus time data, the areas where the extensometer does not move indicate the time of manual data recording. It should also be noted that there was a relaxing of the system, as indicated by the load cell data, this phenomena will be discussed later in the chapter. The input shaft was rotated roughly 2150 times. At this point the wedge was visibly above the pressure plate, ensuring that the experiment worked as planned. The vertical displacement was recorded with the extensometer and the load at this point was significant indicating that a large transverse force was being applied to the sample. It should be noted that it became noticeably harder to rotate the input shaft as the experiment progressed. This is indicative that the cable in transverse loading resisted the pressure applied to it.

During the room temperature experiment, the data was collected from the load cell as well as the extensometer. The voltage excitations for the load cell and the extensometer were 5 V and 2 V respectively. The signal was collected every second a total of 7928 data points.

5.3 Experimental results and discussion.

The data from the extensometer and the load cell was compiled together and analyzed. Since the voltage for both devices started at a particular level, both devices had to be normalized to start at 0 V.

Extensometer has a maximum travel of 25.4 mm. Thus to calculate the instantaneous displacement, the following formula was used.

$$Displacement_{ext} = \frac{total\_displacement * measured\_voltage}{applied\_voltage}$$

$$= \frac{25.4\ mm * measured\_voltage}{2\ V}$$

To calculate the transverse load cell $F_{transverse,}$ the $F_{vertical\text{-}load}$ needs to be calculated. The full load of the load cell was 907 kg. The full scale output of the load cell is 1.329 mV/V and was provided by the manufacturer. The voltage signal of the load cell at full load for an excitation voltage of 5 V is 6.645 mV. To calculate the vertical load V/kg needs to be determined. 6.645 mV / 907 kg = .00733 mV/kg. The data collected has an output of V, so dividing by 1000 gives the right units. Multiplying these two together gives the vertical load in kg. To calculate Newtons multiply the kg by the acceleration of gravity 9.81 m/s^2. Once $F_{vertical\text{-}load}$ is calculated, Eq. 2.2 is used to calculate the $F_{transverse.}$

One of the difficult parts of the design is determining the precise location when the pressure plate is touching and applying load to the 3-strand cable. In this experiment, there is no indication when the pressure plates make contact with the cable. Due to the fact that the experiment is done remotely in a cryogenic cryostat, it would be impossible to directly observe when this would happen. Currently, there are two sources of collecting the displacement and load information during the engagement, the load cell and the extensometer. Unfortunately, since there is no way to measure the transverse displacement and the load directly they have to be calculated from the vertical values. The reason for not having a way to directly measure the contact is due to the lack of space in the area transverse loading area. Future experiments, described in chapter 6, are set out to determine the correlation between the vertical load and the transverse load. Until that time, the cable loading point has to be inferred.

The voltage data taken directly from the load cell and the extensometer is shown in Fig. 5.3. The data is then converted from the raw voltages to displacement in mm and load in kN.

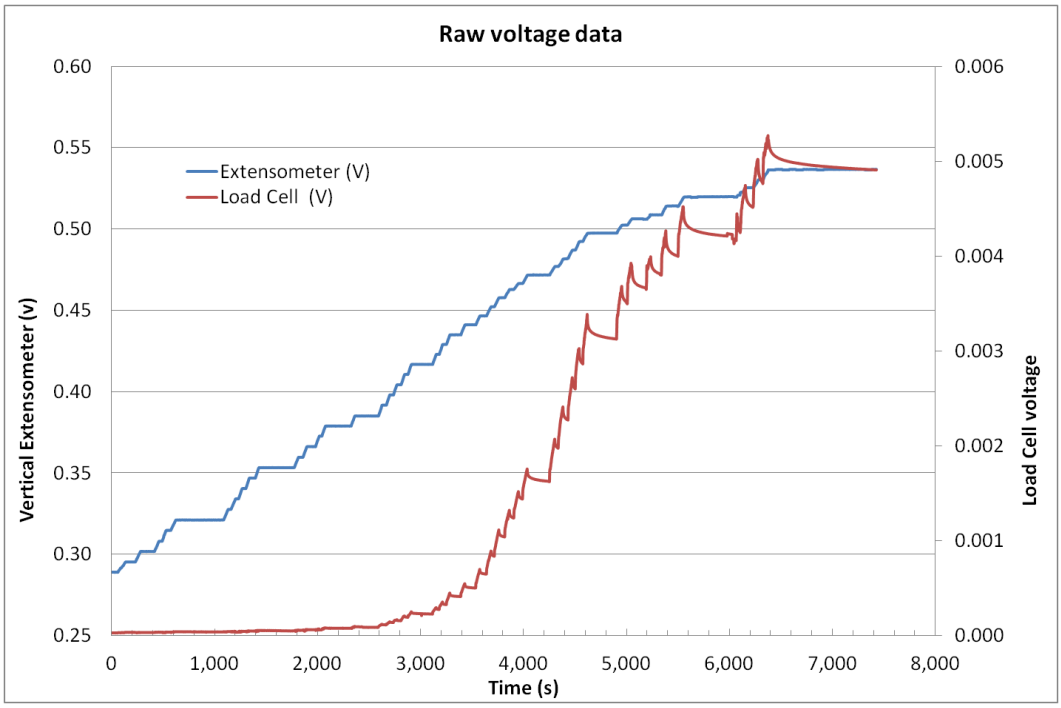

Fig. 5.3 Raw voltage from the load cell and extensometer.

Fig. 5.4 shows the converted load cell and the extensometer data plotted against time. Period before the pressing plate makes contact with the cable needs to be investigated. This area is examined in Fig. 5.5

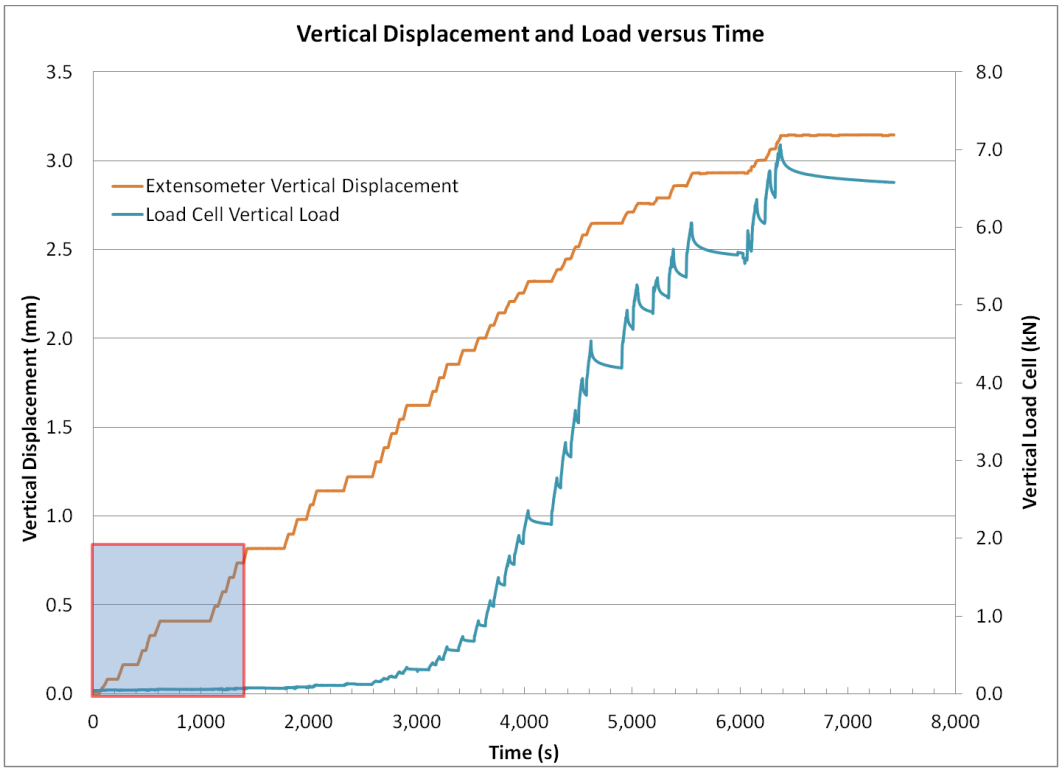

Fig. 5.4 Vertical displacement and load versus time.

Fig. 5.5 shows the zoomed in area from Fig. 5.4, representing the starting point of the room temperature experiment. Initially, as the wedge was moving up vertically, the pressing plates are not applying positive load to the cables, as shown in the graph. The load cell started to show positive increase in load around 1,100 seconds, roughly 0.4 mm of vertical displacement. This is the point where the load cell started applying positive pressure to the cable and will be considered the starting point of the transverse load. This off-set is taken in consideration for the figures following Fig. 5.5.

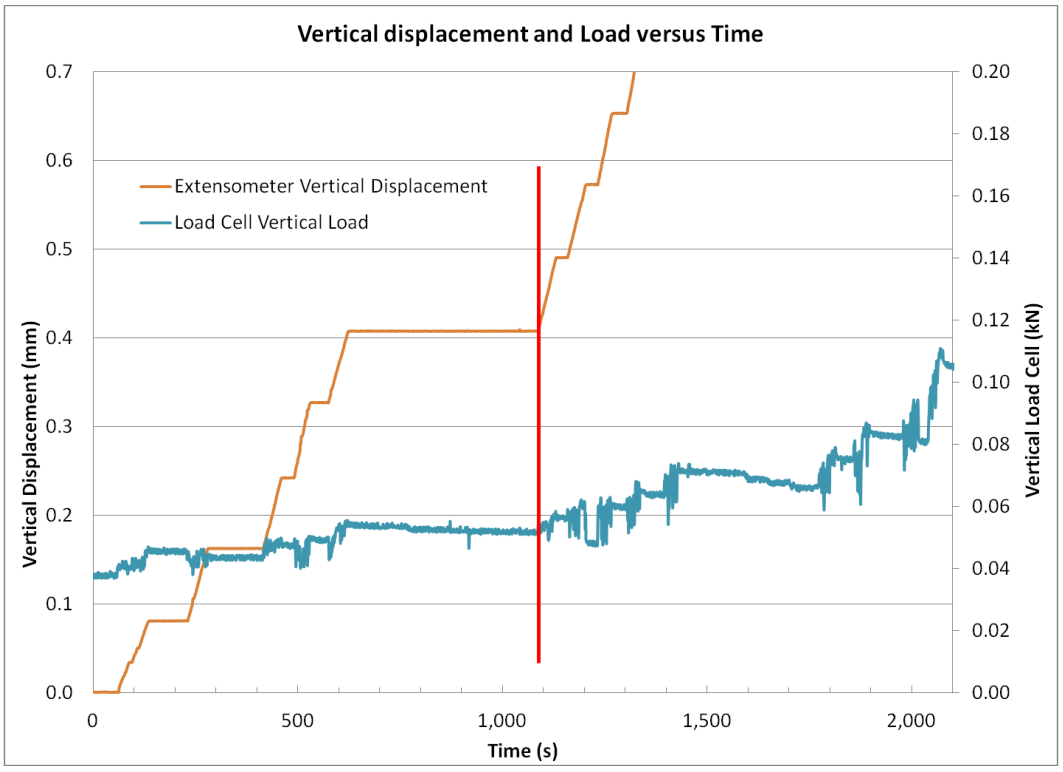

Fig. 5.5 Zoomed in vertical displacement and load versus time, showing the start of the transverse loading.

It is important to discuss the starting point of transverse loading of the cable. In most experiments, it is assumed that the loading of the cable is uniform from the beginning of the loading, this might not represent what is physically happening. It is important to be reminded of the construction of the cable. The 3-strand cable is twisted together using three individual Nb_3Sn strands with a certain twist pitch. The diameter of the twisted cable is not uniform throughout the length of the cable, thus, it would be impossible for the pressing plate to apply equal pressure throughout the whole length of the transverse loading. Initially, the pressing plate is applying load in a few places throughout the length of the cable and the cable acts more similarly to a soft material. As the load is increasing, more area of the cable is being compressed. Theoretical and FEA analysis can be found in [6] and [4]. The data in Fig. 5.6 shows this phenomenon. Initially, the displacement is high while the load applied to the

cable system is very small, this represents the transverse loading process starting and the cable being pushed only in few locations and settling in place. At ~1.2 mm of the vertical displacement, there is a transition period, after which there is a linear correlation between the compressing load and the displacement. This indicates a more uniform load is applied to the cable that now acts more like a solid material, in which the three strands support one another very well.

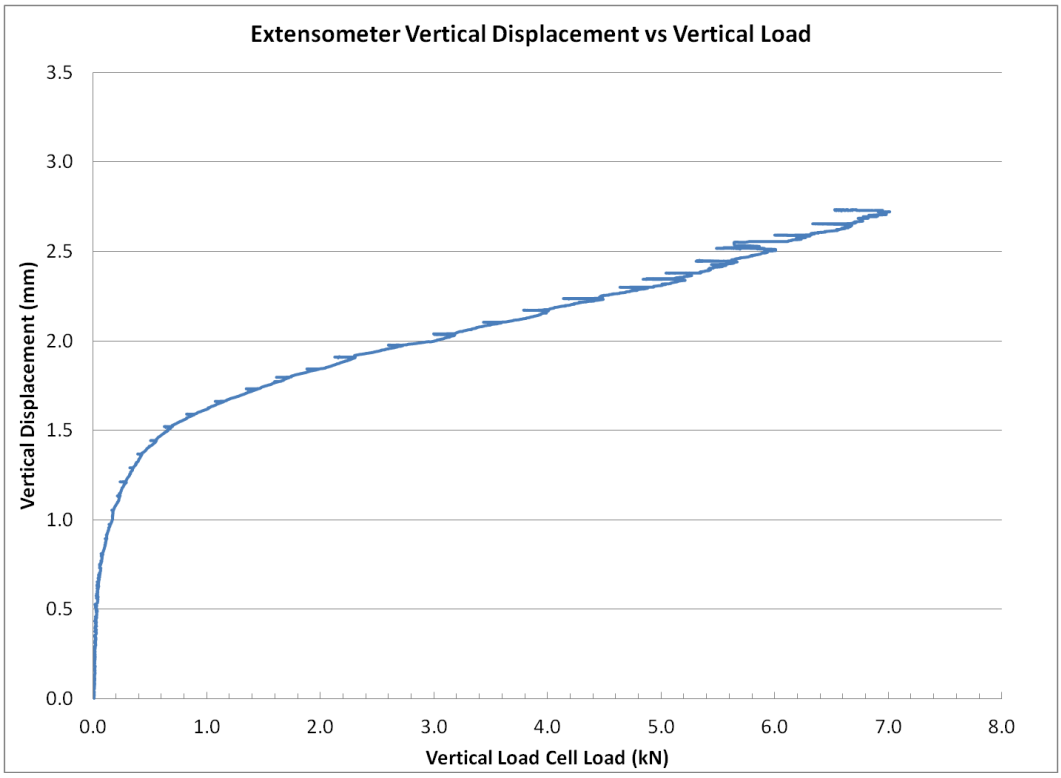

Fig. 5.6 Vertical extensometer displacement versus vertical load during the room temperature experiment.

The transverse movement of the pressure plate versus the transverse load applied to the 3-strand cable is shown in Fig. 5.7. The room temperature plot is similar in shape to the old 3-strand experiment performed by L. Chiesa [6]. One of the main differences between those two sets of data is that for the room temperature tests just described a non-heat-treated sample was used. It is expected that the data

shown in Fig. 5.6 will be slightly different with a heat treated sample and in cryogenic environment. Nevertheless, the room temperature experiment with non-heat treated 3-strand Nb_3Sn cable data closely resembles the range of desired transverse displacement of previous experiment.

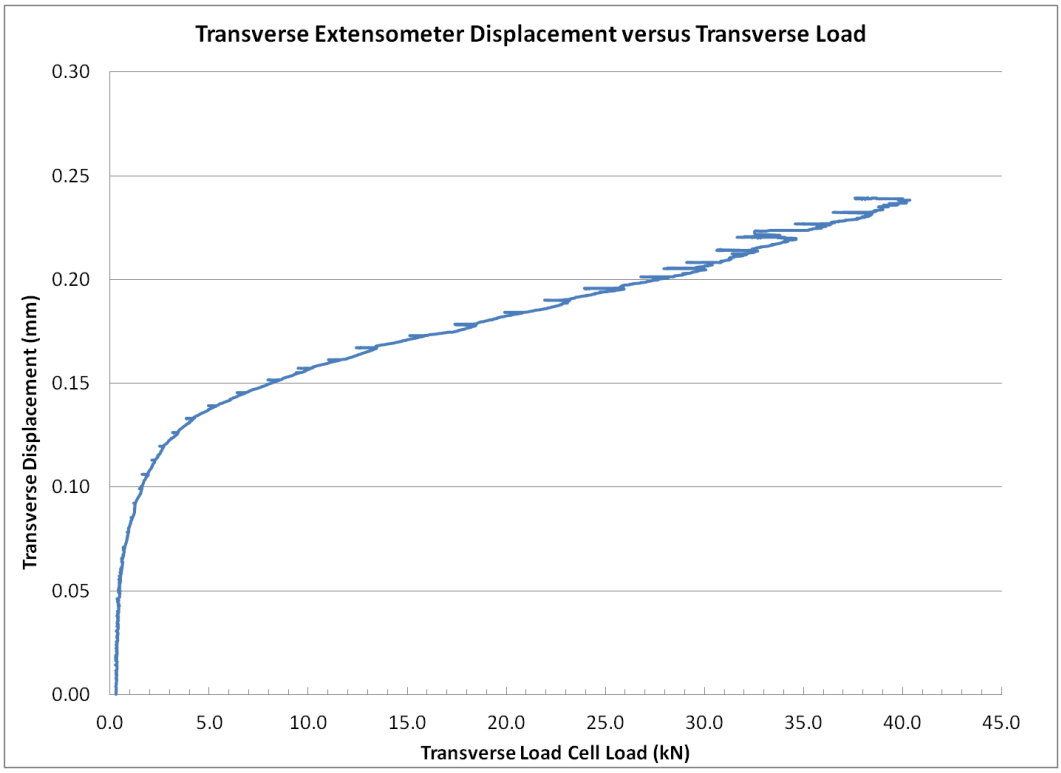

Fig. 5.7 Transverse pressure plate movement versus transverse pressure plate loading. The red line shows the experimental data from previous experiment [6].

It is also important to understand the relation of the vertical displacement versus the transverse loading. Currently, this relationship is calculated instead of being directly measured. In the real experiment, the curve will be slightly different as there are factors that this calculation does not take into account, such as friction between components.

The data from the room temperature experiment was collected and analyzed. Vertical displacement with vertical load cell load was plotted against time. The analysis showed that compression point can be obtained from looking at the extensometer vertical displacement and vertical load versus time. Although this point was determined roughly, during the experiment a similar procedure will be used and it was important to determine the range of loads and displacements that should be expected.

A careful observer will notice a relaxation of the system, at the time where the loading process stops for a period of time. This is shown in the load cell versus time plots, Fig. 5.3 and Fig. 5.4. The root cause of this relaxation is not fully understood. It should be noted that the extensometer does not appear to be moving down during this relaxation. A finite element analysis was done to investigate this relaxation further by analyzing the force structure of the system. Fig. 5.8 shows the results of the study that took in consideration the displacements of various mechanical components as a function of vertical load to evaluate the overall compliance of the structure. It appears that there is minimal vertical movement of the system during the loading and it is not clear that this small displacement has caused the relaxation. A possible source of this relaxation might be a backlash effect of the gear box system. This effect will not be covered in this thesis as it requires a careful investigation but will be addressed in the near future to fully understand the overall behavior of the system. One way to investigate if this effect is caused by the gear box, will be to place a rigid object in place of the cable and begin loading the device. With everything rigid, the source of relaxation could be attributed to the gear box if the relaxation is still observed.

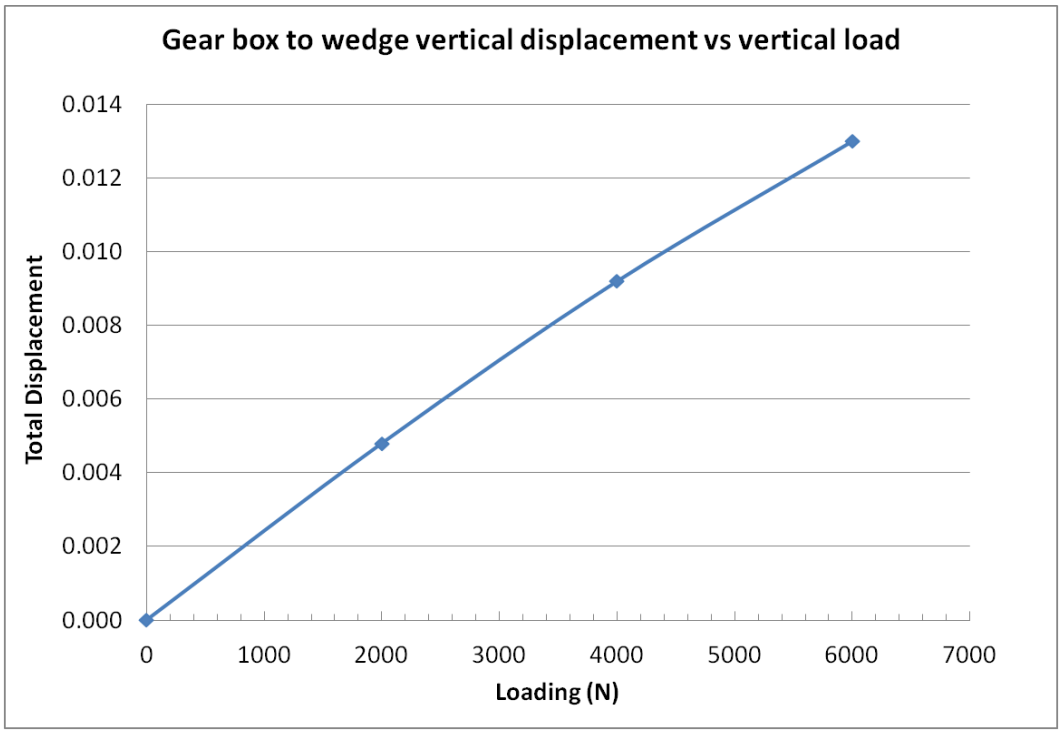

Fig. 5.8 System force displacement versus load.

Chapter 6 Conclusions and Further Research

An experimental device to electromechanically characterize 3-strand superconducting Nb_3Sn samples under transverse mechanical load was designed, manufactured and assembled. The room temperature experiment of the device demonstrated that the design performed as expected and has collected data similar to the previous experiment of the 3-strand cable. A completion of this project is the first step in the process of understanding and characterizing the 3-strand Nb_3Sn cable that is of interest for the ITER fusion energy research.

The new device is designed to continue research to characterize the transverse loading of the Nb_3Sn cable. The device is designed to be used multiple times with very few throw away parts. It was one of the major goals of the design, as the cost per experiments is large, from traveling to paying for the liquid helium. This is a compact device where the load cell and the wedge are at a minimal distance from the experiment, thus eliminating the need to account for material contraction under cryogenic conditions. Due to the small footprint of the components above the load cell, the load cell has great fidelity of the data. This device can be modified to be used with various diameter 3-strand cables for future experiments to better understand the relationship between the transverse loading and the degradation of the critical current.

As with any research topic there are a few things that require further improvement or development.

A direct correlation of the vertical load to the transverse load is important. For the work presented here and the experimental results shown, the transverse load was calculated based on the wedge design. Some work is currently in progress to address this issue and perform a calibration of the device. The basic design for this measurement is to have a cantilever arm, with two strain gauges on each side of the cantilever. Fig. 6.1 shows the proposed design. This analysis will correlate the vertical load measured with the load cell to the transverse load applied to the samples through the reading of the strain of the cantilever beam component. The FEA analysis of the cantilever arm showed that only limited loads could be applied to the arm before the metal starts yielding. The result of this experiment will give an understanding whether the beginning stage of the loading is accurate. The same structure as the experimental device will be used but both the test section cable holder and the pressure plate will be modified for this experiment.

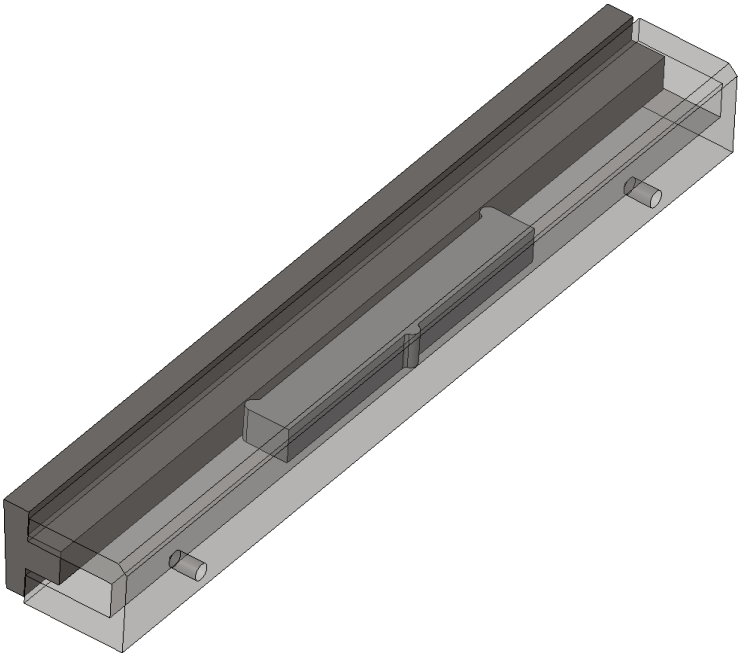

Fig. 6.1 Cantilever experiment designed to measure the transverse loading.

Another area of improvement is a possible cable engagement notification system. This information as it is important to understand when the wedge starts applying load on the 3-strand cable.

Lastly, the gear box mechanism needs a slight improvement as well. For this experiment, brass shims were developed and implemented as way to reduce galling of the material on the bottom of the input shaft and the two worm gears. Minor galling was experienced during the cryogenic experiment in the top area of the input shaft. In order to address this concern, the shims will also be implemented to the top part of input shaft to address this issue.

The transverse loading experiment described in this work was a successful demonstration of designing experiment from concept to the actual experiment. The device will be used to study the Nb_3Sn superconducting wire used in the Toroidal Field and Central Solenoid coils of the ITER fusion machine. It will be used to understand the mechanism behind the degradations due to transverse strain caused by the Lorentz forces. The design took concepts from previously performed experiments [6], [9], and improved the design. This experiment fulfilled all the requirements to compress the cable and performed in within the ranges of operation expected and satisfies the requirements for testing in the NHMFL facility.

The design of a completely new loading mechanism has been developed and successfully tested to sustain and react transverse forces up to 60 kN on a cable length of ~215 mm. The structural integrity of the mechanism and its operational functionality was verified with preliminary tests performed at room temperature.

Cryogenic experiments of the device have been successfully performed at the NHMFL facility.

Chapter 7 Drawings

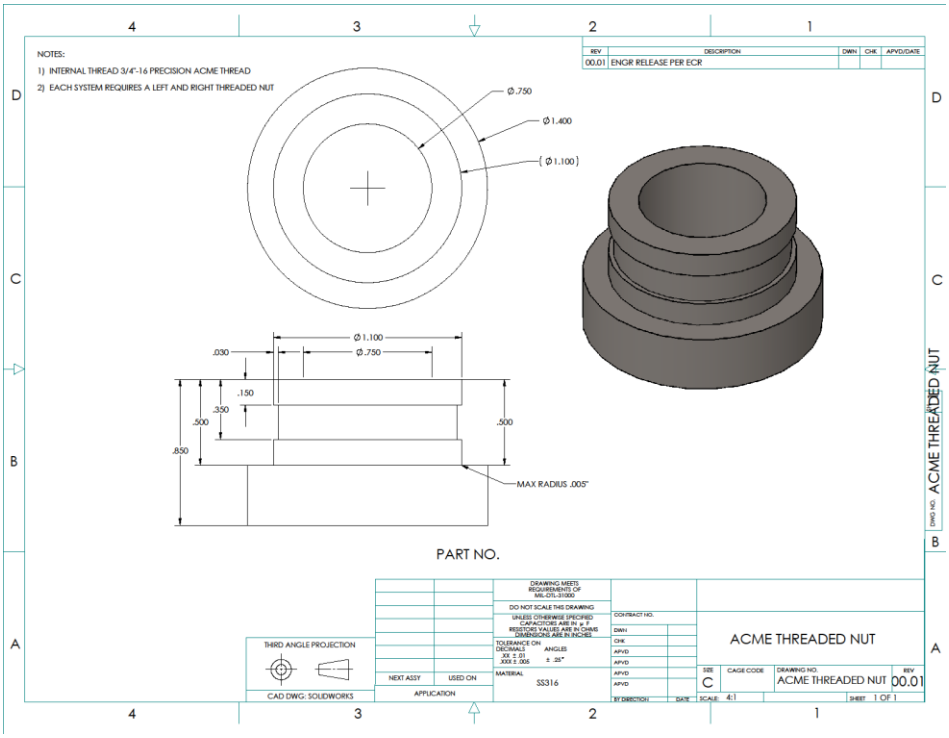

Fig. 7.1 ACME threaded nut

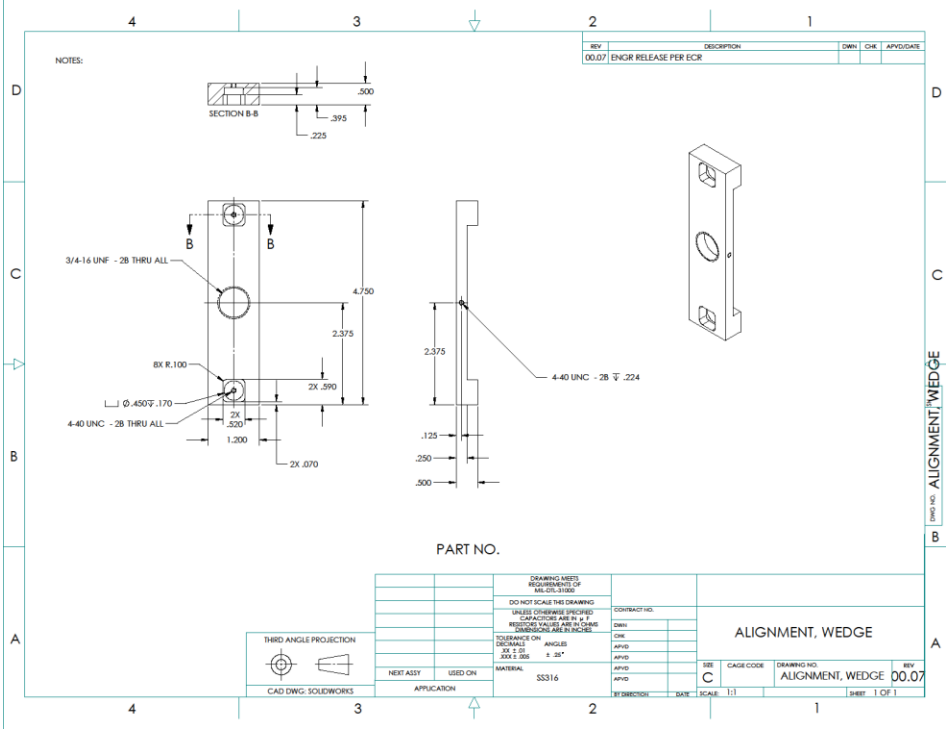

Fig. 7.2 Alignment, wedge

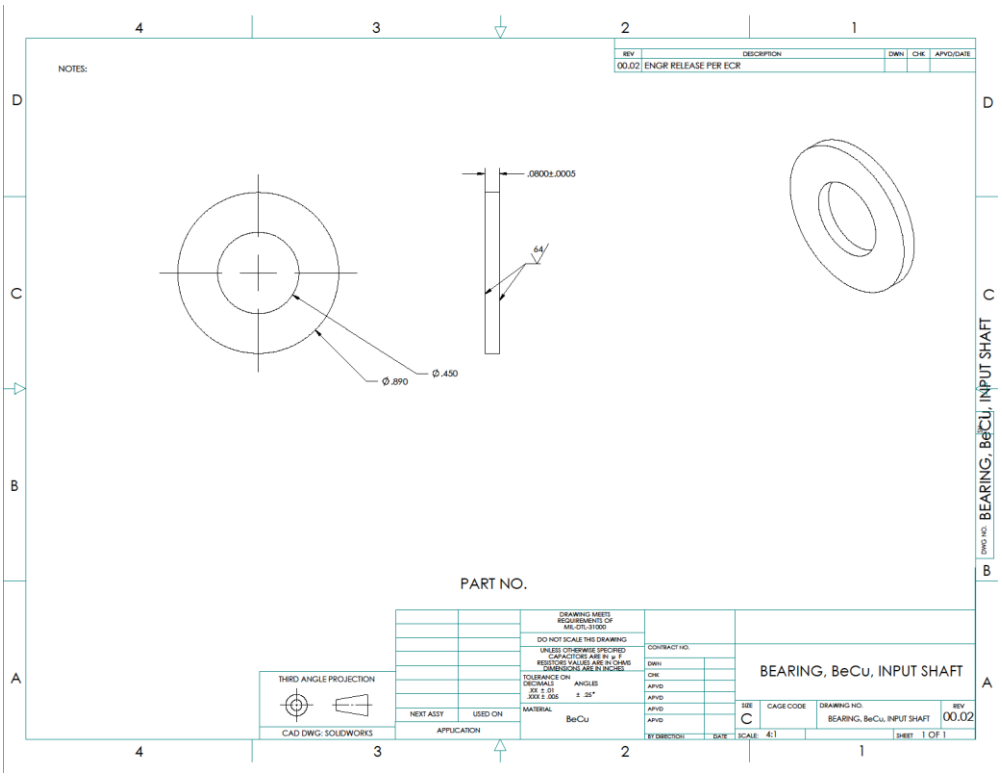

Fig. 7.3 Bearing, BeCu, input shaft

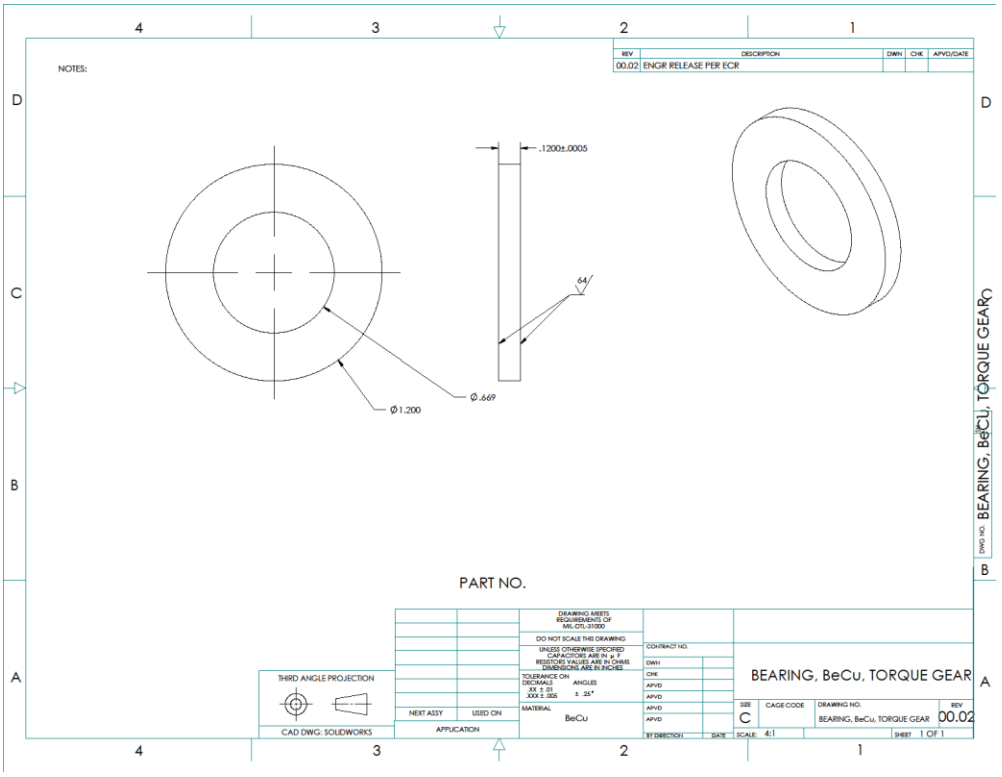

Fig. 7.4 Bearing, BeCu, torque gear

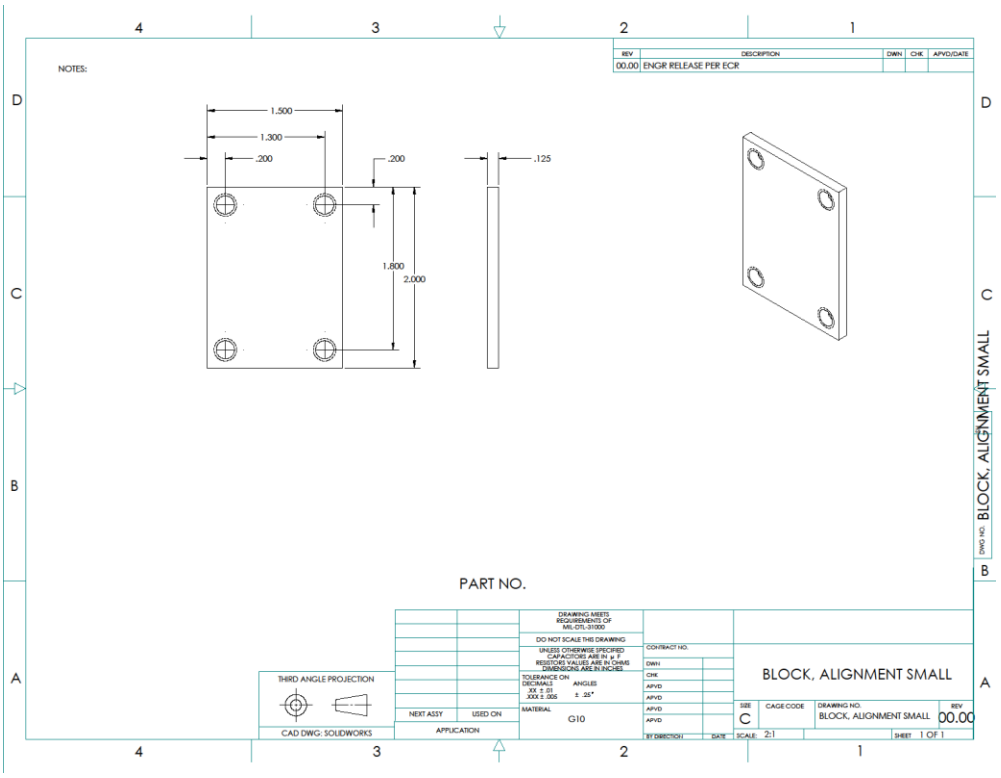

Fig. 7.5 Block, alignment small

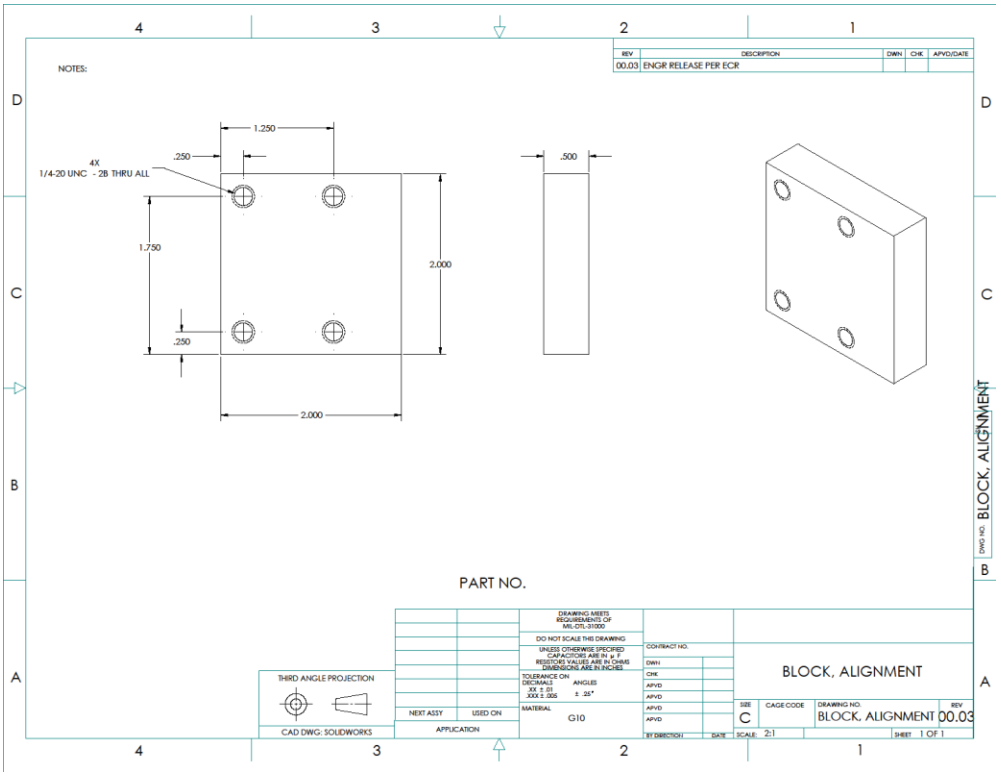

Fig. 7.6 Block alignment

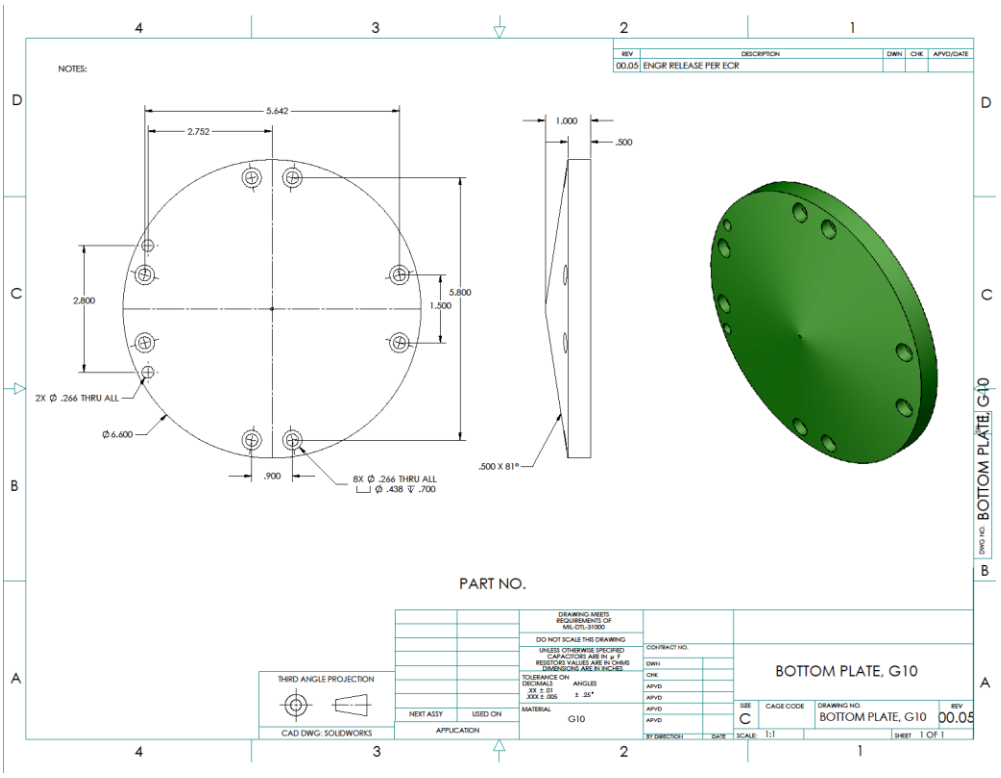

Fig. 7.7 Bottom plate, g10

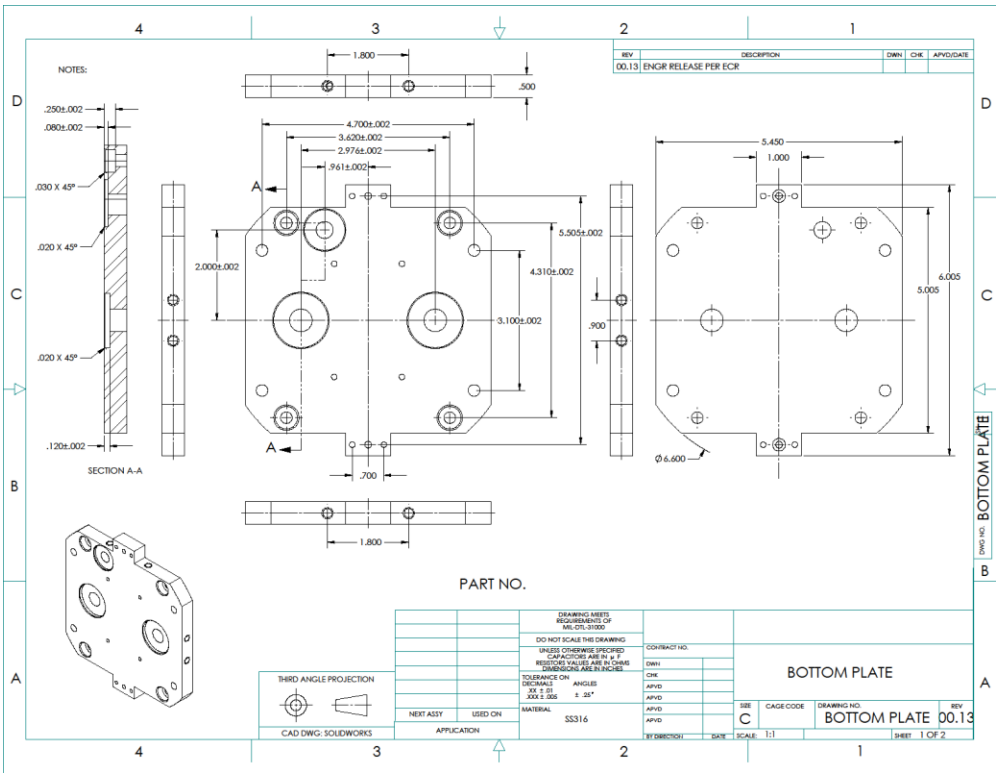

Fig. 7.8 Bottom plate

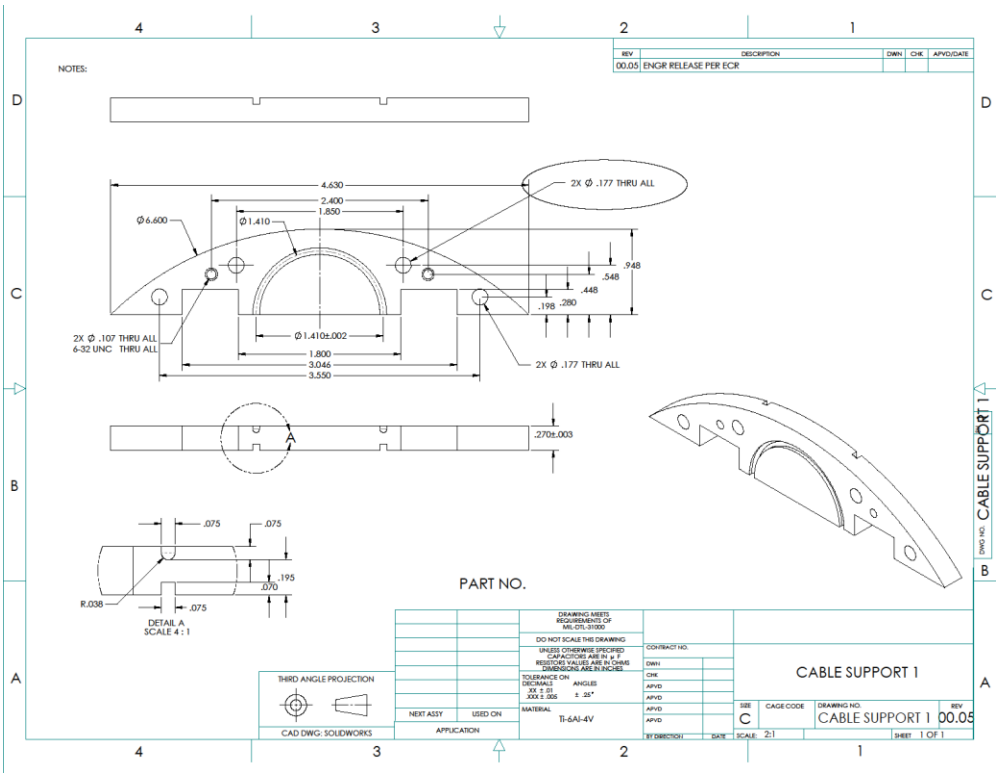

Fig. 7.9 Cable support 1

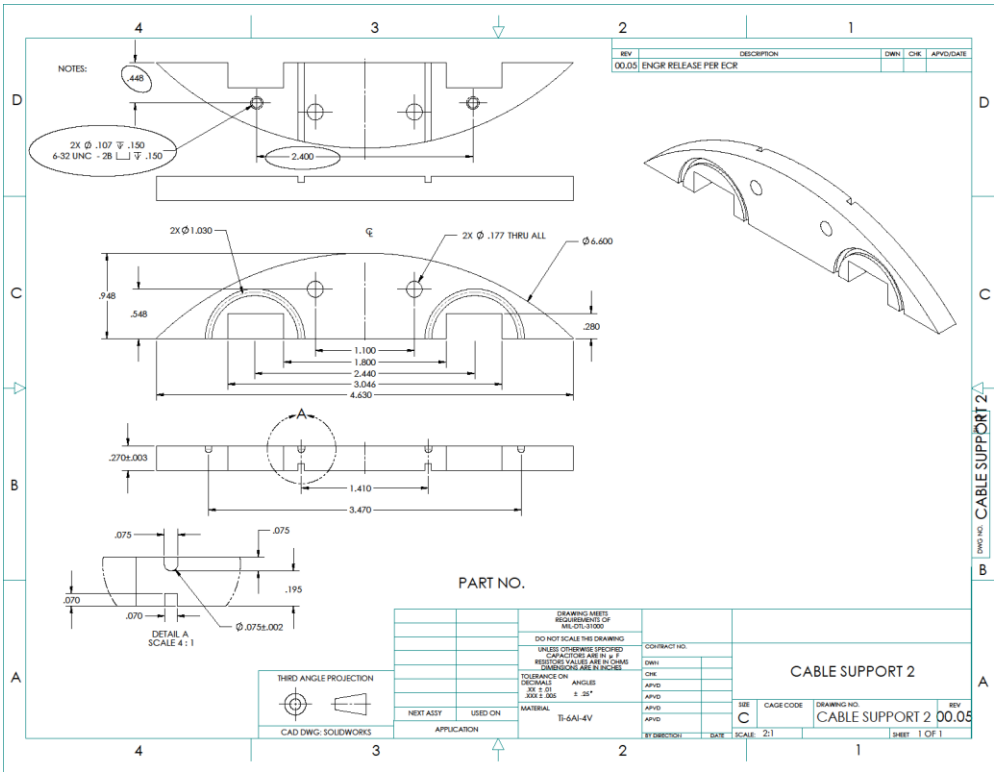

Fig. 7.10 Cable support 2

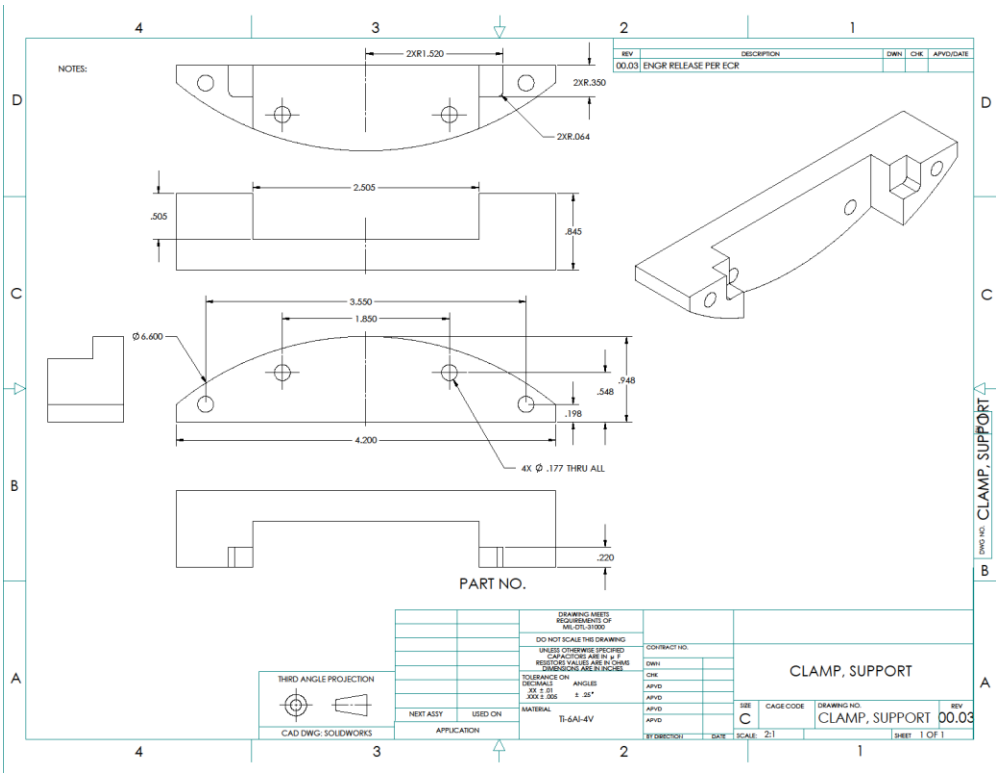

Fig. 7.11 Clamp support

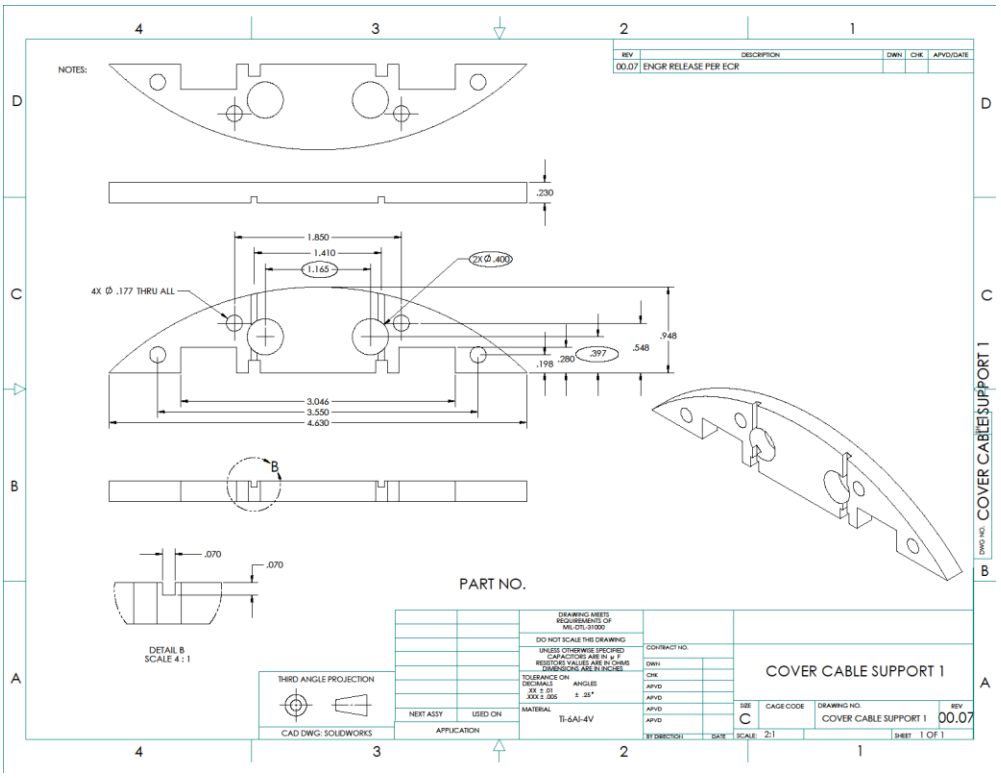

Fig. 7.12 Cover cable support 1

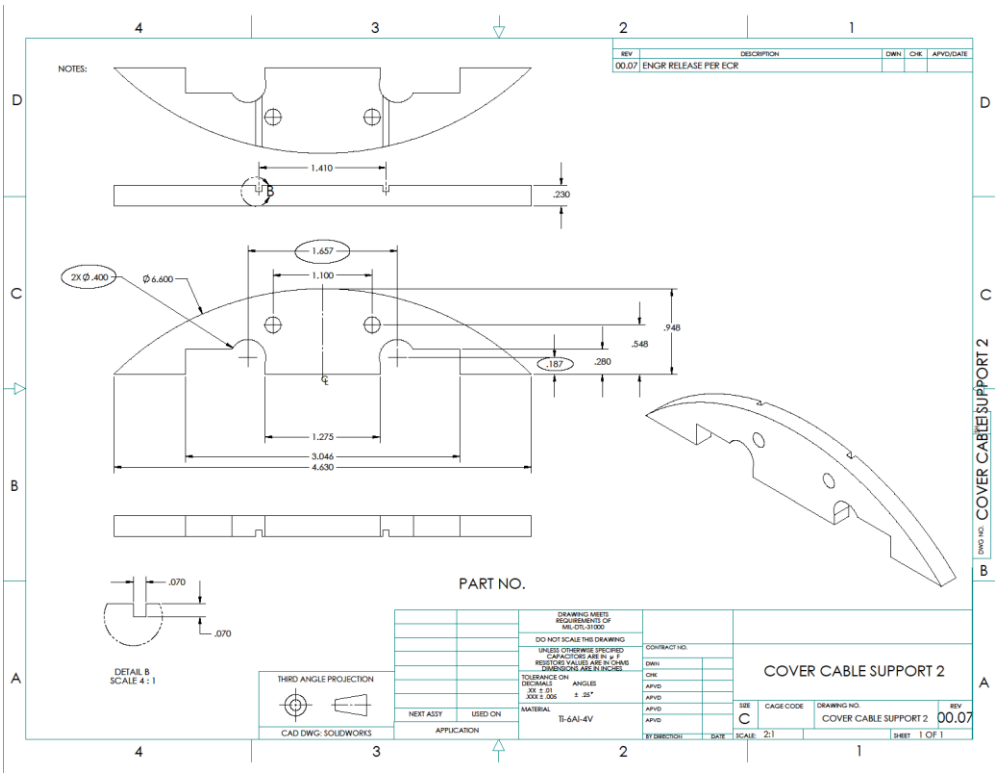

Fig. 7.13 Cover cable support 2

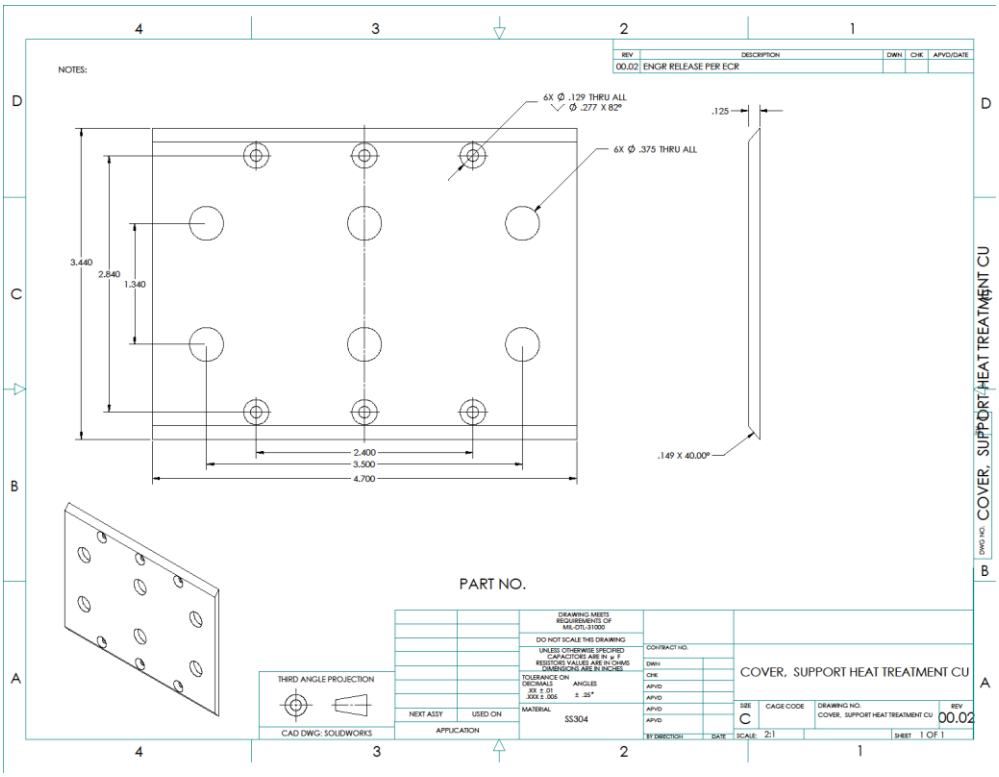

Fig. 7.14 Cover, support heat treatment Cu

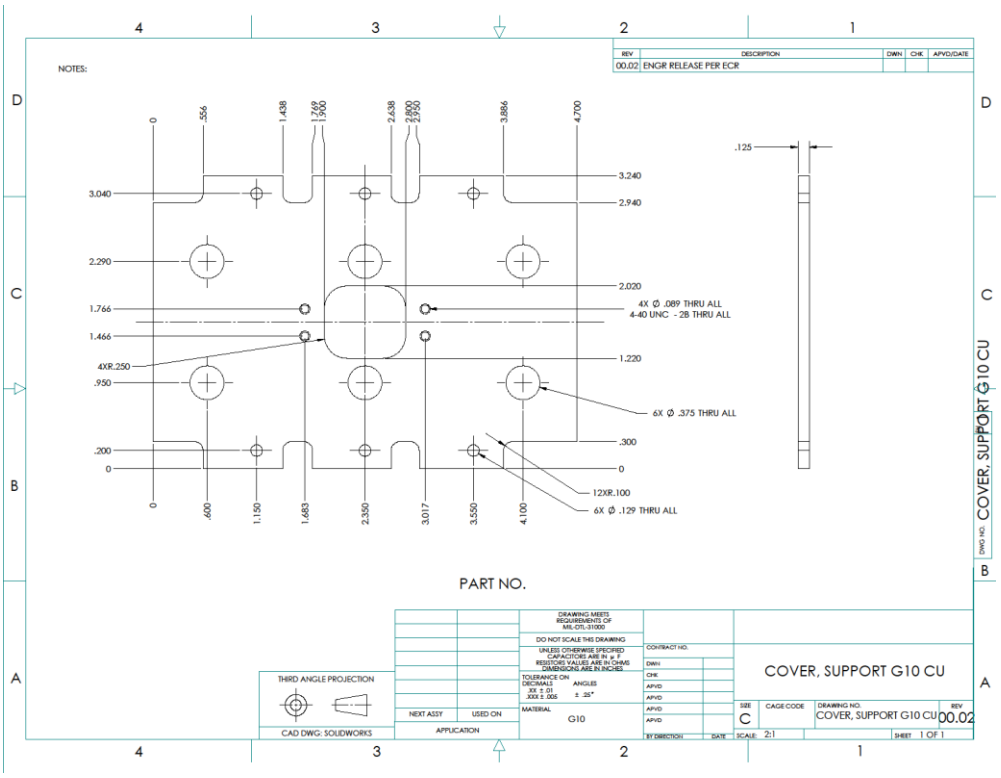

Fig. 7.15 Cover, support g10 Cu

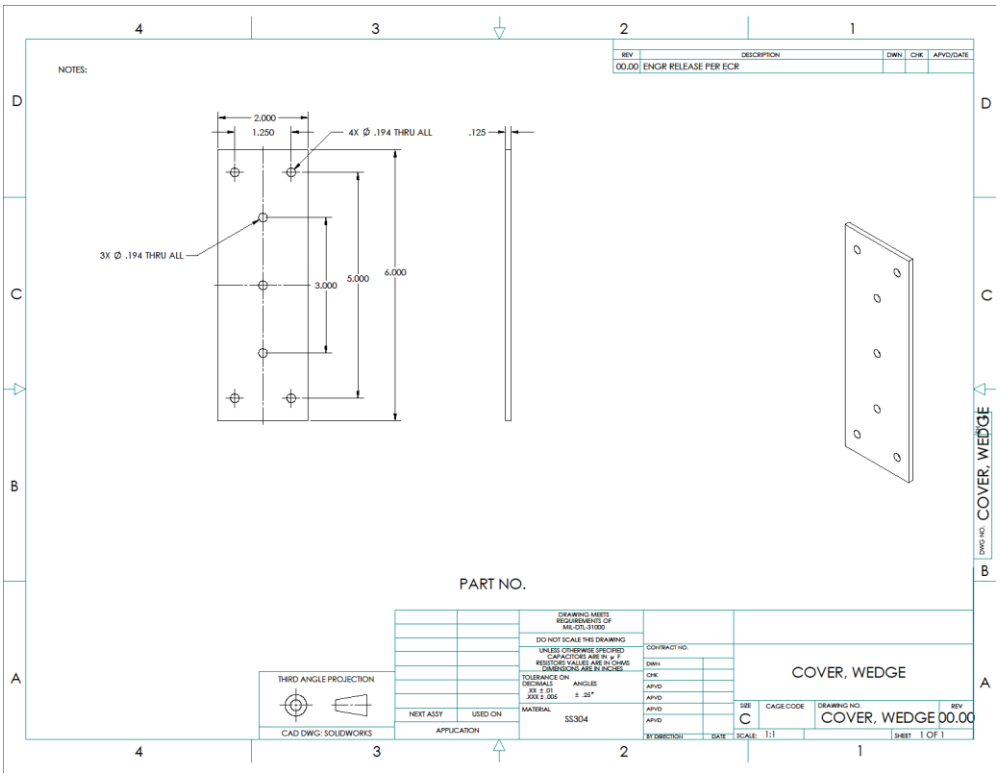

Fig. 7.16 Cover, wedge

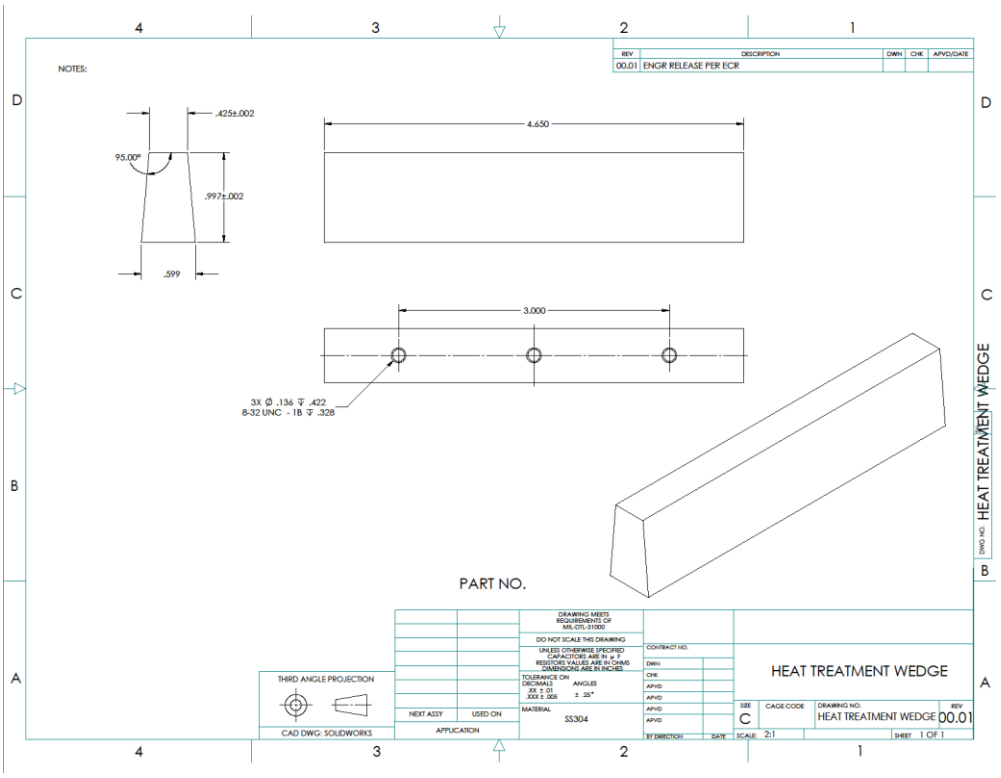

Fig. 7.17 Heat treatment wedge

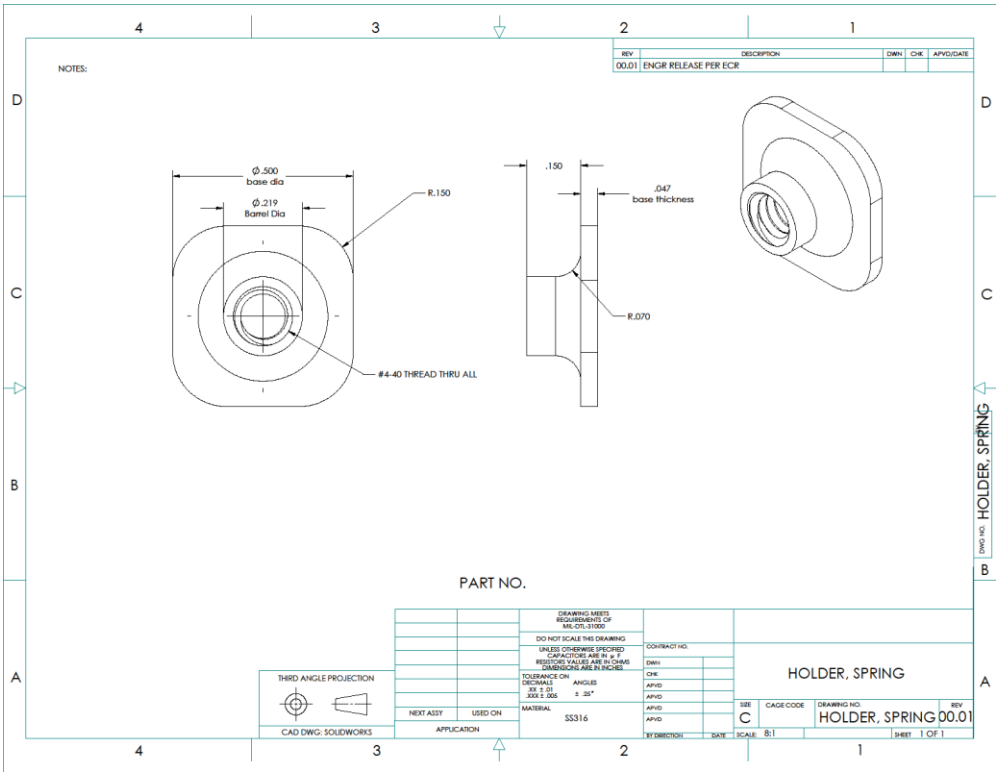

Fig. 7.18 Holder spring

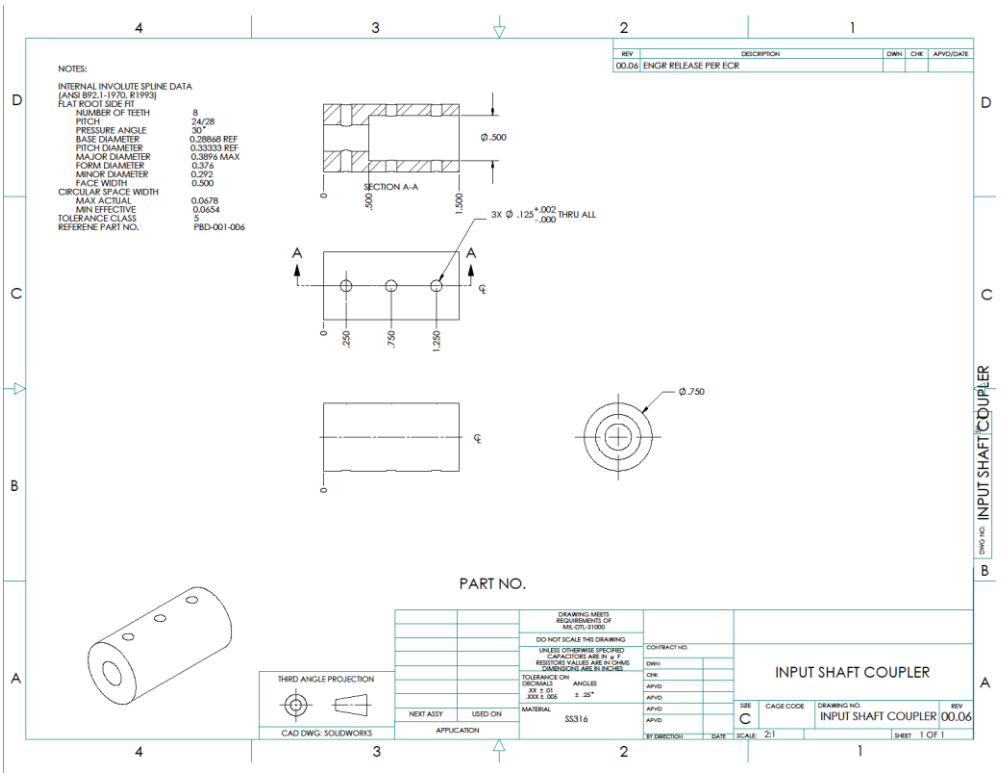

Fig. 7.19 Input shaft coupler

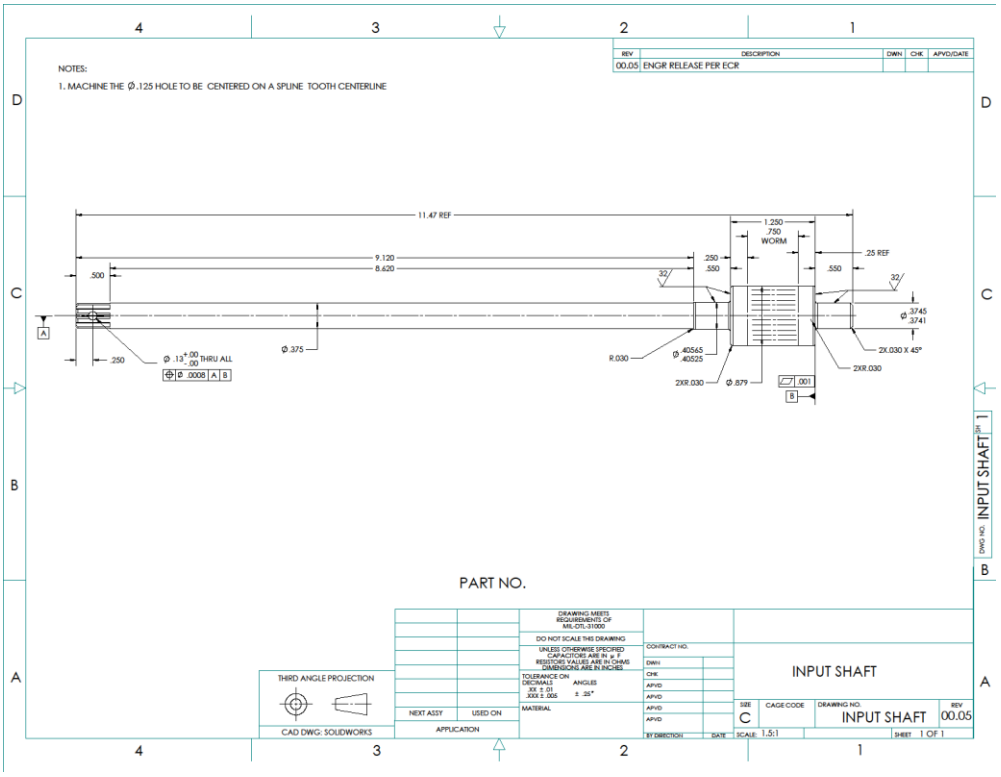

Fig. 7.20 Input shaft

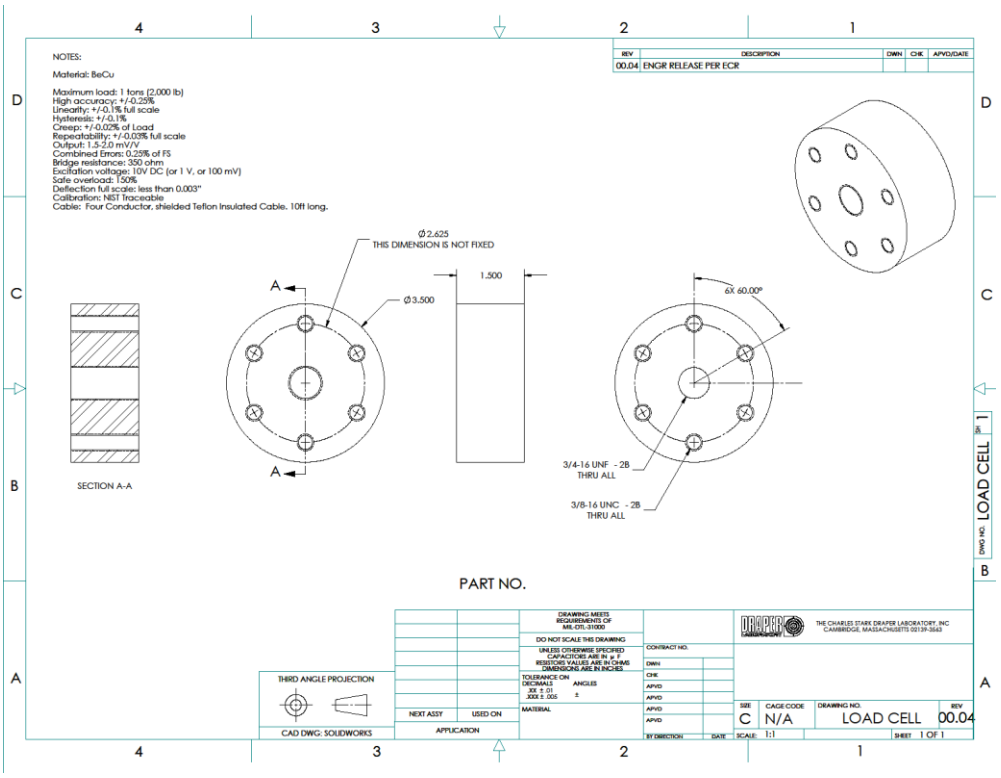

Fig. 7.21 Load cell

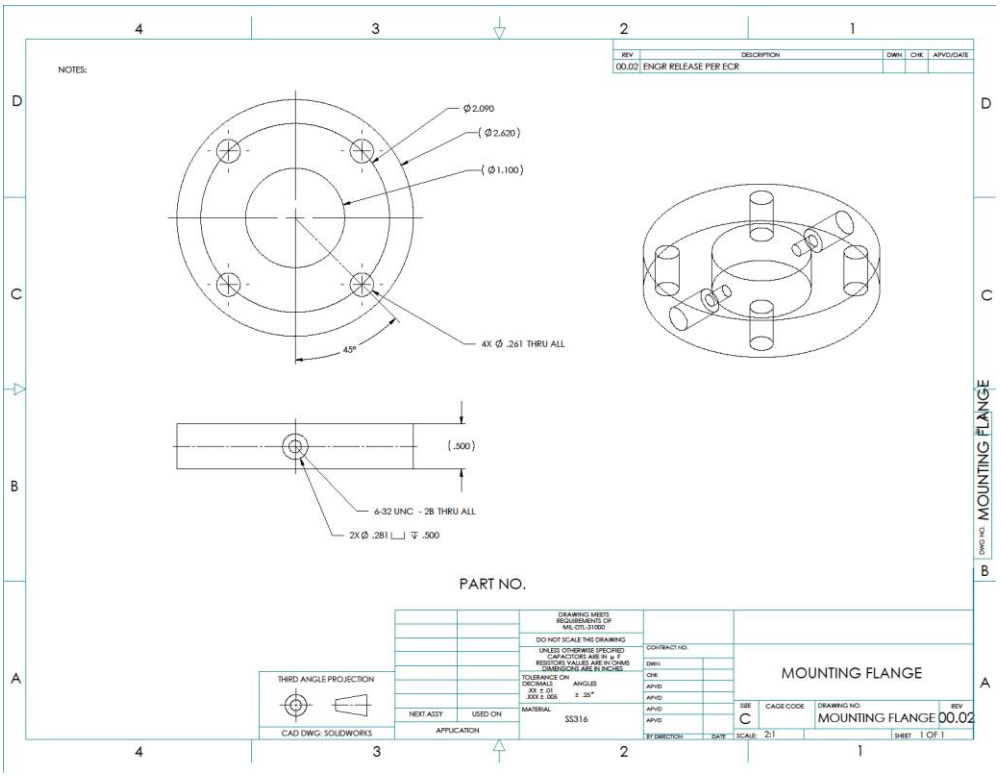

Fig. 7.22 Mounting flange

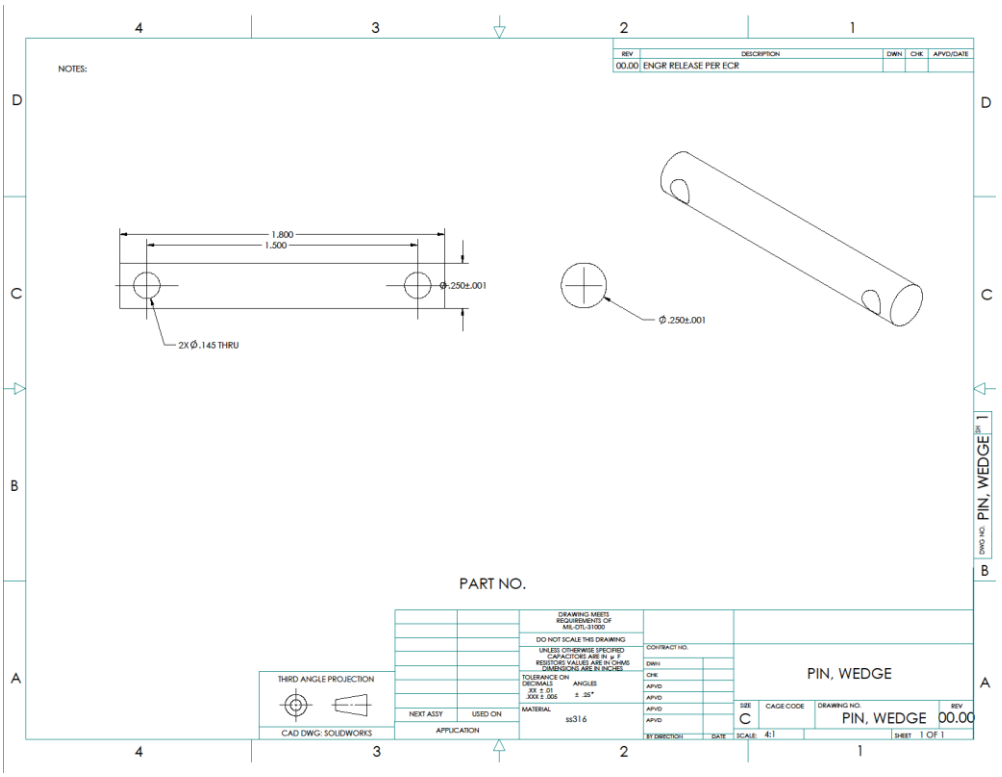

Fig. 7.23 Pin wedge

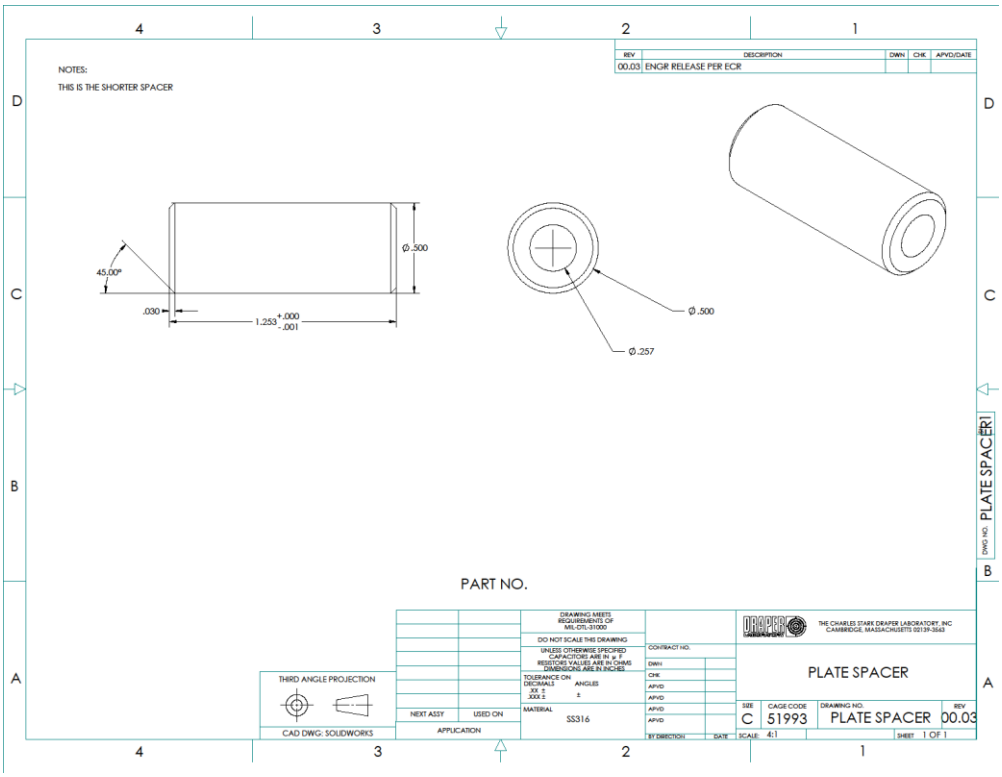

Fig. 7.24 Plate spacer

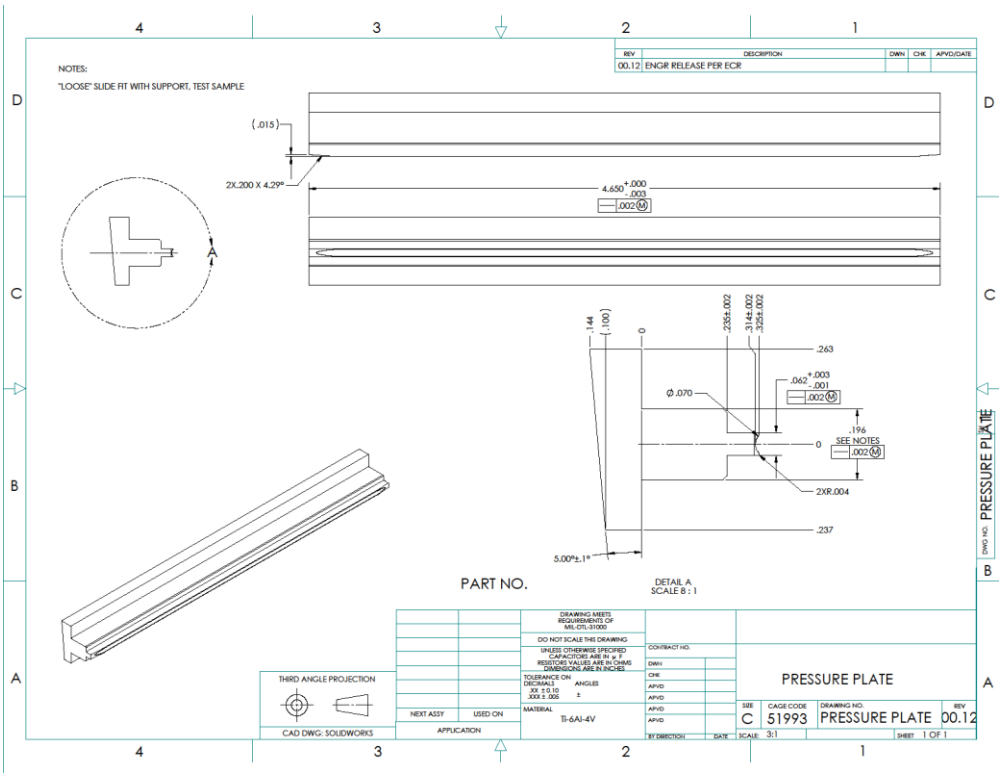

Fig. 7.25 Pressure plate

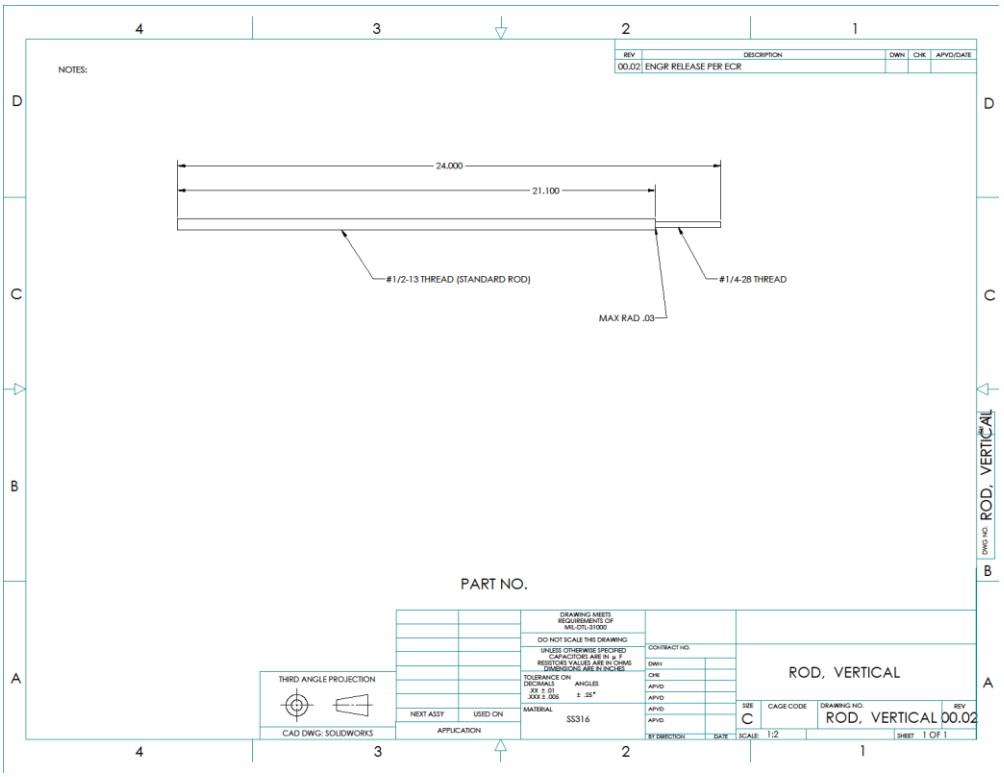

Fig. 7.26 Rod vertical

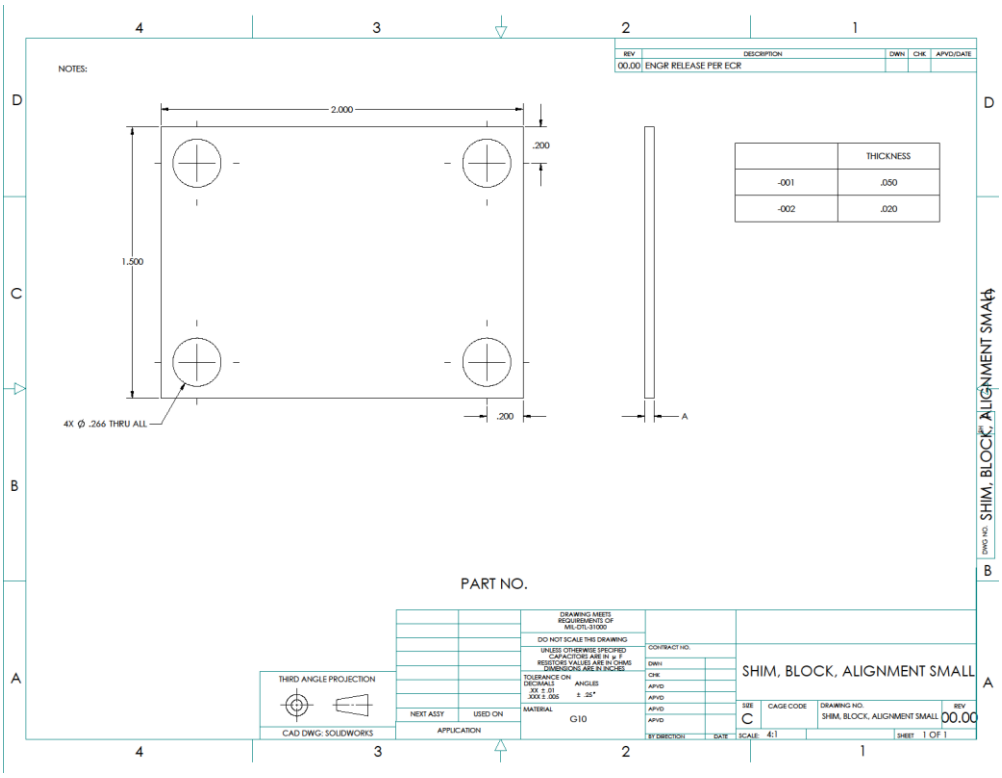

Fig. 7.27 Shim, block alignment small

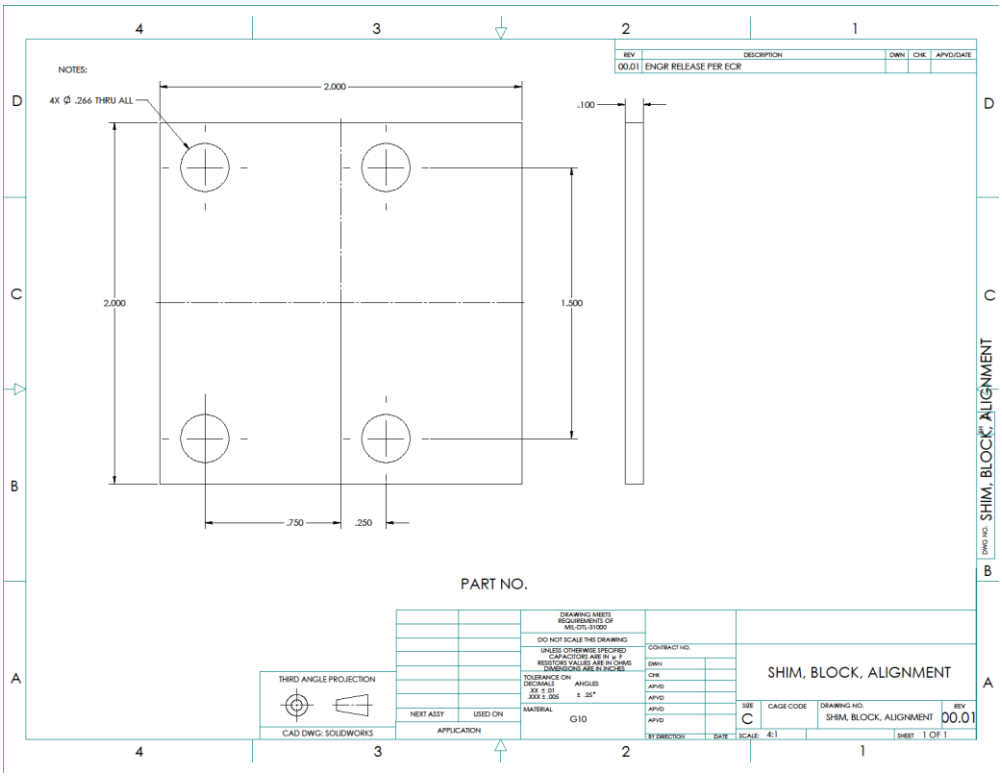

Fig. 7.28 Shim block alignment

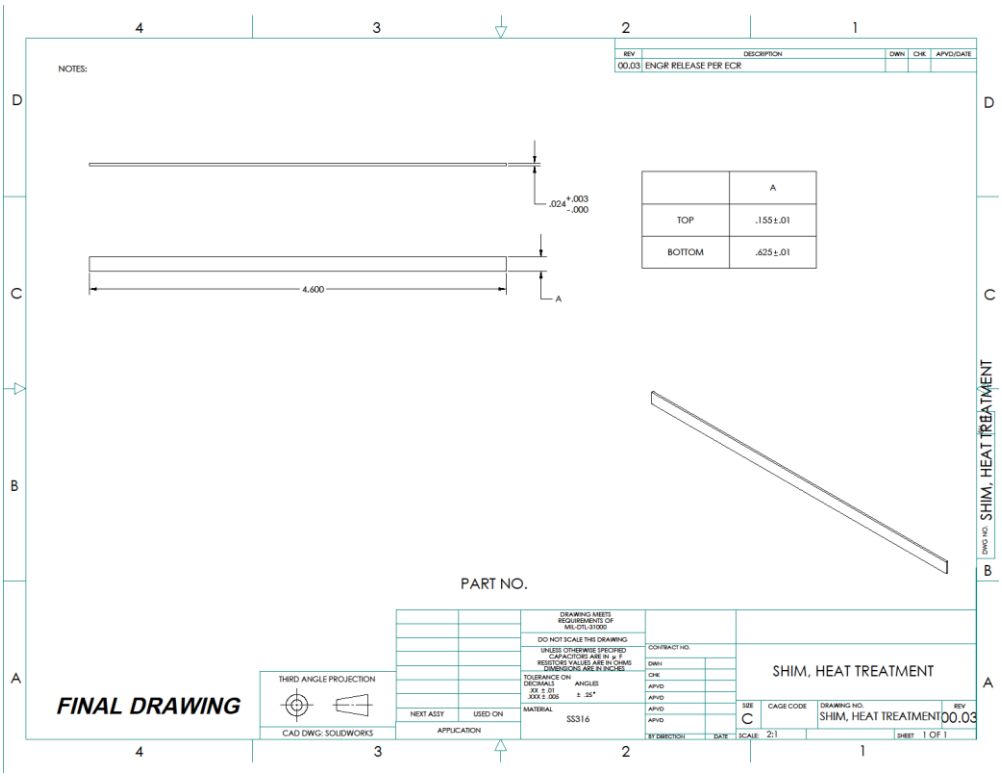

Fig. 7.29 Shim, heat treatment

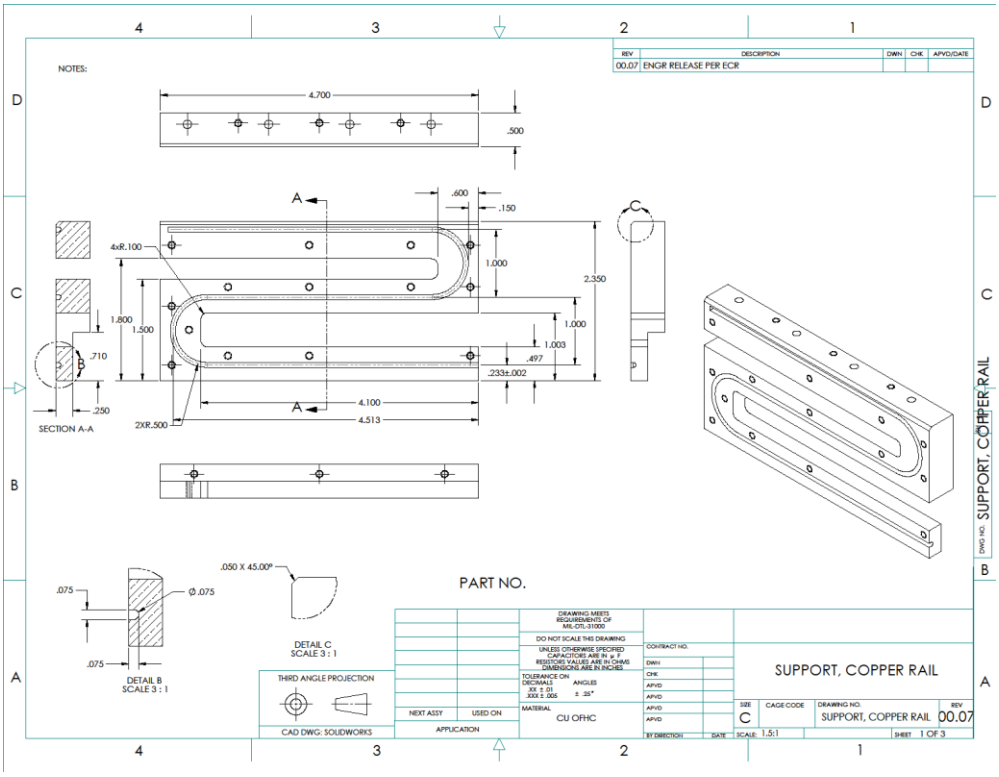

Fig. 7.30 Support copper rail

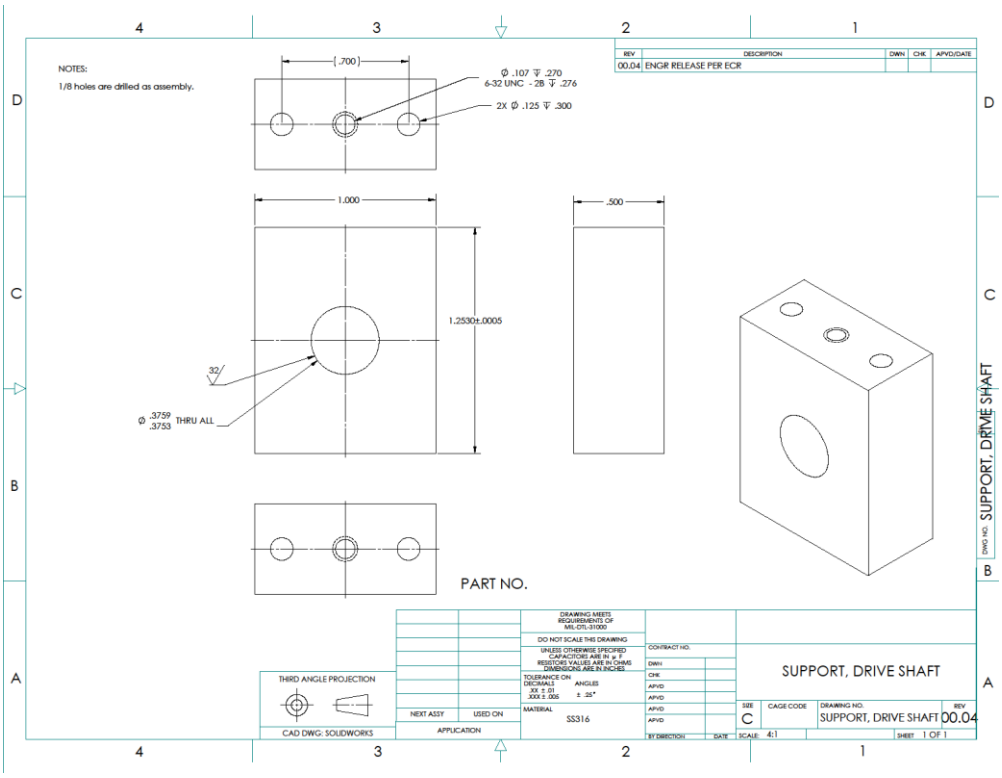

Fig. 7.31 Support drive shaft

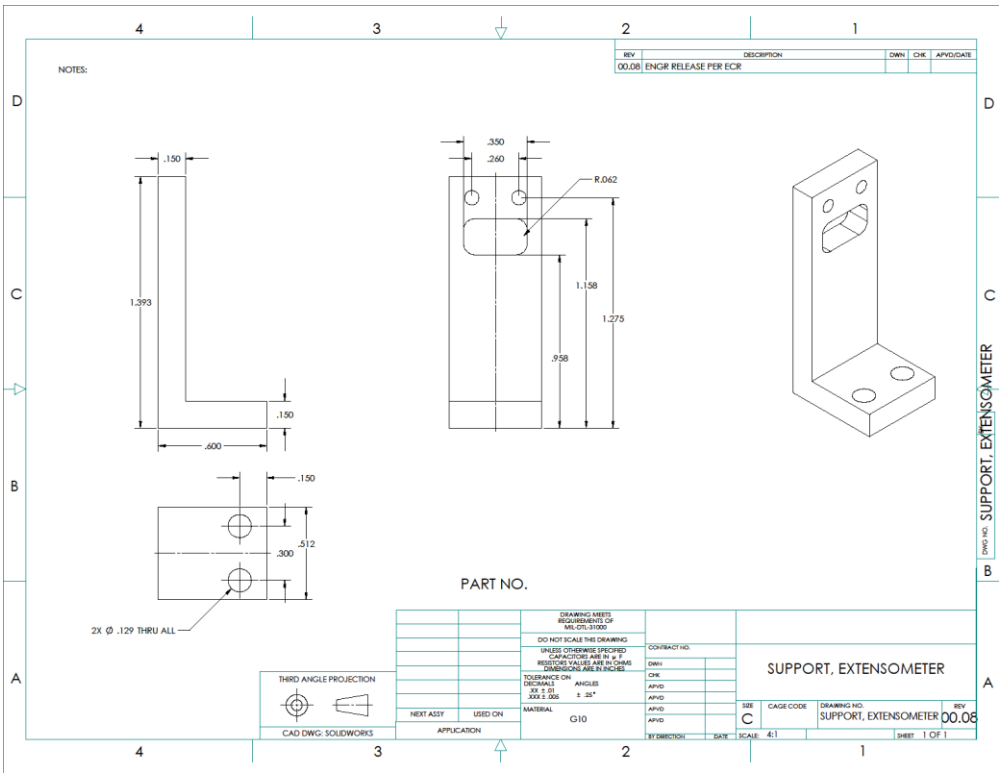

Fig. 7.32 Support extensometer

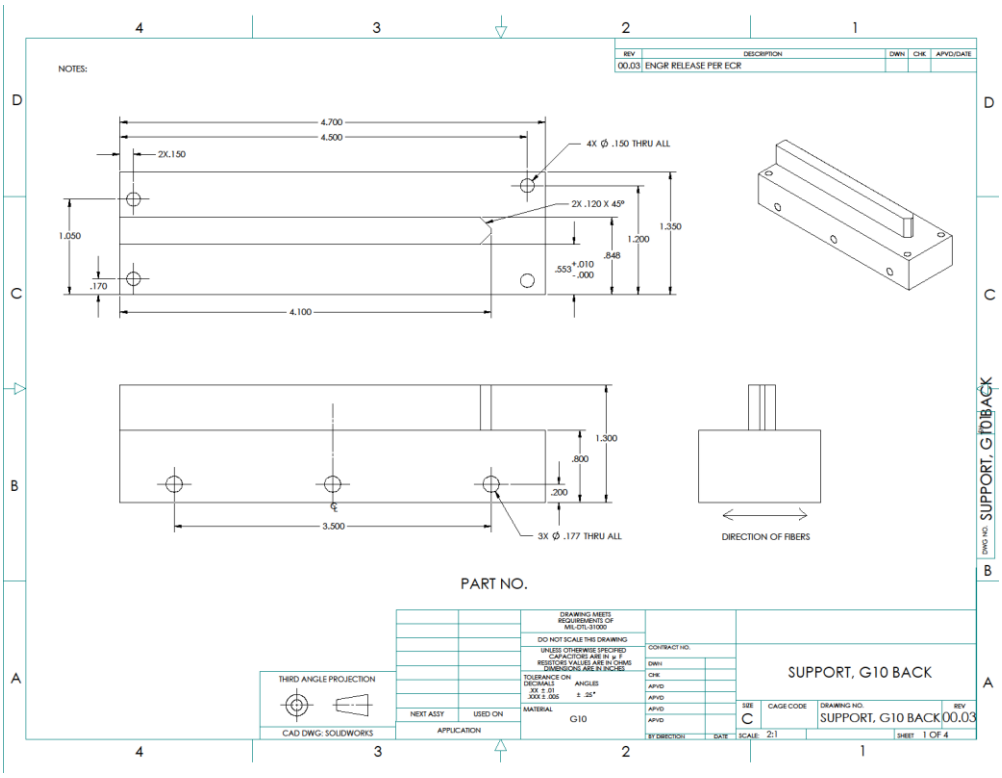

Fig. 7.33 Support G10 block

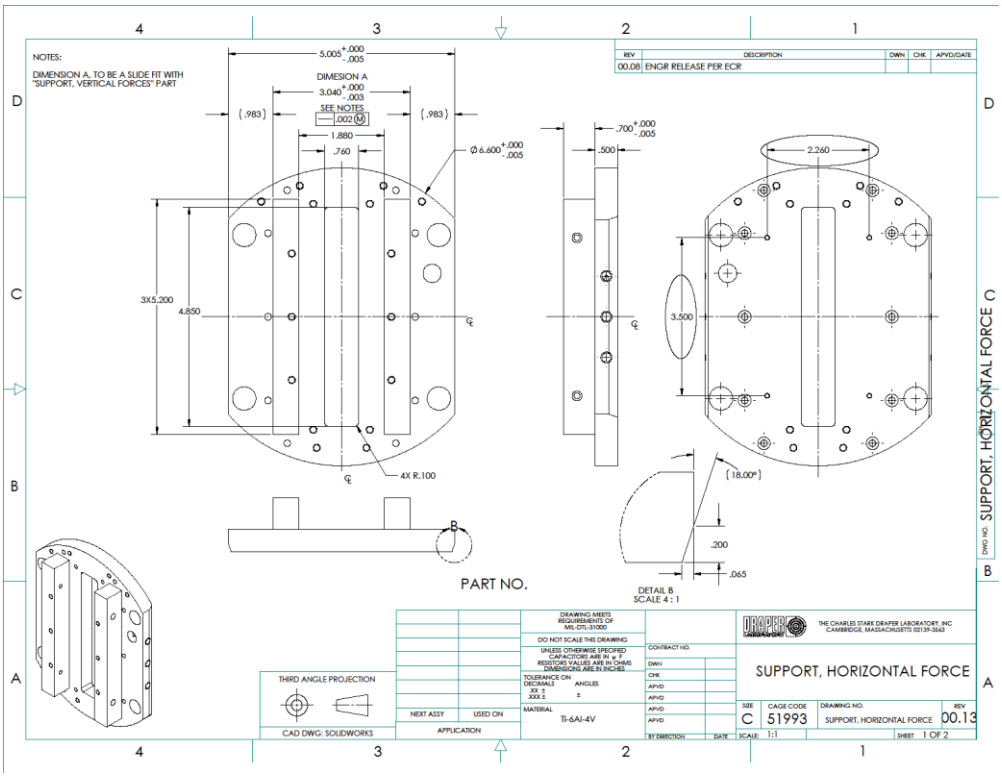

Fig. 7.34 Support horizontal force

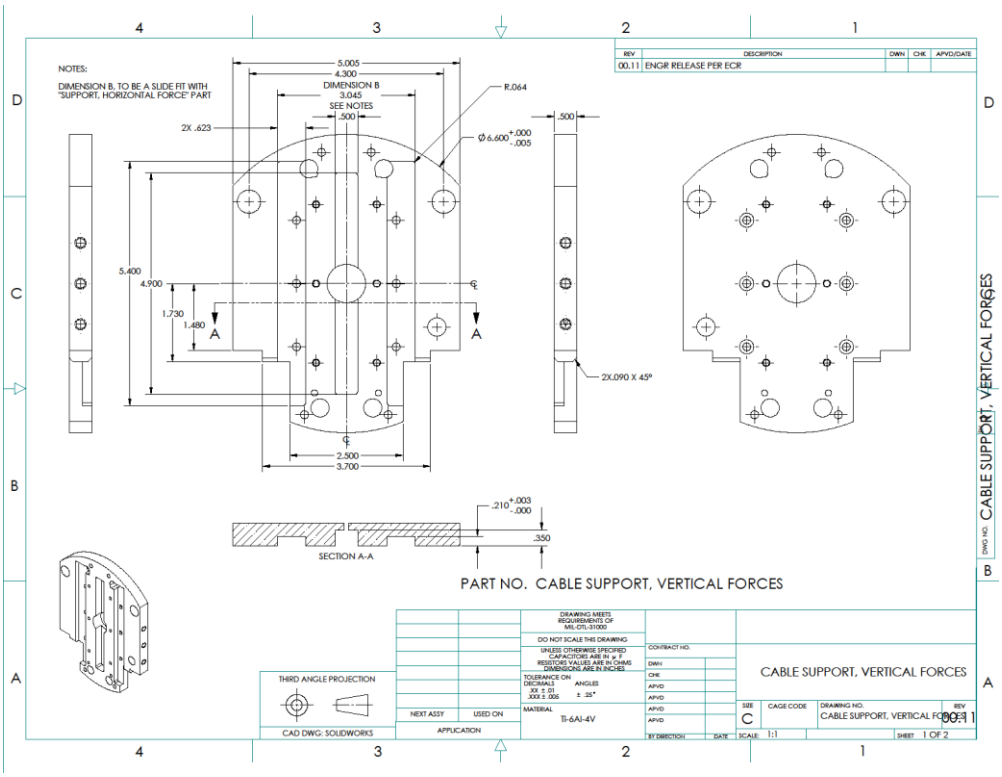

Fig. 7.35 Cable support vertical forces

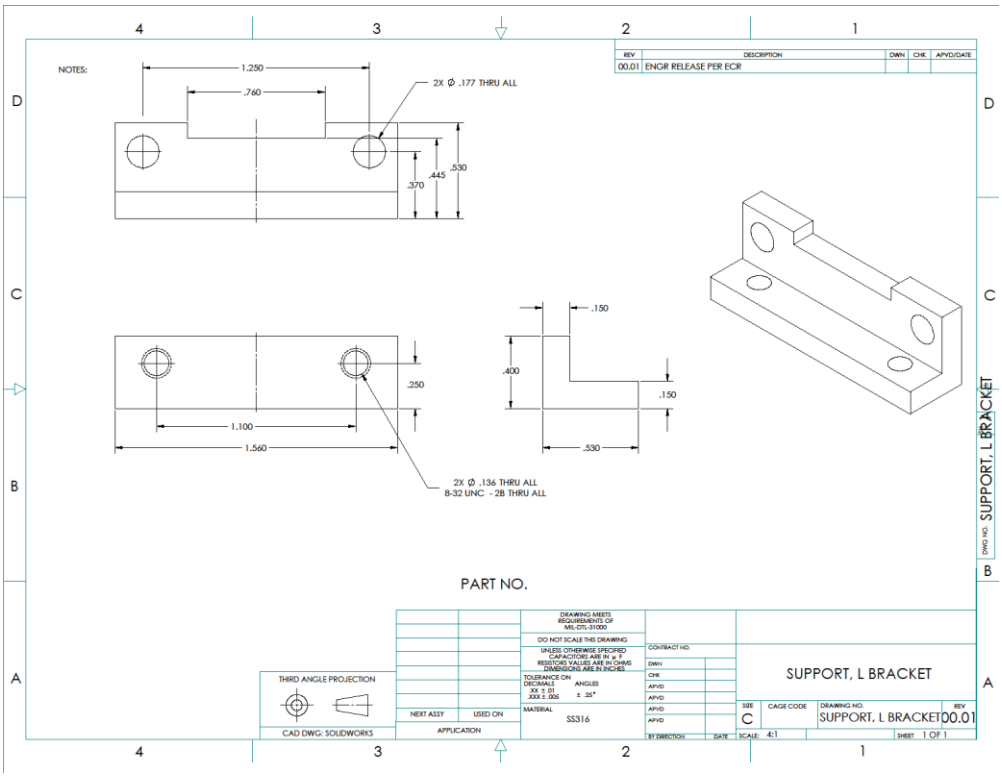

Fig. 7.36 Support L bracket

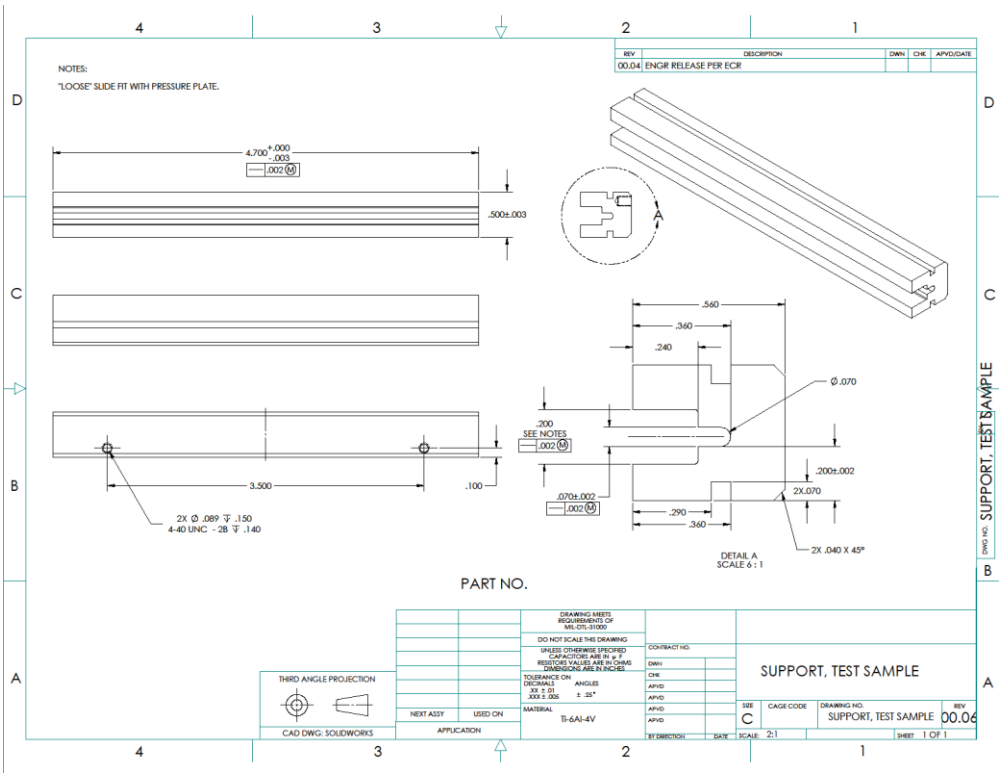

Fig. 7.37 Support test sample

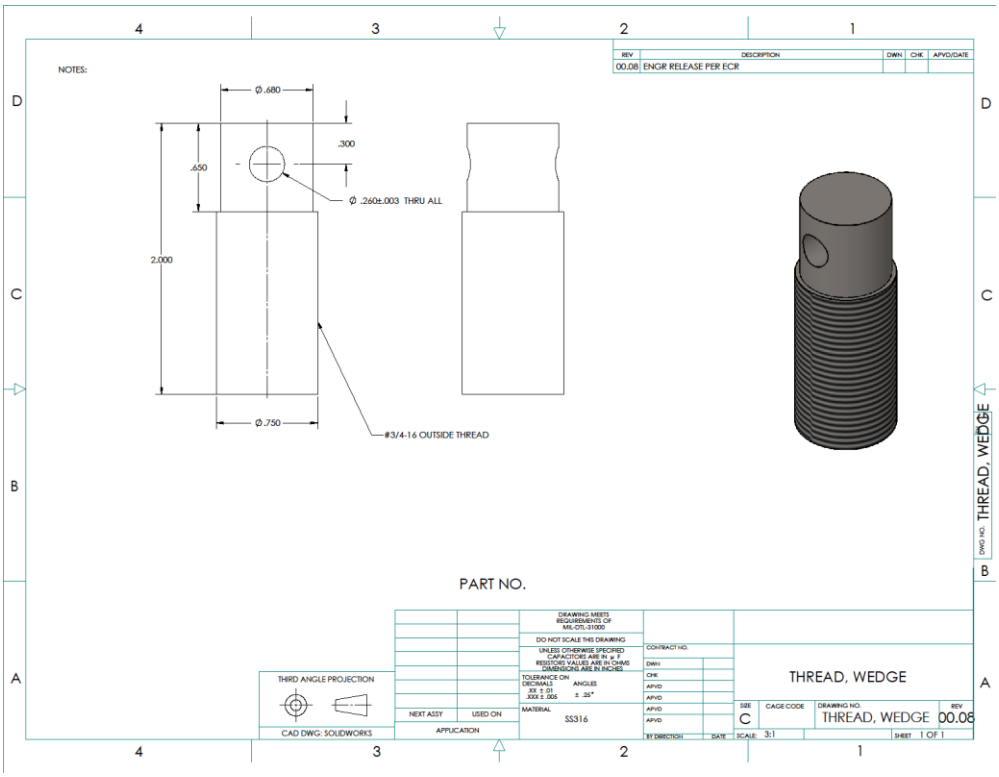

Fig. 7.38 Thread wedge

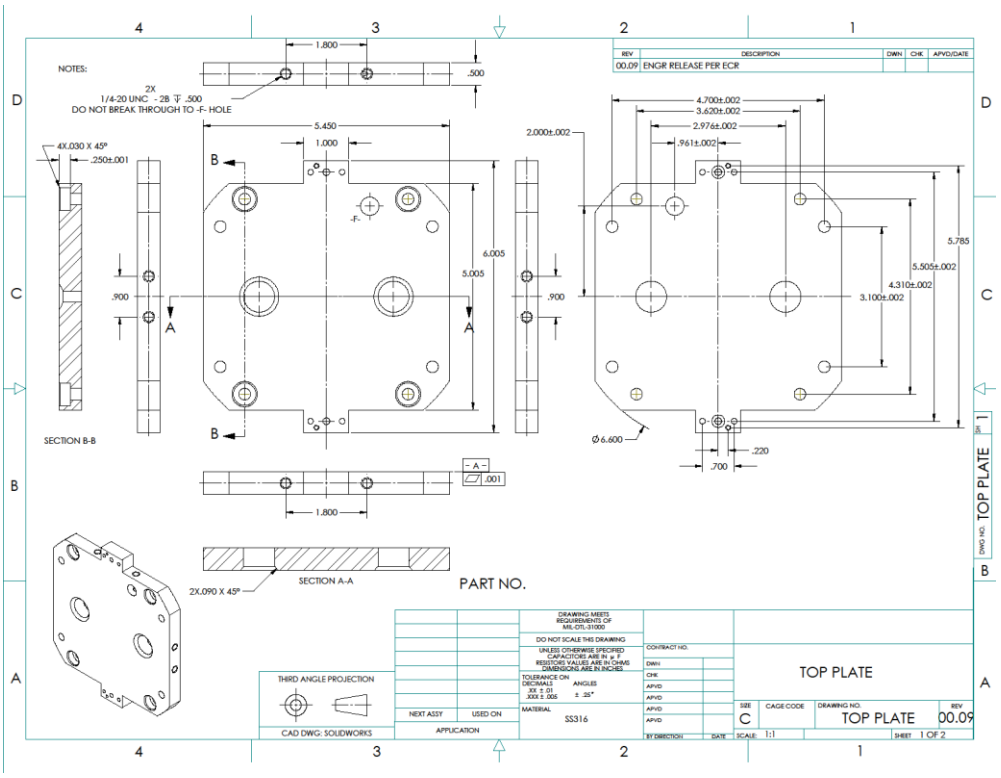

Fig. 7.39 Top plate

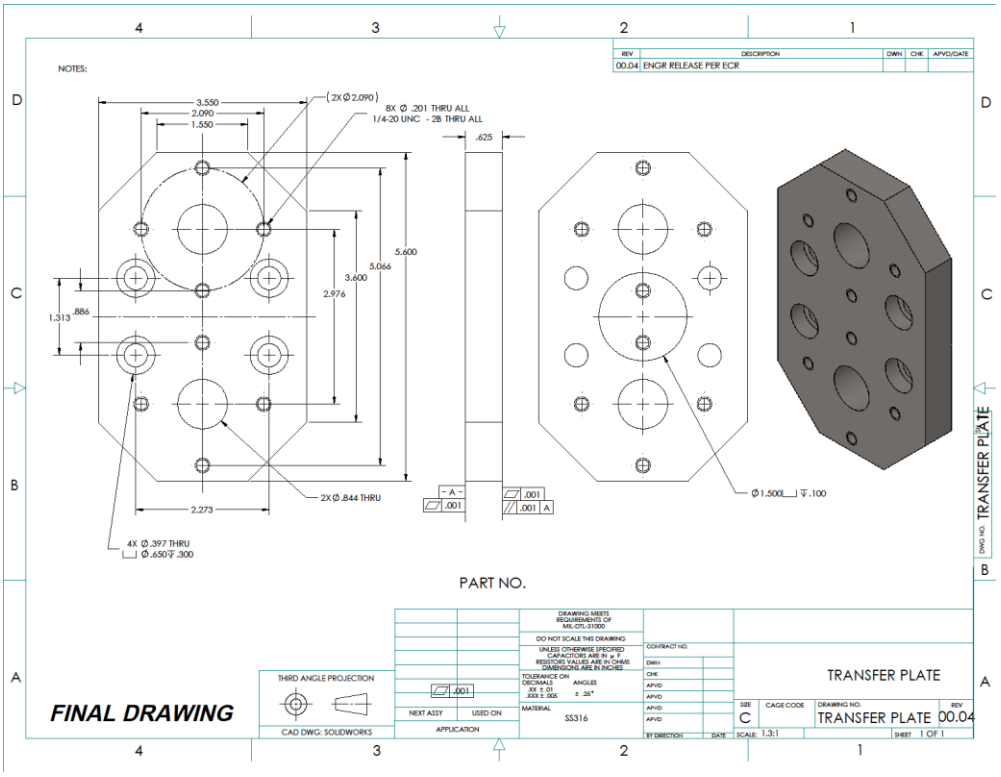

Fig. 7.40 Transfer plate

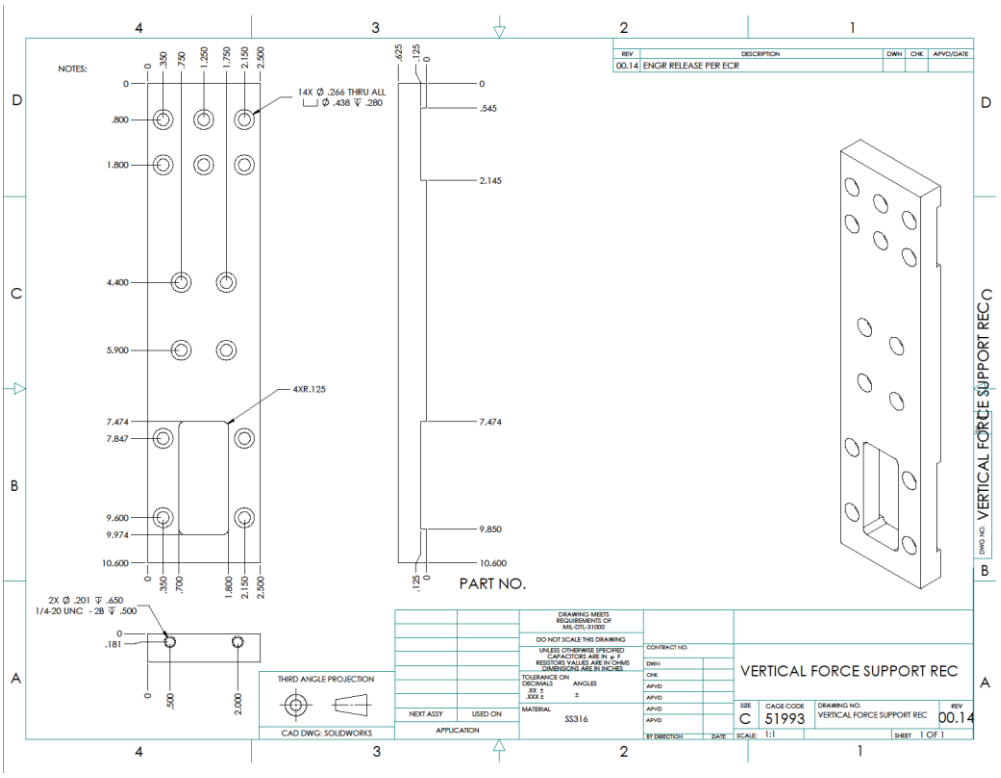

Fig. 7.41 Vertical force support rec

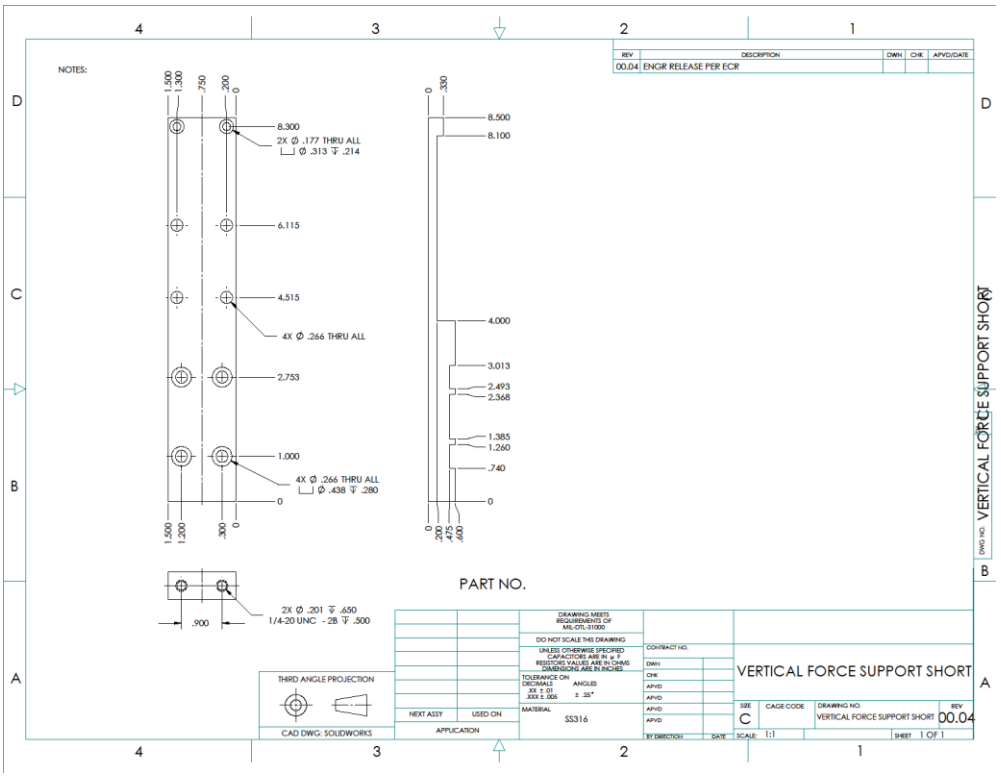

Fig. 7.42 Vertical force support short

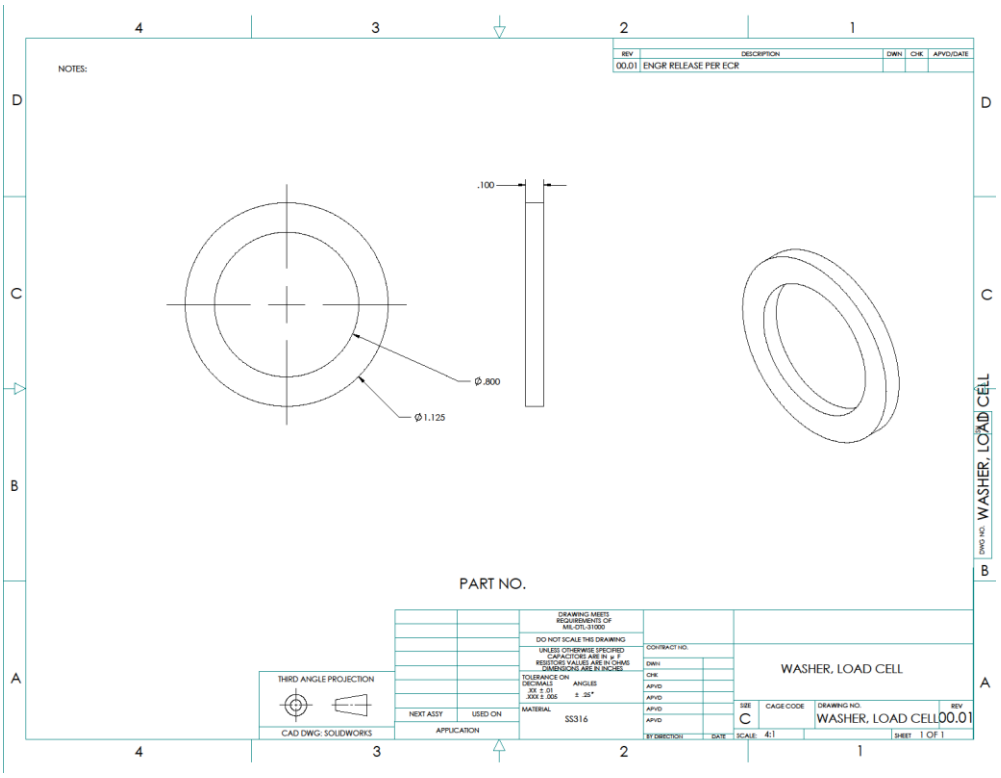

Fig. 7.43 Washer load cell

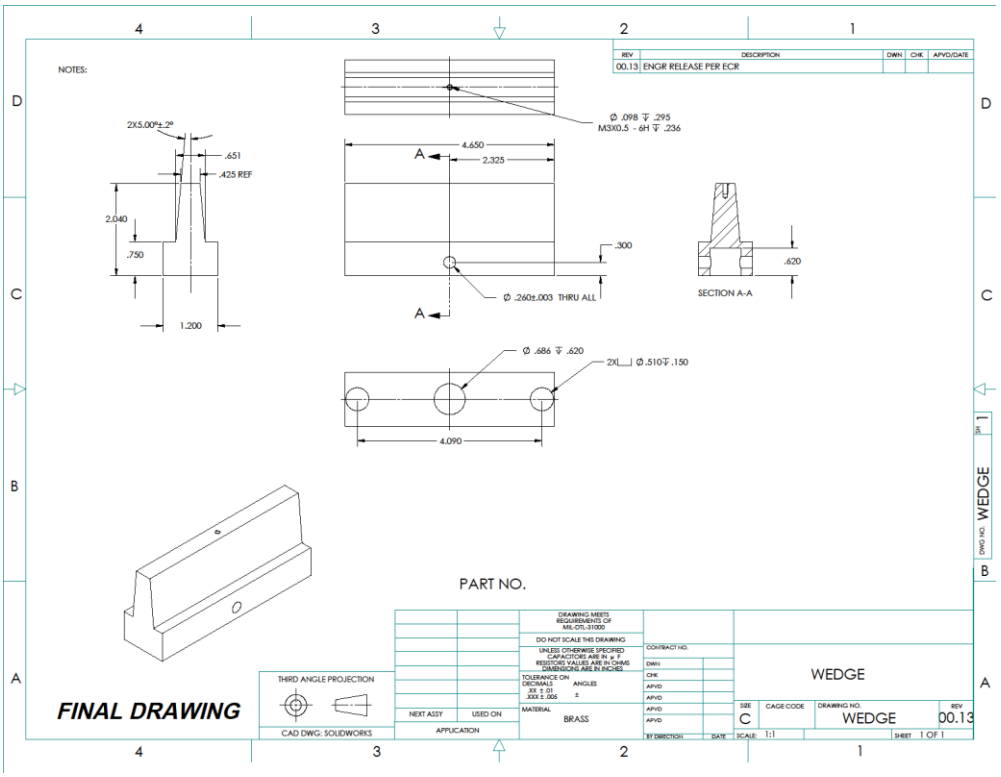

Fig. 7.44 Wedge

References

(2011, March) www.futurescience.com/scintro.html.
1]

Chad Matthew Fischer, "Investigation Of The Relationships Between
2] Superconducting Properties And Nb3Sn Reaction Conditions In Powder-In-Tube Nb3Sn Conductors," University of Wisconsin, Madison, Master of Science 2002.

Yukikazu Iwasa. (2009) Case studies in Superconducting Magnets, 2nd
3] Edition, Massachusetts Institute of Technology.

Tiening Wang, "Stress analysis of transverse load on superconducting
4] Nb3Sn strand(s)," Tufts University, 2010.

I.M. Davidson, G.E. Tuck C.R. Walters, "Long sample high sensitivity
5] critical current measurements under strain," *Cryogenics,* vol. 26, no. 7, pp. 406-12, July 2086.

L Chiesa, "Mechanical and Electromagnetic Transverse Load Effects On
6] Superconducting Niobium-Tin Performance," Massachusetts Institute of Technology, Ph.D. Thesis 2009.

Fritz London and Heinz London, *The Electromagnetic Equations of the*
7] *Supraconductor*. London: Proc. Roy. Soc., 1935.

W Meissner and R Ochsenfeld, *Ein neuer effekt bei eintritt der*
8] *supraleitfähigkeit, Naturwissenschaften*., November, 1993, vol. Vol 21, N. 44, p.787-788.

D. L. Harris, "Characterization of Nb3Sn Superconducting Strand Under
9] Pure Bending," Massachusetts Institute of Technology, M.S. in Mechanical Engineering 2005.

Arno Godeke, "Performance boundaries in Nb3Sn superconductors,"
10] University of Twente, Enschede, The Netherlands, Ph.D. Thesis 2005.

MICHAEL THOMAS NAUS, "OPTIMIZATION OF INTERNAL-Sn
11] Nb3Sn COMPOSITES," University of Wisconsin-Madison Ph.D. Thesis, 2002,.

ITER website. (Accessed February 2012) www.iter.org.
12]

Philip Mallon, "Characterization of Nb3Sn Superconducting Strands
13] under," Tufts University, 2011.

M. Takayasu, P.J. Lee, J.V. Minervini, D.C. Larbalestier B. J.
14] Senkowicz, "Effects of bending on cracking and critical current of Nb3Sn ITER wires," *IEEE Transactions on Applied Superconductivity*, vol. 15, no. n2, pt. III, pp. 3470-3473, June 2005.

J.W. Ekin, "Effect of transverse compressive stress on the critical current
15] and upper critical field of Nb3Sn," *J. Appl. Phys.*, vol. 62, p. 4829, Dec 1987.

J.W. Ekin, "Transverse stress effect on multifilamentary Nb3Sn
16] superconductor," *Adv. Cryogenics Eng.*, vol. 34, pp. 547-552, 1988.

W. Specking, "Effect of transverse compression on Ic of Nb3Sn
17] multifilamentary wire," *Adv. Cryogenics Eng.*, vol. 34, p. 569, 1988.

M. Takayasu, "Current Sharing Temperature And Critical Current
18] Analyses Based On Single Strand Data," in *CSMC and CSIC Workshop*, JAERI, Naka, Japan, November 9-10, 2000.

National High Magnetic Field Laboratory. name of lab. [Online].
19] www.magnet.fsu.edu

A.C. Rose-Innes and E.H. Rhoderick, *Introduction to superconductivity*.
20] Oxford: Pergamon Press, 1978.